AD-A276 227

(2)

REGIONAL CHARACTERIZATION OF MINE BLASTS, EARTHQUAKES, MINE TREMORS, AND NUCLEAR EXPLOSIONS USING THE INTELLIGENT SEISMIC EVENT IDENTIFICATION SYSTEM

DTIC
ELECTE
FEB 2 8 1994
S A

FINAL REPORT
SAS-TR-94-12
July 31, 1993

Sponsored by:
Advanced Research Projects Agency (DoD)
Nuclear Monitoring Research Office

ARPA Order 6731, Amendment 14
Issued by Phillips Laboratory
Contract F29601-92-C-0009

This document has been approved for public release and sale; its distribution is unlimited

Name of Contractor: ENSCO, Inc.
Effective Date of Contract: 26 March 1992
Contract Expiration Date: 31 December 1993

Principal Investigator: Dr. D.R. Baumgardt
Phone Number: 703-321-9000
Reporting Period: 1 April 1992-1 July 1993

DISCLAIMER

"The views and conclusions contained in this document are those of the authors and should not be interpreted as representing the official policies, either expressed or implied, of the Advanced Research Projects Agency, or the U.S. Government."

94-06451

94 2 25 175

REGIONAL CHARACTERIZATION OF MINE BLASTS, EARTHQUAKES, MINE TREMORS, AND NUCLEAR EXPLOSIONS USING THE INTELLIGENT SEISMIC EVENT IDENTIFICATION SYSTEM

FINAL REPORT
SAS-TR-94-12
July 31, 1993

Sponsored by:
Advanced Research Projects Agency (DoD)
Nuclear Monitoring Research Office

ARPA Order 6731, Amendment 1
Issued by Phillips Laboratory
Contract F29601-92-C-0009

Accesion For
NTIS CRA&I
DTIC TAB
Unannounced
Justification
By
Distribution /
Availability Codes
Dist | Avail and / or Special
A-1

DTIC QUALITY INSPECTED 2

Name of Contractor: ENSCO, Inc.
Effective Date of Contract: 26 March 1992
Contract Expiration Date: 31 December 1993

Principal Investigator: Dr. D.R. Baumgardt
Phone Number: 703-321-9000
Reporting Period: 1 April 1992-1 July 1993

DISCLAIMER

"The views and conclusions contained in this document are those of the authors and should not be interpreted as representing the official policies, either expressed or implied, of the Advanced Research Projects Agency, or the U.S. Government."

UNCLASSIFIED

SECURITY CLASSIFICATION OF THIS PAGE

REPORT DOCUMENTATION PAGE

1a. REPORT SECURITY CLASSIFICATION UNCLASSIFIED	1b. RESTRICTIVE MARKINGS
2a. SECURITY CLASSIFICATION AUTHORITY	3. DISTRIBUTION/AVAILABILITY OF REPORT Unlimited
2b. DECLASSIFICATION/DOWNGRADING SCHEDULE	
4. PERFORMING ORGANIZATION REPORT NUMBER(S) SAS-TR-94-12	5. MONITORING ORGANIZATION REPORT NUMBER (S)
6a. NAME OF PERFORMING ORGANIZATION ENSCO, Inc. — 6b. OFFICE SYMBOL (If applicable) SAS	7a. NAME OF MONITORING ORGANIZATION Phillips Laboratory/PKRA
6c. ADDRESS (CITY, STATE, AND ZIP CODE) 5400 Port Royal Road Springfield, VA 22151-2388	7b. ADDRESS (CITY, STATE, AND ZIP CODE) Directorate of Contracting Kirtland AFB, NM 87117-5320
8a. NAME OF FUNDING/SPONSORING ORGANIZATION ARPA/NMRO — 8b. OFFICE SYMBOL	9. PROCUREMENT INSTRUMENT IDENTIFICATION NUMBER F29601-92-C-0009
8c. ADDRESS (City, State, and Zip Code) 3701 North Fairfax Drive Arlington, VA 22203-1714	10. SOURCE OF FUNDING NUMBERS PROGRAM ELEMENT — PROJECT NO. — TASK NO. — ACCESSION NO. WORK UNIT

11. TITLE (Include Security Classification)
Regional Characterization of Mine Blasts, Earthquakes, Mine Tremors, and Nuclear Explosions Using the Intelligent Seismic Event Identification System

12. PERSONAL AUTHOR(S).
Dr. Douglas Baumgardt

13. TYPE OF REPORT	13b. TIME COVERED	14. DATE OF REPORT (Year, Month, Day)	15. PAGE COUNT
Final Report	FROM 04/01/92 TO 07/01/93	1993 JUL 31	77

16. SUPPLEMENTARY NOTATION

17. COSATI CODES			18. SUBJECT TERMS (Continue on reverse if necessary and identify by block number)
FIELD	GROUP	SUB-GROUP	Seismic, discrimination, ISEIS, regional, mine blasts, mine tremors, earthquakes, expert system

19. ABSTRACT (Continue on reverse if necessary and identify by block number)
See reverse page.

20. DISTRIBUTION/AVAILABILITY OF ABSTRACT	21. ABSTRACT SECURITY CLASSIFICATION	
☐ UNCLASSIFIED/UNLIMITED ☒ SAME AS REPORT ☐ DTIC USERS	UNCLASSIFIED	
22a. NAME OF RESPONSIBLE INDIVIDUAL	22b. TELEPHONE (Include Area Code)	22c. OFFICE SYMBOL

DD FORM 1473, 84 MAR

UNCLASSIFIED

SECURITY CLASSIFICATION OF THIS PAGE

Block 19.

This report describes the results of a study of the Intelligent Seismic Event Identification System (ISEIS) which was installed at the Center for Seismic Studies and applied to regional events in the Intelligent Monitoring System (IMS) database. A subset of IMS data has been collected for known events in a database called the Ground Truth Database (GTD) and these events were processed by ISEIS. This has shown that the regional high-frequency *P/S* ratio discriminates between explosions and earthquakes in the Vogtland region recorded at the GERESSS array. Mine tremors in the Lubin and Upper Silesia resemble earthquakes. *Lg* spectral ratio was found to separate explosions and earthquakes in the Vogtland region, but the Lubin and Upper Silesia region mine tremors had large scatter. An evaluation was made of the discrimination rules in the ISEIS expert system on the events in four regions (Vogtland, Lubin, Upper Silesia, and Steigen) in the GTD.

This report also describes the results of the analysis of the December 31, 1992 event which occurred near the Russian test site on Novaya Zemlya. Analysis of *Pn/Sn* ratios at NORESS indicated that these ratios were comparable to those measured for Kola Peninsula mine blasts, although the propagation paths were different. The ratios were only slightly greater than those observed for earthquakes in the Greenland Sea. The August 1, 1986 event recorded was re-analyzed and also found to resemble mine blasts. However, other discriminants indicate that the event was probably an earthquake. A statistical analysis of the relative log *Pn/Sn* ratios, compared to nuclear explosions at Novaya Zemlya, of the December 31, 1992 event, recorded at ARCESS, and the August 1, 1986 event, recorded at NORESS, indicated that the two events were very similar. Since the August 1, 1986 event was apparently an earthquake, its similarity to the December 31, 1992 event suggests that the latter was also an earthquake.

TABLE OF CONTENTS

ABSTRACT

This report describes the results of a study of the Intelligent Seismic Event Identification System (ISEIS) which was installed at the Center for Seismic Studies and applied to regional events in the Intelligent Monitoring System (IMS) database. A subset of IMS data has been collected for known events in a database called the Ground Truth Database (GTD) and these events were processed by ISEIS. This has shown that the regional high-frequency *P/S* ratio discriminates between explosions and earthquakes in the Vogtland region recorded at the GERESSS array. Mine tremors in the Lubin and Upper Silesia resemble earthquakes. *Lg* spectral ratio was found to separate explosions and earthquakes in the Vogtland region, but the Lubin and Upper Silesia region mine tremors had large scatter. An evaluation was made of the discrimination rules in the ISEIS expert system on the events in four regions (Vogtland, Lubin, Upper Silesia, and Steigen) in the GTD.

This report also describes the results of the analysis of the December 31, 1992 event which occurred near the Russian test site on Novaya Zemlya. Analysis of *Pn/Sn* ratios at NORESS indicated that these ratios were comparable to those measured for Kola Peninsula mine blasts, although the propagation paths were different. The ratios were only slightly greater than those observed for earthquakes in the Greenland Sea. The August 1, 1986 event recorded was re-analyzed and also found to resemble mine blasts. However, other discriminants indicate that the event was probably an earthquake. A statistical analysis of the relative log *Pn/Sn* ratios, compared to nuclear explosions at Novaya Zemlya, of the December 31, 1992 event, recorded at ARCESS, and the August 1, 1986 event, recorded at NORESS, indicated that the two events were very similar. Since the August 1, 1986 event was apparently an earthquake, its similarity to the December 31, 1992 event suggests that the latter was also an earthquake.

1.0 INTRODUCTION

1.1 OBJECTIVES

The overall objective of this project is to utilize a new research prototype for seismic discrimination, called the Intelligent Seismic Event Recognition System (ISEIS) and described by Baumgardt et al (1991a, b), to evaluate regional seismic discrimination methods utilizing the databases produced by the Intelligent Monitoring System (IMS), described by Bache et al (1991). The IMS detects regional seismic events, recorded primarily by the four regional seismic arrays, NORESS, ARCESS, FINESA, and GERESS, as well as selected three-component stations, identifies key regional seismic phases, and locates events using combined phase travel times and array-parameter measurements. This process has been running online at NORSAR, processing data from all four arrays since the beginning of 1991, and has produced waveform edits for many thousands of regional seismic events in Scandinavia, southern Europe, and western Russia which have been stored at the Center for Seismic Studies (CSS) in an Oracle database. Our goal in this study is to interface the ISEIS system with this database at the CSS and evaluate waveform discrimination techniques on this very large database.

1.2 OVERVIEW

During this reporting period, a number of different projects were initiated, both in the improvement and CSS implementation of ISEIS and in the use of ISEIS to investigate in detail multivariate waveform discriminants. This final report follows up previous work described in our earlier report (Baumgardt et al, 1992). In Section 1.2.1, we summarize the work that has been completed and in Section 1.2.2, we present the conclusions of the research studies accomplished to date.

1.2.1 Research Accomplished

The first major task of this study was the implementation of the Intelligent Seismic Events Identification System (ISEIS) at the Center for Seismic Studies (CSS). The details of this implementation were described in Baumgardt et al (1992) and an outline of the approach and the discriminant rules are given in Section 2.0.

The major focus of this study has been the ISEIS analysis of data in the Ground Truth Database (GDT), described by Grant et al (1993a), which contains many events for which we have some ground truth; i.e., there is independent information about the accurate location of the events, in some cases including depth of focus, and identification of the events.

Another major focus of this project was a seismic event that occurred on the island of Novaya Zemlya on December 31, 1992. The proximity of this event to the Russian nuclear test site at Matochkin Shar has raised suspicions that it could have been an unannounced nuclear explosion. The available seismic data from this event, consisting primarily of ARCESS recordings, have been analyzed in detail and compared with historical events in the region. Also, NORESS recordings of an earlier event recorded at Novaya Zemlya, which occurred on August 1, 1986, were also re-examined and compared with a nuclear explosion recorded there. The results of this study are described in Section 3.0.

1.2.2 Overall Conclusions

(1) The regional *P/S* ratio discriminant, which we have studied in four different geographic regions, has proven to be a very good discriminant at high frequency. We have found it to be a very stable discriminant for events in the Scandinavian shield as well as in the more tectonically active regions of Germany and Poland. Mine tremors seem to resemble earthquakes in that they have small *P/S* ratios. Even for events which may be combined mine blast and tremor, we have observed earthquake-like *P/S* ratios.

(2) The *Lg* spectral ratio has given somewhat enigmatic results. It seems to effectively separate the explosion and earthquake populations at Vogtland in the way observed by Bennett and Murphy (1986) for nuclear explosions and earthquakes; i.e., the earthquakes seem to have higher frequencies than the explosions. Our analysis of the spectra have shown that the reason that this discriminant works at Vogtland is that Vogtland earthquakes have a strong spectral peak at about 4 Hz which seems to be missing in the explosions, and hence, earthquakes have much flatter spectra than the explosions. We have suggested possible source effects, including depth of focus differences and source-mechanism differences, as the cause of the success of this discriminant. However, we have found greater scatter in these spectral ratios for the Lubin and Upper Silesia events. Moreover, our studies in other regions of Scandinavia have shown that this discriminant is not as effective in shield regions in separating earthquake and explosions as it has been in the Vogtland region.

(3) Our analysis of the performance of the ISEIS discrimination rules have shown them to be surprisingly successful. As expected, the *P/S* ratio discriminants works best to classify earthquakes whereas ripple fire works best to classify mine blasts. Also, at Vogtland, *Lg* spectral ratio helps to classify many of the events. We have a large number of "unidentified" events, many of which could later be identified by an analyst using the ISEIS interactive graphics visualization

tools. Moreover, the addition of an *Rg* discriminant would eliminate many of the unidentified blasts, although care must be used for very shallow mine tremors and also earthquakes.

(4) The Lubin and Upper Silesia events need more analysis. We have found that these events tend to look earthquake-like, which we might expect for such events, but we have also observed some explosion-like character as well. For many mines in Scandinavia, we have frequently observed large scatter in the *P/S* ratios which may be due to induced spall. However, many of these events may actually not be pure blasts but rather some combination of blast and induced tremor. This has significance for conceiving of possible evasion scenarios, because it appears to be possible to generate very earthquake-like sources in mines. Thus, it might be possible to detonate a nuclear explosion in a mine, perhaps with some combination of conventional blasts, in such a way as to produce strong shear waves at the observing stations which might be identified as mine tremor or earthquake.

(5) Comparison of ARCESS waveforms from the December 31, 1992 (921231) event with historical nuclear explosions at Novaya Zemlya shows that the event generates more *Sn* energy, relative to *Pn* energy, than the nuclear explosions. Nuclear explosions produce very large *Pn/Sn* amplitude ratios in frequency bands above 4 Hz. Ratios for the 921231 event are not as high as those of nuclear explosions, but are slightly larger than those produced by earthquakes in the same distance range. Spectral analysis of the *Pn* and *Sn* indicates that the event is not ripple-fired since the spectra are not scalloped. The *Sn* spectral ratio fails to discriminate between small earthquakes and chemical blasts. Re-analysis of an earlier larger (*mb* = 4.6) Novaya Zemlya event, which occurred on August 1, 1986 (860801) and identified as an earthquake, reveals that it has similarities to the 921231 event in terms of its waveform features compared to reference events recorded at NORESS. A statistical comparison was made, relative to the Novaya Zemlya nuclear explosions, of the *Pn/Sn* amplitude ratios in four frequency bands (2-4 Hz, 2.5-4.5 Hz, 3-5 Hz, 4-6 Hz) of the 921231 event at ARCESS and the 860801 event at NORESS. This analysis shows that the log *Pn/Sn* amplitude ratios scale almost exactly the same relative to the nuclear explosions. Thus, had the 921231 event been large enough to be recorded at NORESS, it would have had the same *Pn/Sn* amplitude ratios as the 860801 event. We conclude that both events are not nuclear explosions and that their *Pn/Sn* ratios are comparable to many observed chemical blasts. However, since the 860801 event has been identified as an earthquake based on other discriminants (location, magnitude, *Ms* - *mb*), the *Pn/Sn* relative scaling argument indicates that the 921231 event is more likely an earthquake than a chemical blast.

2.0 REGIONAL SEISMIC EVENT IDENTIFICATION OF EARTHQUAKES, MINE BLASTS, AND MINE TREMORS USING ISEIS

2.1 INTRODUCTION

The Intelligent Seismic Event Identification System (ISEIS) is a combined signal processing and X-Window-based interactive graphics visualization system for applying and analyzing seismic discriminants to regional seismic data (Baumgardt et al, 1991a, b). The two primary objectives of this project were to: (1) implement ISEIS at the Center for Seismic Studies (CSS) to interface with databases of the Intelligent Monitoring System and (2) investigate its performance in the discrimination of regional seismic events in the IMS. The first objective was achieved early on in this project and was described in detail by Baumgardt et al (1992).

To meet the second objective, we chose to analyze in detail seismic events which have been collected at the CSS as part of a "ground-truth" database (Grant et al, 1993a). Most of the events in the GTD consist of mine blasts, earthquakes, and mine tremors in mining districts of Germany (Vogtland) and Poland (Lubin, Upper Silesia) recorded at the GERESS array and the Steigen earthquake swarm in northern Norway, recorded at ARCESS and NORESS. The previous report (Baumgardt et al, 1992) covered the analysis of the earthquakes and explosions in the Vogtland region and the earthquake swarm in the Steigen region. In this section, we include the analysis of events in the Lubin and Upper Silesia regions of Poland, most of which are believed to be mine tremors, and compare the results with the events for the Vogtland region. A description of the discrimination rules in ISEIS then follows, concluding with a discussion of the performance of the discriminants on events in the GTD.

2.2 ISEIS OPERATIONAL APPROACH

Figure 1 shows a flow diagram of how data from the CSS Oracle databases are migrated into the ISEIS database and processed through ISEIS, both in automated and interactive modes. Database relations, including event parameters, analyst phase picks, and waveform pointers, are first copied to the Oracle database account ISEIS_IMS database for selected events of interest. These relations are the basic CSS 3.0 core relations described by Anderson et al (1990), which include *origin*, *origerr*, *assoc*, *arrival*, *wftag*, and *wfdisc*. ISEIS is "current event driven" which means that a specific event to be identified is processed by the system once it has been associated and located by the IMS.

ISEIS processing is keyed initially to phase identifications and time picks made by the IMS and/or the analyst review in the Analyst Review Station (ARS). ISEIS computes incoherent

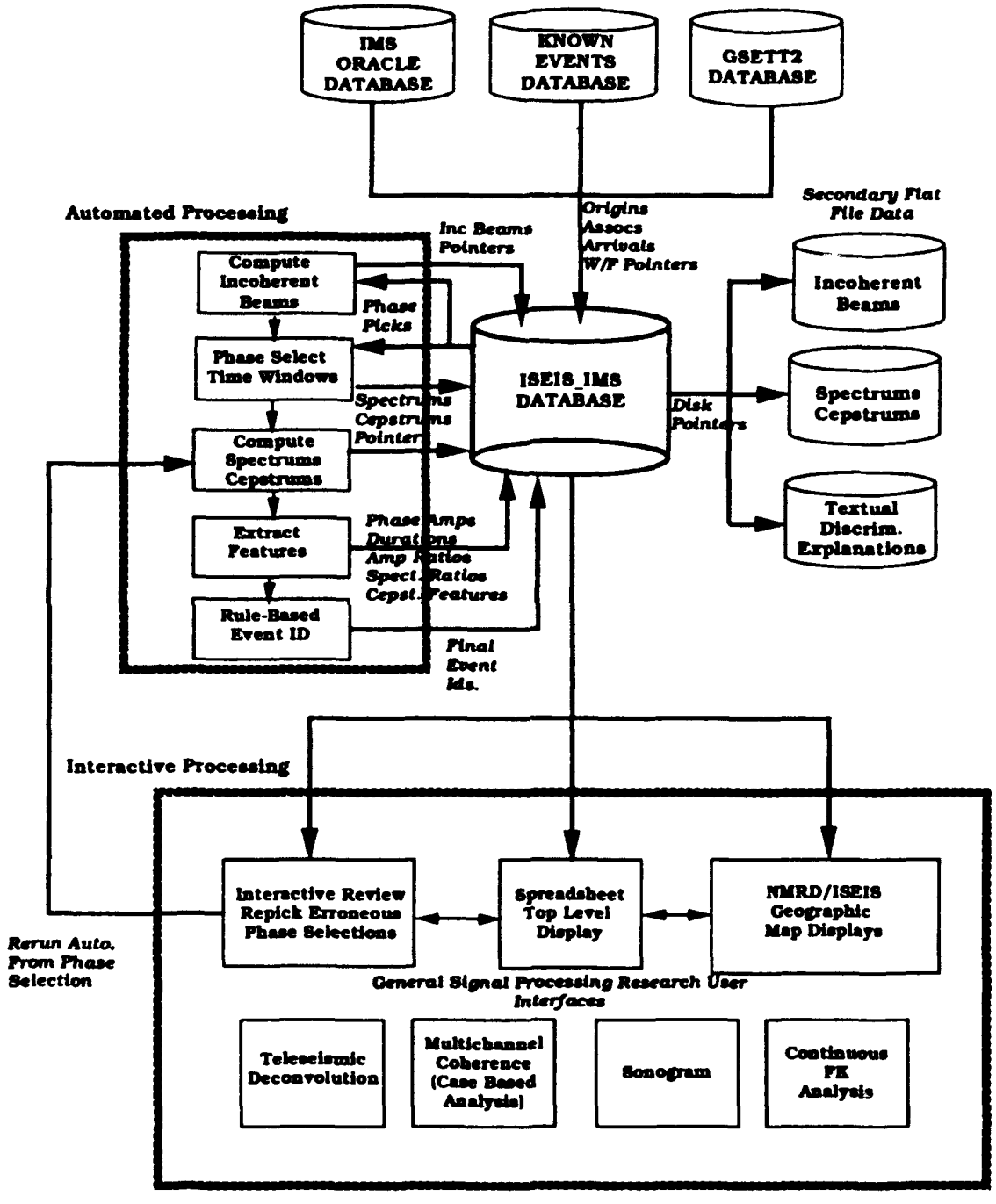

FIGURE 1: Schematic diagram showing how the ISEIS system has been interfaced at the CSS with IMS.

beams, makes phase selections, computes spectra and cepstra, and extracts features based on the phase picks. Initial event identifications by an expert system using rules coded in the NASA expert system shell, CLIPS, and the results are displayed in two user interfaces, *Spreadsheet* and *Top Level Summary (TLS)*. Interactive processing in ISEIS provides the capability to review the automated phase selections and re-pick them, and then automated ISEIS can be rerun with the corrected phase selections. Descriptions of these interfaces and the important *phase selection process* have been given in previous reports (Baumgardt et al, 1991a; Baumgardt et al, 1992). It is essential that complete consistent phase selections be made in order for reliable discriminants to be extracted, which makes the phase identification function of IMS critical for successful event identification.

2.3 EVENT LOCATIONS

Figures 2a and 2b show maps of the locations of events in Germany and Poland contained in the GTD and processed by ISEIS. The Vogtland events consist of known earthquakes and explosions, which have been processed by Baumgardt et al (1992) and Wuster (1993). The Lubin and Upper Silesia regions have event clusters whose locations are based on determinations by local networks (see Grant et al, 1993b). These events appear to be a combination of mine tremors, perhaps induced by blasting, and rock bursts associated with the mining activities in the region, but which do not appear to be associated with blasts (Gibowicz, 1984; 1985). For details about the event locations and how they were determined, see Grant et al (1993a, b).

Figures 3a and 3b show examples of incoherent beam plots for the GERESS array for events from the Lubin and Upper Silesia regions, respectively. These traces were made by averaging across the array the RMS amplitude on each seismogram of the array, averaged in moving 1 second time windows on the seismogram, beginning 30 seconds in the noise prior to the first arrival and extending to 100 seconds after the last detection, which is usually *Lg* or *Rg*. A total of 9 incoherent beams are computed for each array for 9 bandpass filters ranging from 0.5 to 2.5 Hz on the low end to 8 to 16 Hz on the high end.

Phase picks are shown in Figure 3 for phase identifications made by the analyst. Most of the events in the GTD were originally processed by the IMS. Subsequently, an analyst reviewed and checked the phase identifications and timings, making corrections where necessary. For both the Lubin and Upper Silesia regions, four regional phases were generally recognized, including *Pn*, *Pg*, *Sn*, and *Lg*.

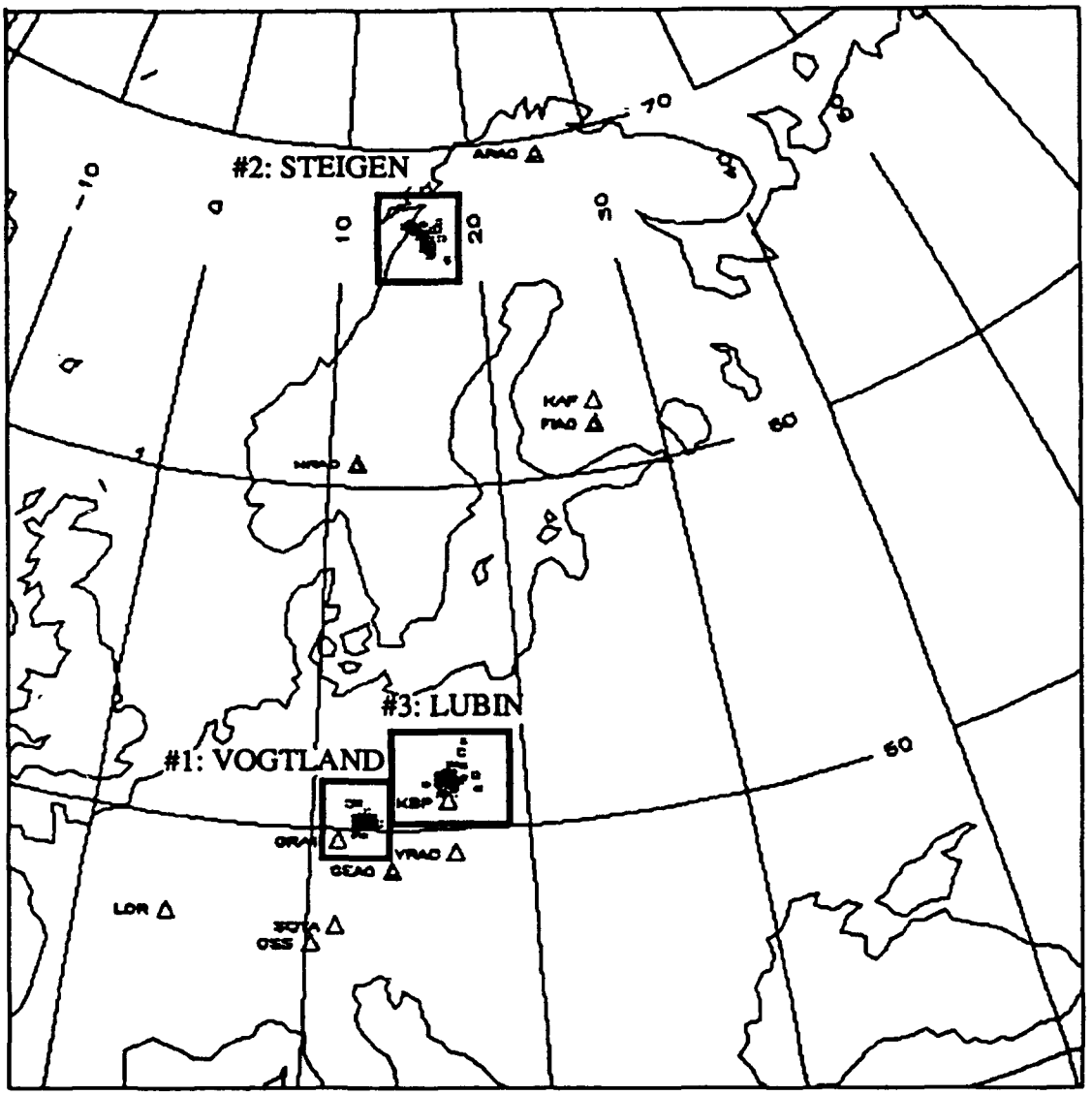

FIGURE 2 (a): Map showing the location of the Steigen, Vogtland, and Lubin regions (from Grant et al, 1993a).

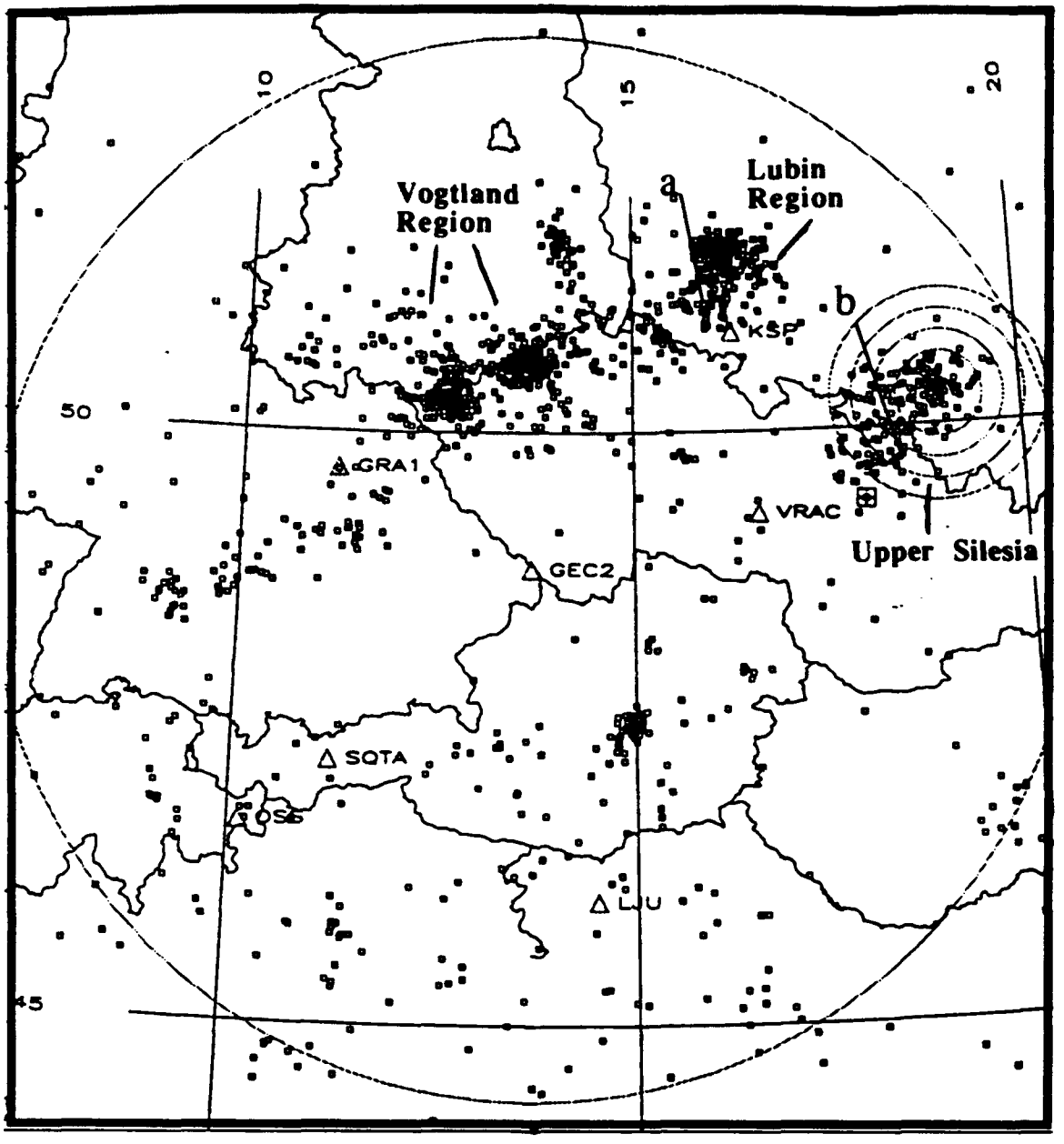

FIGURE 2 (b): Map showing locations of the seismicity in the Vogtland, Lubin, and Upper Silesia regions (from Grant et al, 1993b).

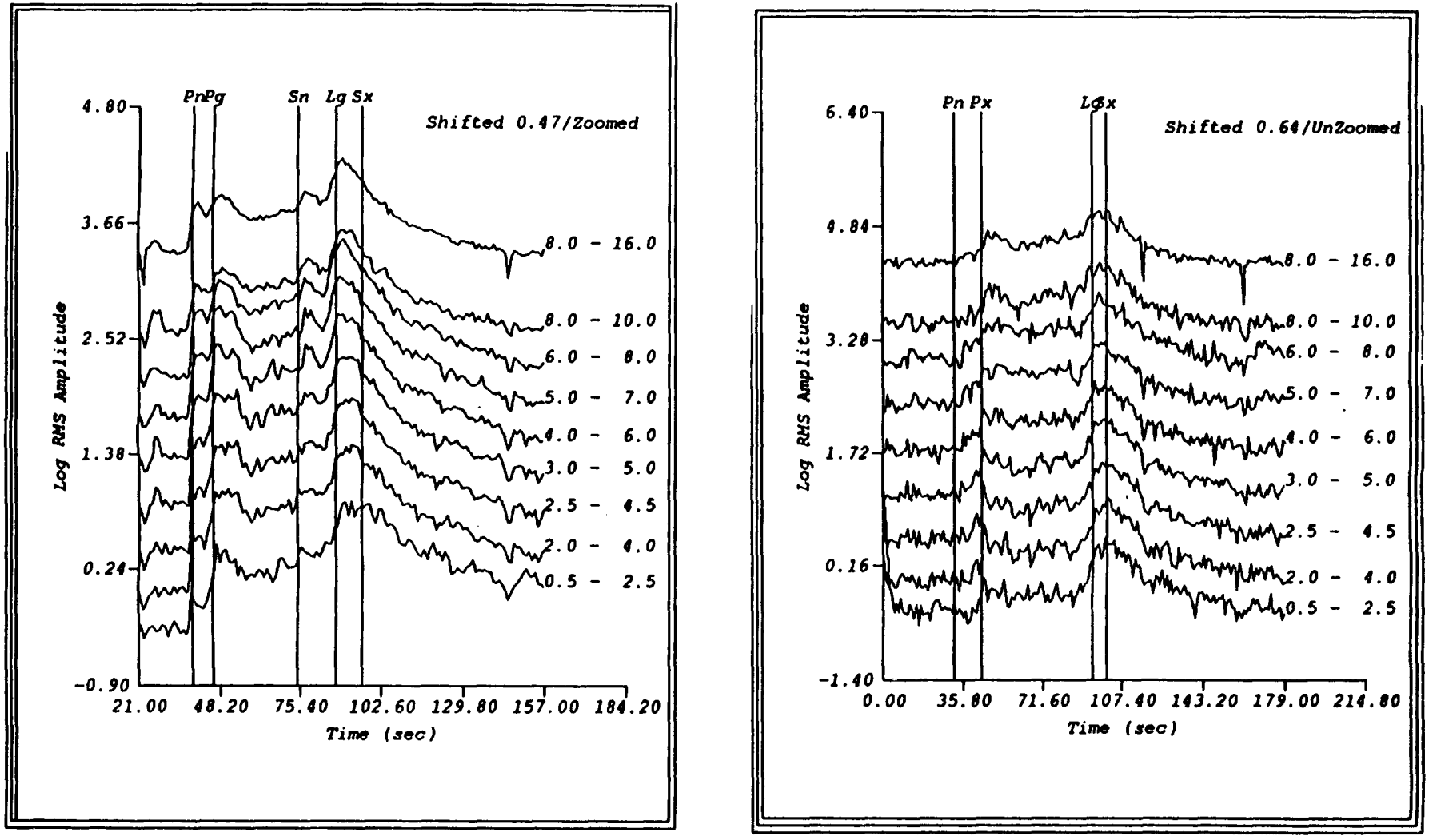

FIGURE 3: Examples of GERESS incoherent beams for events in the (a) Lubin and (b) Upper Silesia regions. The analyst picks are indicated.

Sometimes, *Rg* was also identified by the analyst for events in these regions, mostly at the Polish station KSP. Figure 3a for the GERESS incoherent beams for a Lubin event shows an "*Sx*" phase identification in the coda of the *Lg*. This *Sx* phase, which denotes regional *S* of uncertain origin, seems to be associated with energy enhancement on the 0.5 to 2.5 Hz beam and thus, could be associated with an *Rg* phase arrival at GERESS. More KSP *Rg* detections were made for the Lubin events than for the Upper Silesia, perhaps because the Lubin region is closer to KSP than the Upper Silesia region. *Rg* detection is usually thought to be an indication of shallow depth. Many such *Rg* detections at GERESS were made for the Vogtland mine blasts, as shown by Wuster (1993) and Baumgardt et al (1992), but none for the earthquakes. Thus, *Rg* detection itself might be a discriminant, where its presence indicates explosion. However, the Lubin and Upper Silesia events are all believed to be mine tremors. Thus, the identification of *Rg* waves associated with these events may mean either that the mine tremors are very shallow, thus exciting strong *Rg* waves, or they are associated with shallow mine blasts.

2.4 WAVEFORM FEATURES

The two main discriminants we examine in this study are the high-frequency regional *P/S* amplitude ratio and the *Lg* spectral ratio. The first of these has been found by a number of authors (e.g., Bennett et al, 1989; 1991; Baumgardt and Young, 1990; Baumgardt, 1992; Baumgardt et al, 1992) to be discriminatory between blasts, both mine blasts and nuclear explosions, and earthquakes. The second discriminant, low-to-high frequency spectral ratio in *Lg*, was found by Murphy and Bennett (1982), Bennett and Murphy (1986), Taylor et al (1988; 1989) to discriminate nuclear explosions and earthquakes in the western U.S., with earthquakes having more high-frequency content than explosions. Baumgardt (1992) and Baumgardt et al (1992) tested higher-frequency versions of this discriminant on mine blasts and earthquakes in Scandinavia and found it to be generally ineffective. However, Baumgardt et al (1992) did find that the discriminant worked to separate the Vogtland mine blasts and earthquakes, recorded at GERESS. Wuster (1993) also found that a spectral discriminant, using autoregressive coefficients, classified these events. In this section, we continue to examine these discriminants, expanding the analysis of the Vogtland events to include the Lubin and Upper Silesia events.

Also, in this section, we describe in detail the different features which are extracted by ISEIS for discrimination analysis and specific discrimination rules. It should be noted that measurements and spectra are determined for all phases identified by the IMS or the analysis afterwards, so that there are many more feature measurements than what may be used in actual event

identification. These extra features were recorded in order to support research in discriminant-feature trends.

For the regional *P/S* amplitude ratio discriminant, all amplitude measurements in different frequency bands are made from the incoherent-beam traces. In Figure 3, for example, each phase pick marks the start of a time window, whose width is set automatically based on an assumed group velocity range for each phase. After this window is defined, two measurements, called *stapicks*, are made of the amplitude in the incoherent beams: the maximum RMS amplitude and the average of RMS amplitudes in each *stapick* window on the incoherent beams in each of the nine filter bands. After computing the incoherent beams and storing the *stapicks*, the different waveform features are computed.

Grant et al (1993) pointed out some uncertainties in phase identifications of *Pn* and *Pg* from events in this region and more careful analyses of these events were made to correctly identify these phases. Mispicking *Pg* as *Pn* can cause severe errors in event location. They are also important in discrimination in that ISEIS has two discriminants based on *Pn* (high-frequency *Pn/Sn* and *Pn/Lg* amplitude ratio) and others based on *Pg*. Thus, it is important also in discrimination. The same also holds true for *Sn* and *Lg*; i.e., mispicking *Sn* as *Lg* or *Lg* as *Sn* and using the erroneous phase picks in the amplitude ratios can cause serious errors in the discriminants and in the identification of seismic events.

Our approach in regional waveform discrimination has emphasized always making consistent phase identifications and using the same phases when using the *P/S* type ratio. Some investigators, such as Bennett et al (1989), use a regional phase ratio like *Pmax/Lg*, where *Pmax* is the maximum *P* phase on the seismogram. However, this may cause high scatter in the phase ratios if a large number of different paths and frequencies are used, because *Pmax* may sometimes be a *Pg* type phase and other times a *Pn* type phase. Moreover, we have found in our studies that the *Pn* phase may be more stable for amplitude ratios than *Pg*, as we discuss below. Therefore, whenever possible, the phases should be identified as accurately as possible and used consistently in the amplitude ratio features, so as to avoid comparing phase ratios formed by different phases.

Another possible problem associated with *P/S* type relates to distance dependent effects of differential *P* and *S* amplitude variations. For example, Kennett (1993) has studied the distance dependence in the *Lg/Pn* and *Sn/Pn* ratio and has shown strong distance dependent effects for the distance range of 0 to 700 km. Many of these effects may be due to local site scattering and also some of the measurement techniques used in the study; e.g., measuring the ratios in the 1 to 12 Hz band, which is a broader band than we have used. We have observed, based on measurements at

the regional arrays, that these ratios are stable with distance, in the range of 100 to 500 km, for ratios measured in narrower frequency bands, as we will discuss later. However, there is no doubt that over distances greater than 700 to 1000 km, there are significant distance dependent variations, as was evident in the study of Lynnes and Baumstark (1991). In Section 3.0 of this report, we will also discuss possible distance dependent effects of the *Pn/Sn* ratio over distances over 2000 km. These effects appear to be due to differential attenuation affects in *Pn* and *Sn*.

2.5 DISCRIMINANT FEATURE RESULTS

We now examine how the these features measured for the Lubin and Upper Silesia events compare with the previous results from the Vogtland region, discussed by Baumgardt et al (1992). Both the *Pg/Lg* and *Pn/Lg* ratios were studied where in the previous study, we only investigated the *Pn/Lg* amplitude ratio. It should be noted that most of the Vogtland events were close to the crossover distance at GERESS for *Pn* and *Pg*, so that some of the *Pg* picks at Vogtland may be suspect. However, these two phases were well separated at the distances of the Lubin and Upper Silesia events.

In the scatterplots that follow, a specific set of symbols always represents different event classes, shown on the legends in each plot. Squares represent earthquakes, including the presumed mine tremors in the Lubin and Upper Silesia regions. Circles, triangles, and plus signs represent mine blast, underwater blast, and nuclear explosion, respectively.

Pn/Lg and Pg/Lg Amplitude Ratios

Figures 4a and 4b show a comparison of maximum amplitude *Pn/Lg* and *Pg/Lg* ratios, respectively, for all the events, compared with the Lubin event plotted in Figure 3a. This event is plotted in Figures 4a and 4b as a square symbol with an embedded asterisk. Square symbols denote earthquakes, and circles, quarry blasts. For the purposes of this comparison, the mine tremors and rock bursts of Lubin and Upper Silesia have been assigned the square symbol for earthquake along with the Vogtland earthquakes. The mean value of the ratios and the standard deviations, represented by the error bars, have been plotted for each source type.

Figures 4a and 4b show the increasing separation of earthquake and explosion source types with increasing frequency which we have often seen in our previous studies. The source types overlap at low frequency, below 2.5 to 4.5 Hz, but the separation is very clear at frequencies above 8 Hz. In our previous studies, we have focused primarily on the *Pn/Lg* ratio. However, this plot shows just as strong discrimination using *Pg/Lg* ratios, where *Pg* is often an easier phase to pick than *Pn*, particularly in the Upper Silesia region.

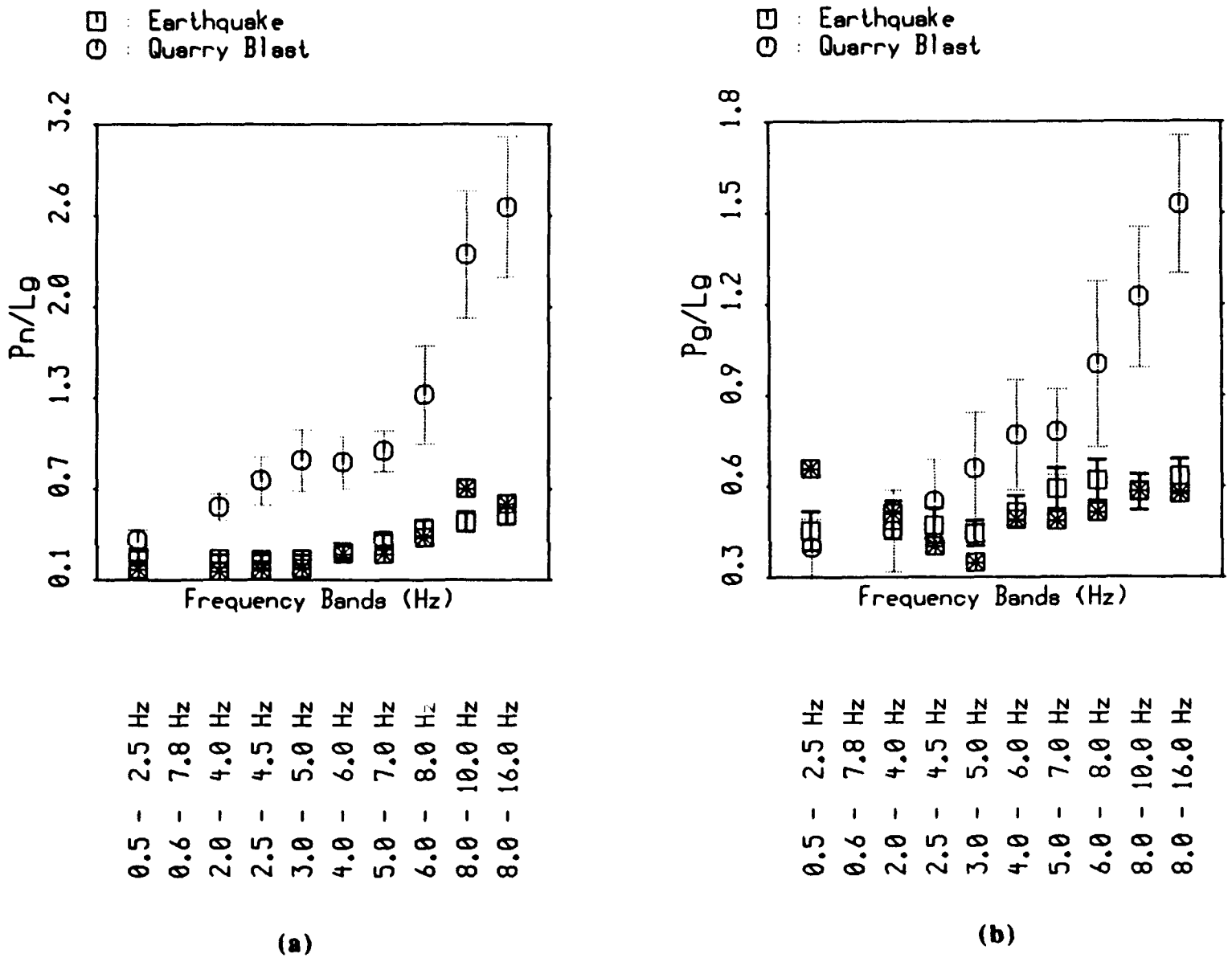

FIGURE 4: Scatterplots of (a) *Pn/Lg* and (b) *Pg/Lg* ratios as a function of frequency for the combined Vogtland, Lubin, and Upper Silesia events. The amplitudes are maximum amplitudes on the RMS incoherent beams.

Figures 5a and 5b compare the same ratios measured in the 8 to 10 Hz band plotted as a function of distance. Note again that these amplitudes are maximum RMS measured in each phase selection window on the incoherent beams. Figure 5a shows that *Pn/Lg* amplitude ratios for the Lubin and Upper Silesia events have almost the same range of values as those of the earthquakes at Vogtland, which are well below the values of the Vogtland mine blasts. The range of *Pn/Sn* ratio values for the earthquakes at Vogtland is about 0.1 to 0.7, which is about the same as those of the Lubin and Upper Silesia regions. Figure 5b shows that the *Pg/Lg* ratios have considerably more scatter, particularly in the Upper Silesia group. Some of the *Pg/Lg* ratios exceed and overlap the Vogtland blast group. We have noticed this before in our studies of Norwegian events at NORESS. In general, ratios involving *Pn* seem to be more stable in terms of scatter and separate blast and earthquake source types better than the ratios using *Pn*.

Figure 5a shows the stability of the *Pn/Lg* measurements as a function of distance for the earthquakes and the Lubin and Upper Silesia events. The range of values for the Lubin and Upper Silesia events, at distances of between 350 and 420 km, are nearly the same as those for the Vogtland earthquakes between 140 and 252 km. Thus, over the distance range of 140 to 420 km, the *Pn/Lg* ratios exhibit very little variation for earthquakes. The strong variability we observe for the explosions is not systematic and appears to be caused by source variations rather than by propagation effects.

Comparison of Maximum and Average RMS Amplitude Ratios

As we noted above, two different measurements are made on the phases, the maximum RMS and the average RMS. Plots of the average RMS amplitude measurements are shown in Figures 6a and 6b for *Pn/Lg* and *Pg/Lg* ratios, respectively. This method for measuring amplitudes appears to be less stable than the maximum amplitude method in that the explosion and earthquake ratios are not as well separated. However, the variance of the ratios appears to be about the same for the RMS measurements as it is for the maximum amplitude measurements.

In a recent discrimination study of high-frequency *Pg/Lg* ratios in New York (Kim et al, 1993; also see Shi et al, 1993), the claim was made that RMS measurements of amplitudes were very stable. These measurements were made by centering a Gaussian-shaped window on the phase and measuring the RMS amplitudes inside the window. This approach would seem to produce a very robust estimate, but would probably be very similar to a maximum amplitude measurement, since the Gaussian-shaped window centered on the phase would place more weight on the maximum amplitude in the RMS average. In our study, we have found that the maximum amplitude on the RMS incoherent beam, shown in Figure 5, to be slightly more stable than

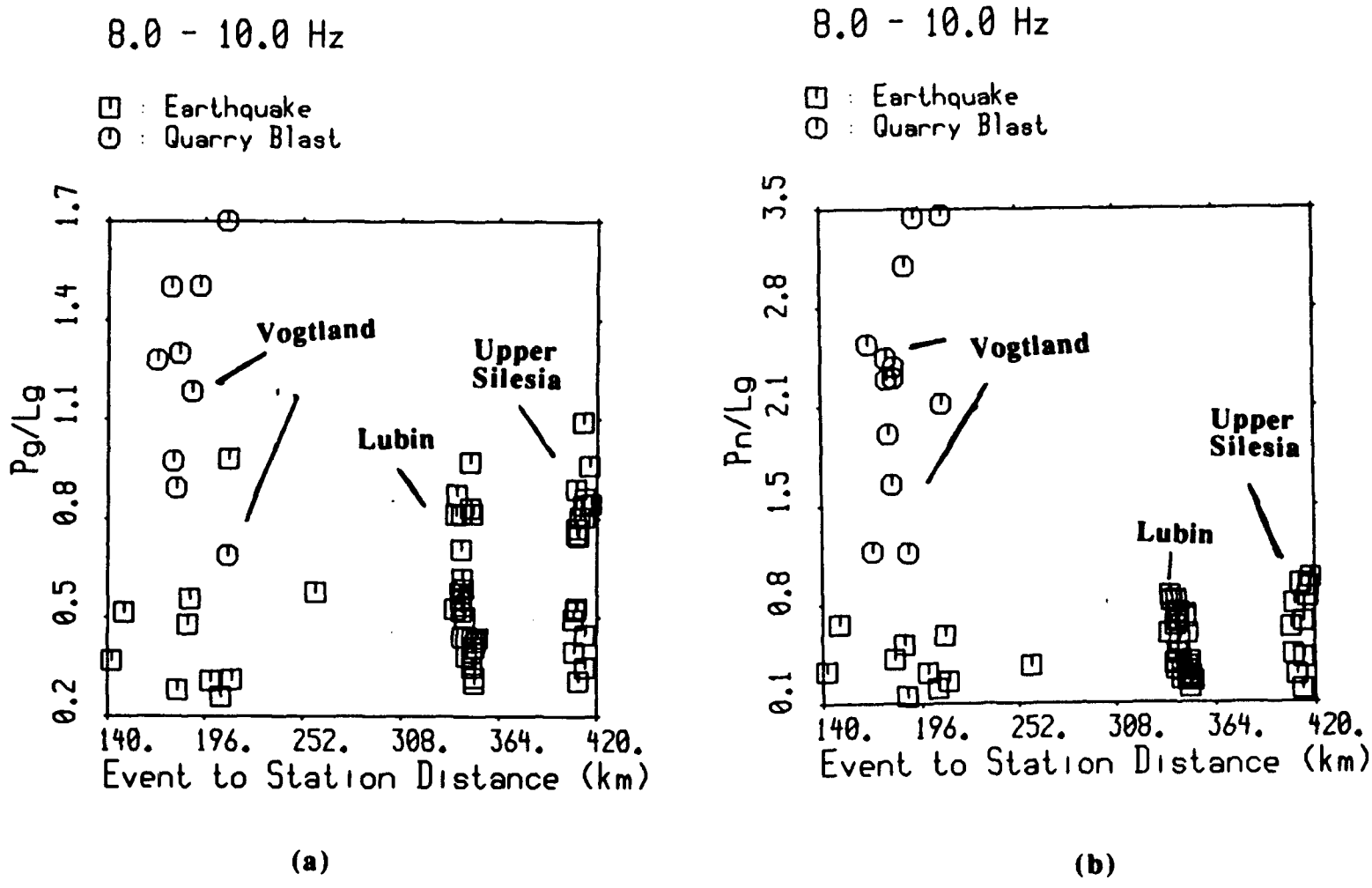

FIGURE 5: Scatterplots of (a) *Pn/Lg* and (b) *Pg/Lg* ratios as a function of distance for the combined Vogtland, Lubin, and Upper Silesia events. The amplitudes are maximum amplitudes on the RMS incoherent beams.

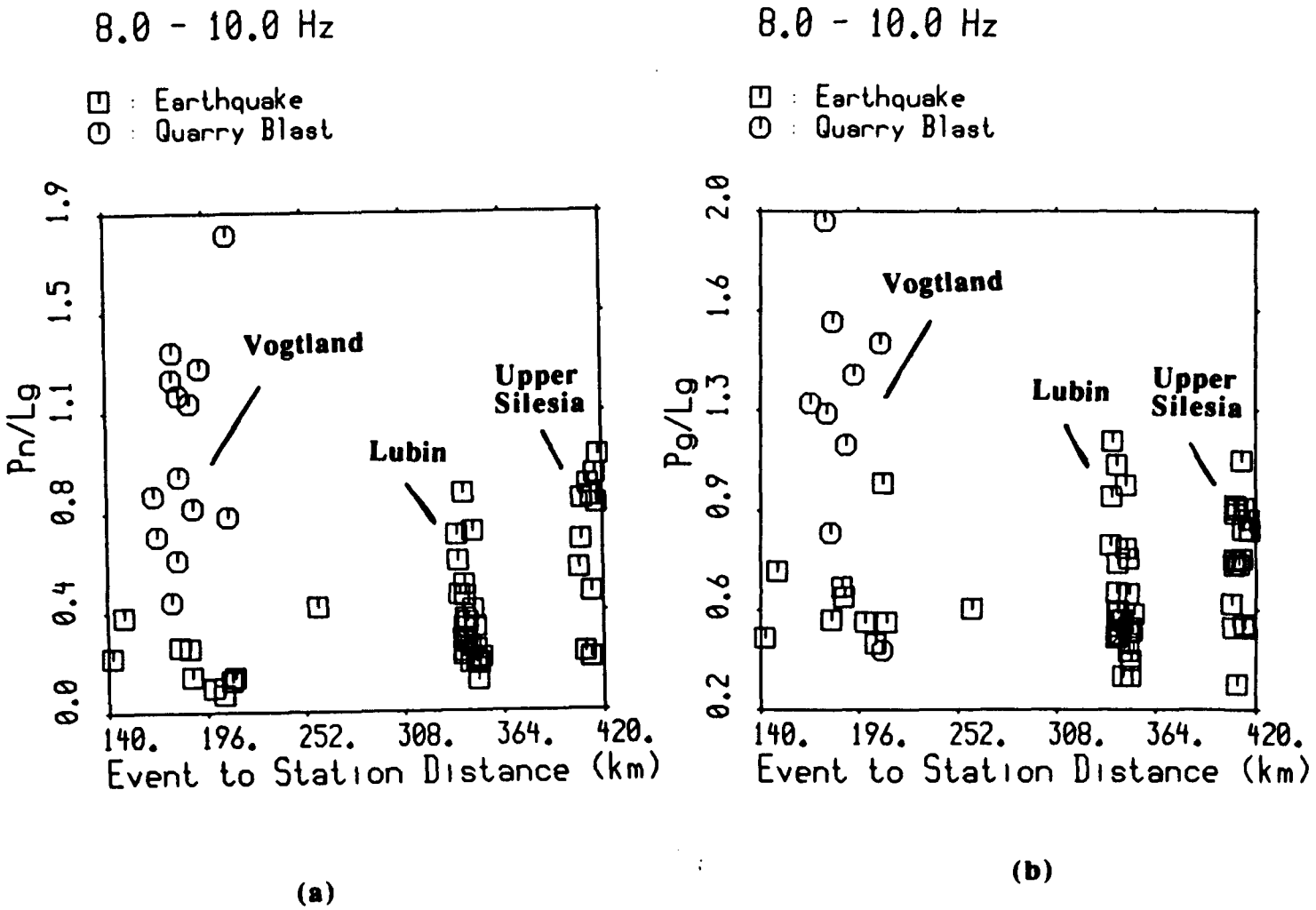

FIGURE 6: Scatterplots of (a) *Pn/Lg* and (b) *Pg/Lg* ratios as a function of distance for the combined Vogtland, Lubin, and Upper Silesia events. The amplitudes are average amplitudes on the RMS incoherent beams.

average RMS in a square window, shown in Figure 6, at least for separating earthquakes and explosions. We have found, however, that for lower signal-to-noise ratios, the maximum RMS amplitude measurement is better than the average RMS. We believe that a maximum RMS amplitude measurement would probably have comparable stability to an average RMS in a Gaussian window.

Lg Spectral Ratio

Figure 7 shows plots of the spectral ratio *R1* and *R2*, defined as

$$R1 = A_{RMS}\,(2\text{-}4\ Hz)/\ A_{RMS}\,(4\text{-}8\ Hz)$$

and

$$R2 = A_{RMS}\,(2\text{-}6Hz)/\ A_{RMS}\,(6\text{-}10Hz),$$

plotted as a function of epicentral distance. Prior to computing these ratios, the instrument response was removed from the spectra. Figure 7a shows the evident separation of Vogtland earthquakes and explosions we observed before (Baumgardt et al, 1992). However, the Lubin ratios show greater scatter than the Vogtland earthquakes, with some points overlapping the Vogtland blasts. The Upper Silesia points have events with greater scatter with some points greatly exceeding the values in the Vogtland blast group. The higher-frequency ratio, *R2*, plotted in Figure 7b, has even greater scatter for the Upper Silesia events.

In order to prove that variations in the spectral ratio are not caused by source scaling, the same ratios are plotted as a function of the local magnitude of the events in Figure 8a for *R1* and Figure 8b for *R1*. If magnitude scaling causes significant spectral effects, we might expect the spectral ratio to systematically increase with magnitude, assuming the corner frequency shifts to lower frequency across the bandwidth of 2 to 10 Hz in the *Lg* as magnitude increases. In both plots, there is no evident systematic trend of spectral ratio with magnitude.

Sample GERESS spectra for all phases associated with selected Vogtland earthquakes and an explosion are plotted in Figure 9 along with the *Lg* spectral-ratio vs. local magnitude (*Ml*) scatterplot to show why this discriminant seems to separate earthquakes and explosions in that region. Both these spectra plotted and those used to compute the spectral ratio have been corrected for a "NORESS-type" instrument correction. (Note: Using the NORESS instrument correction at

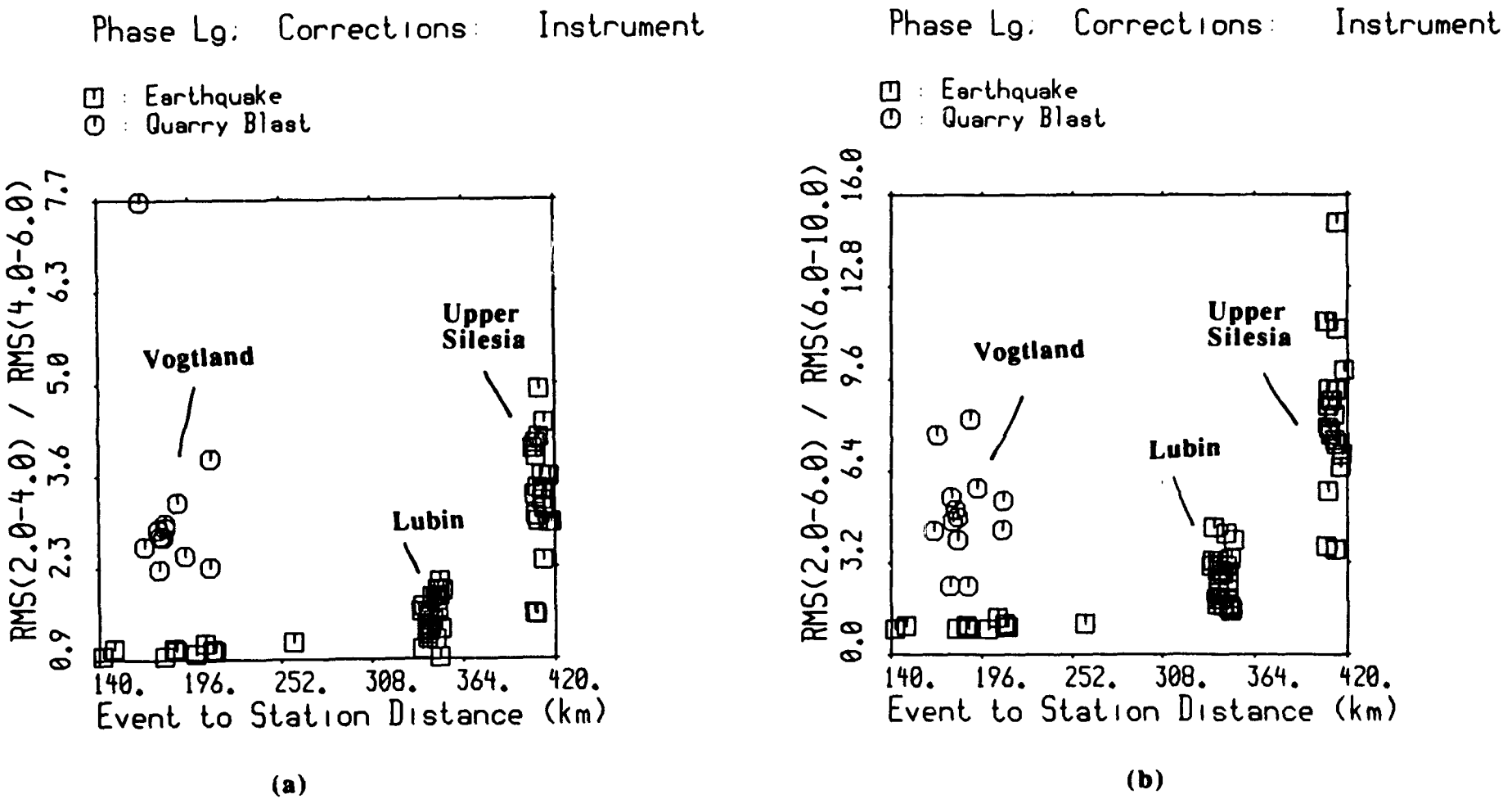

FIGURE 7: Scatterplots of two different spectral ratios for *Lg* against distance: (a) *R1* = ARMS (2-4 Hz)/ARMS (4-6 Hz); (b) *R2* = ARMS (2-6 Hz)/ARMS (6-10 Hz).

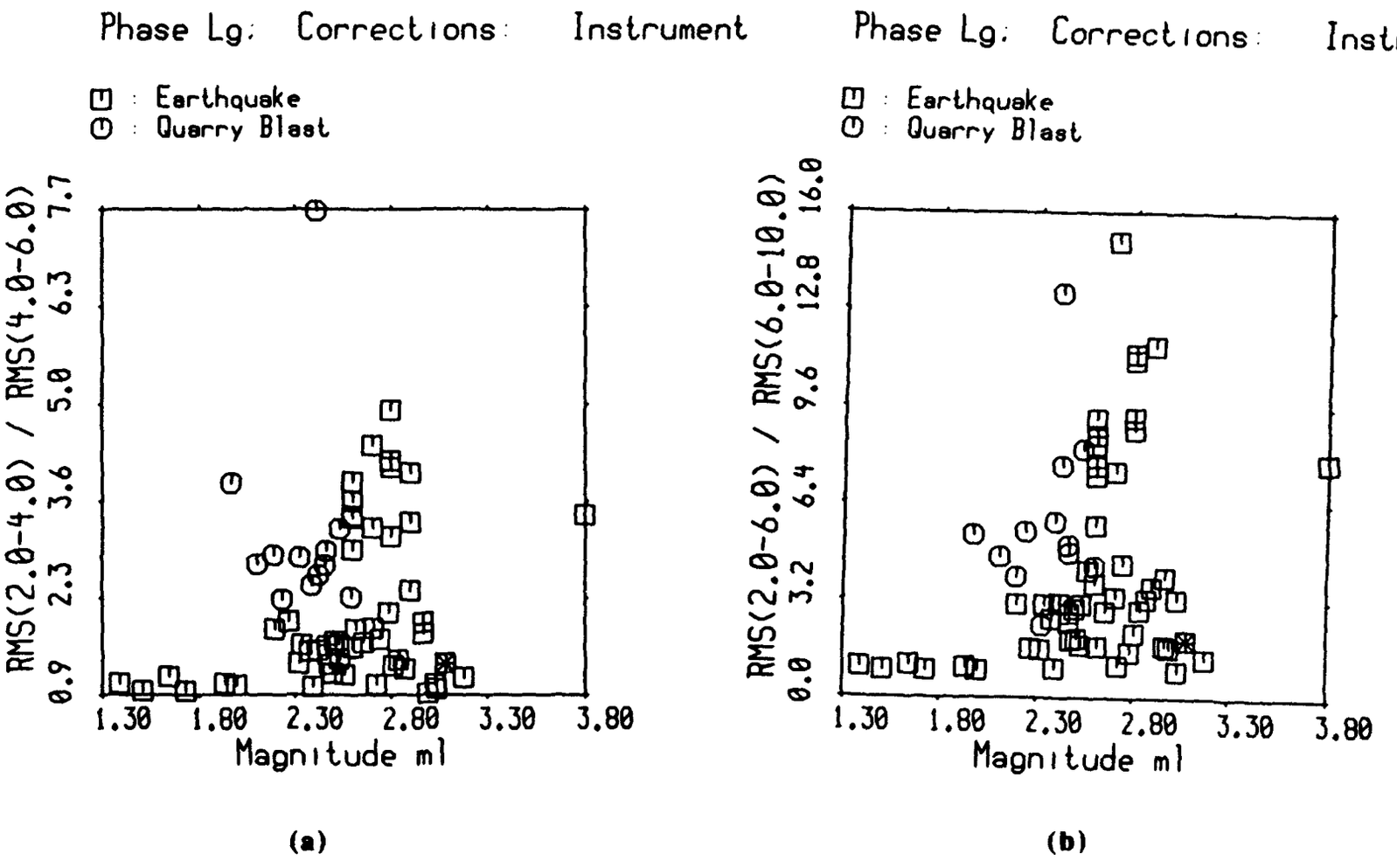

FIGURE 8: Scatterplots of two different spectral ratios for *Lg* against local magnitude: (a) *R1* = ARMS (2-4 Hz)/ARMS (4-6 Hz); (b) *R2* = ARMS (2-6 Hz)/ARMS (6-10 Hz).

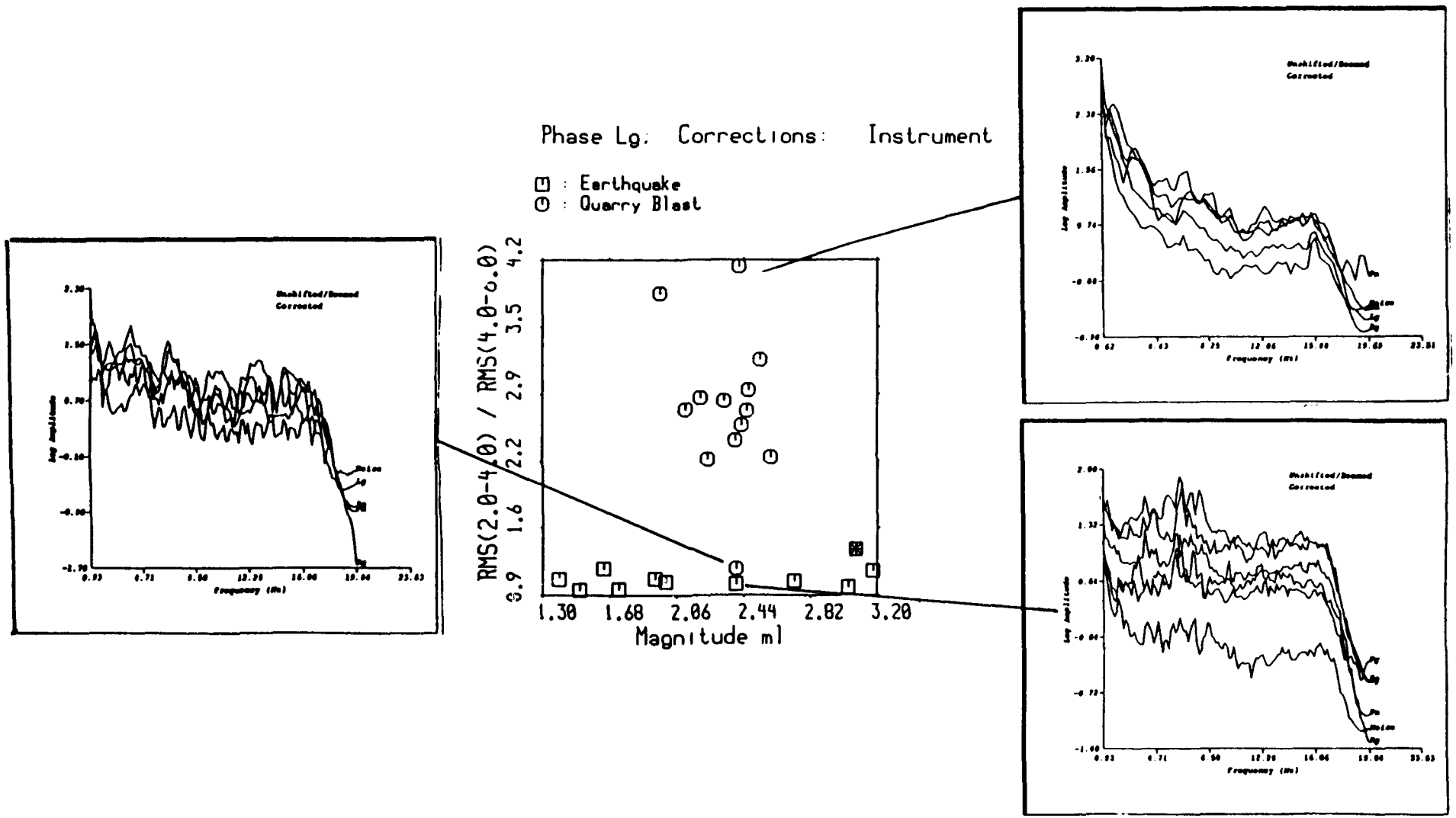

FIGURE 9: Sample spectra which were used to compute *Lg* spectral ratios for the Vogtland explosions and earthquakes.

GERESS is valid for frequencies below about 17 Hz. However, above 17 Hz, there is a very sharp anti-alias filter applied at GERESS which is not present for either NORESS or ARCESS, and it is therefore not removed by the NORESS instrument correction in Figure 9.)

The low spectral ratios of earthquakes are caused by a peak in the spectra of all phases between 5 to 8 Hz, which can be seen on the spectra on the lower right Figure 9. This peak can be seen in all of the earthquake spectra. It usually is missing from the spectra of mine blasts, an example of which is shown in the spectrum on the upper right. The lack of this peak causes the spectra to fall off rapidly from about 1 to 12 Hz for blasts which result in high values of the low-band to high-band spectral ratios, with one exception, which is plotted on the left of Figure 9. This spectrum was produced by a known mine blast which had a spectral ratio value that fell into the earthquake category, as shown in Figure 9. The explanation for the low spectral ratio is that there was strong spectral scalloping which is particularly enhanced at high frequency. However, even for this event, the spectral peak evident in the earthquakes is not present.

The cause of this difference in the earthquake and explosion spectra in the Vogtland region spectra is not clear. We have speculated earlier (Baumgardt et al, 1992) that the spectral peaks in the earthquakes may be caused by some kind of depth effect, in which the earthquakes are deeper which somehow causes the flatter spectra than the shallower explosions. Another possibility is that the low-frequency peak is caused by a low-frequency "corner" caused by effects related to the source mechanism of the Vogtland earthquakes. Whatever causes this peak, we have not observed it for Scandinavian earthquakes. Generally, as we have pointed out repeatedly in past studies (Baumgardt, 1992; Baumgardt et al, 1992), the spectra of Scandinavian earthquakes do not exhibit this effect in general, and the spectral ratio discriminant has not been very effective in separating Scandinavian earthquakes and explosions. Perhaps one of the reasons for this is that blast spectral shapes are strongly distorted by the effects of ripple fire, as in the case of the "anomalous" spectral ratio plotted in Figure 9, which can be very different from one blast to another.

We can also only speculate on the causes of the unusual *Lg* spectral-ratio patterns observed for the Lubin and Upper Silesia events. We have assumed that these events are earthquakes since they are mine tremors and in fact, their *Pn/Lg* amplitude ratios are very earthquake-like. However, some of these events might have been associated with mine blasts or may have actually been induced by blasts (L. Grant, personal reference). So, these events may in fact be some hybrid of source types between earthquake and explosion, which might explain why the spectral ratios span the range of the Vogtland earthquakes and explosions.

Whatever the cause of these spectral-ratio variations, they appear to be source or source-region effects. Figure 7 shows that the wide variance in spectral ratios is observed for events at the same distance, so we cannot appeal to distance-dependent or propagation effects, like anelastic attenuation. Clearly, there is a great deal of variability in the source region, either in the source region structure or in the event mechanisms of the mine tremors themselves, which cause a great deal of variability in the spectral characteristics of the recorded phases at GERESS.

2.6 THE ISEIS DISCRIMINATION EXPERT SYSTEM

In all our previous reports on ISEIS, we have emphasized the visualization and display interfaces and shown research results based on ISEIS feature extraction. Although we have mentioned in past reports that a CLIPS-based expert system has been implemented to make discrimination decisions, based on these features, there has never been a complete description of these rules. In this section, we describe the rules in detail and how they performed on the analysis of the events in the GTD.

2.6.1 Overall ISEIS Event Identification Approach

A schematic of the overall ISEIS approach to discrimination is shown in Figure 10. This figure summarizes the waveform discriminants which we have used to do *model-based reasoning*, in which we try to identify specifically a source type (i.e., explosion, earthquake) based on some kind of model which describes what kinds of signals the source type would generate. For example, we expect that earthquakes, being dislocation sources, should generate stronger shear waves relative to compressional waves than explosions. The regional *P/S* amplitude ratio idea has essentially been based on that idea. The CLIPS rules were then written to try to identify specific event types, based on expectations of the model.

The term *case-based reasoning* refers to the process of comparing events against previous "reference events," which may or may not be known to be of a certain source type. The goal is to then say whether the event looks like the features of the reference events, or looks like the event itself. In ISEIS, a number of tools have been implemented to accomplish case-based reasoning, which include the following:

(1) Interactive displays which allow the comparison of a "current event's" features with those of reference events, which the user can select from specific reference regions to which the events have been assigned. The plots we have shown earlier generally are screen dumps of these interactive displays.

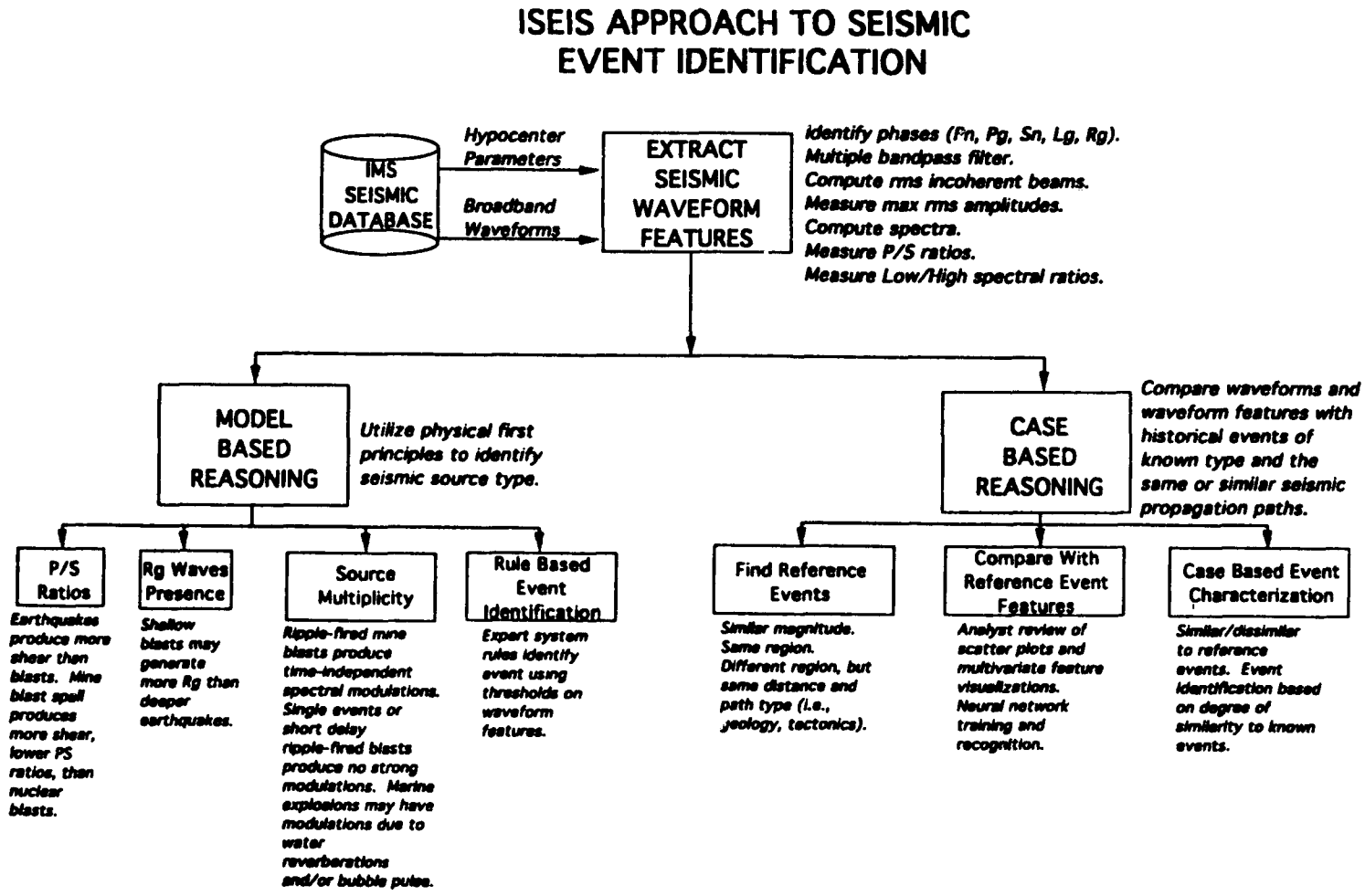

FIGURE 10: Schematic diagram shown the ISEIS approach to discrimination.

(2) Waveform and envelope comparisons, where the user can overlay waveforms or compare incoherent beams, based on a method called *Dynamic Time Warping (DTW)*, which has been described in detail in previous reports.

(3) Multichannel coherence analysis of reference events compared to the current event, using methods described by Der et al (1990; 1991; 1992), and Harris (1991). Interfaces have been implemented to set up this analysis and to display the results.

(4) A neural network interface has been implemented, using the neural network simulator approach described by Der and Baumgardt (1992), in which the neural network weights are "trained" by a least-squares error minimization algorithm to recognized event types which are similar to those with which the neural network has been trained. Currently, the ISEIS neural network has only been designed to recognize events based on the different varieties of regional *P/S* ratios, like those we have discussed above. We categorize neural network recognition as a kind of *case-based reasoning* because neural networks only recognize patterns in features like the "cases" with which they have been trained.

Up to now, the CLIPS rule-based processing has mainly been applied to *model-based reasoning*, with the exception of *DTW*, for which there are CLIPS rules which identify events as *similar* or *dissimilar*.

2.6.2 ISEIS Model-Based Discriminants

In this section, we describe in detail the model-based discriminants which have been implemented in ISEIS. These were initially developed to identify earthquakes and mine blasts in southern Norway (Baumgardt and Young, 1990) and to demonstrate the concept of using an expert system for seismic discrimination. By no means should these discriminants be considered optimal or definitive. We expect to make major modifications to these discriminants, including the addition of many new discriminants, in the future as more data is analyzed.

We also point out that the ISEIS expert system also includes numerous rules for characterizing "data status," as explained in the ISEIS documentation (Baumgardt et al, 1991). These rules determine whether or not sufficient data has been processed in order to apply a particular discriminant. Although these rules can be as extensive and complex as the discriminant rules themselves, we will not describe them here.

The primary discriminants used by ISEIS for identification are the following:

(i) Max *P*/Max *S*.
(ii) High-Frequency *Pn*/*Sn* Amplitude Ratio.
(iii) High-Frequency *Pn*/*Lg* Amplitude Ratio.
(iv) *Sn* Spectral Ratio (2-4Hz/4-6Hz).
(v) *Lg* Spectral Ratio (2-4Hz/4-6Hz).
(vi) Time Independent Spectral Modulation (indication of ripple fire).
(vii) Combined Discrimination.

Other discriminants have also been implemented which utilize *Ms*/*mb*, for teleseismic events, and depth of focus. However, since the IMS does not measure *Ms* or *mb*, nor does it estimate depth of focus, these discriminants will not be described here.

(i) Max P/Max S Amplitude Ratios

The RMS amplitudes of all regional *P* (*Pn, Pg*) and *S* (*Sn, Lg*) phases are measured off the incoherent beams in 8 filter bands, in frequency bands above 2.0 Hz, which are stored in the Oracle database. These amplitudes are accessed from the database, and the maximum of all the regional *P* and regional *S* phases are determined and ratioed. Then, the following rules are applied:

- If *Max P/Max S* < 0.5 at least 1 station => high-confidence earthquake (conf = 0.9).
- If *Max P/Max S* > 0.5 but < 0.7 at 1 station => low-confidence earthquakes (conf = 0.75).
- If *Max P/Max S* > 0.7 but <1.0 at 2 stations => earthquake characteristics (conf = 0.75).
- If *Max P/Max S* > 1.0 but < 1.4 at 2 or more stations => possible explosion (conf = 0.75).
- *Max P/Max S* > 2.0 at least 1 station => possible explosion (conf = 0.75).

Each of these criteria are applied on a station-by-station basis. Each station then votes on the identity of the event, based on the threshold settings.

Note that no corrections are made for distance-dependent attenuation in order to account for different attenuation of the *P* and *S* wave, nor is this discriminant limited to any distance range. Therefore, it is possible to have an event big enough to be recorded at a close-in station, with small *P/S* ratio, and a more distant station with larger ratio. This might be regarded as deficiency.

However, if there is any conflict in the way two or more stations vote, i.e., one station votes earthquake and another votes explosion, the earthquake conclusion will always dominate. This feature has been effective in ensuring that events are not identified as explosion simply because distant stations saw large *P/S* ratios.

(ii) High-Frequency Pn/Sn Amplitude Ratios

RMS amplitudes of *Pn* and *Sn* phases are measured off the incoherent beam in the 8 to 10 Hz band and the maximum RMS amplitudes are ratioed. Then, exactly the same rules as in the case of the *Max P/Max S* are applied to the *Pn/Sn* amplitude ratios.

(iii) High-Frequency Pn/Lg Amplitude Ratios

RMS amplitudes of *Pn* and *Lg* phases are measured off the incoherent beams in the 8 to 10 Hz band and the maximum RMS amplitudes are ratioed. Then, exactly the same rules as in the case of *Max P/Max S* are applied to the *Pn/Lg* amplitude ratios.

(iv) Sn Spectral Ratio

The spectral ratio $R1 = A_{RMS}\ (2\text{-}4\ Hz)/A_{RMS}\ (4\text{-}8\ Hz)$, computed from the spectra of an *Sn* phase which has been corrected for the instrument response, is read in from the database. (Note: Other spectral ratios are available in the database and these rules can easily be modified to utilize these ratios, if desired.) Then, the following rules are applied:

If $R1 > 2.0$, then the event has explosion characteristics.

If $R1 < 2.0$, then the event has earthquake characteristics.

The final identification of the event is based on the calculation of a confidence factor, CF, as follows:

If the event has explosion characteristics, then

$$CF = (CFMAX - 0.5)\ \{\ (R1 - 2.0\ )/(MAXRATIO - 4.0)\} + 0.5$$

where

$$CFMAX = 0.75 \text{ and } MAXRATIO = 3.0.$$

If the event has earthquake characteristics, then

$$CF = (CFMIN - 0.5)\ \{(2.0 - R1)/(2.0 - MINRATIO)\} + 0.5$$

where

$$CFMIN = 0.95 \text{ and } MINRATIO = 1.0.$$

If $R1$ > MAXRATIO, then CF is set to CFMAX, and if $R1$ < MINRATIO, then CF is set to CFMIN.

The final identification is based on the value of the CF. If the event has explosion characteristics (i.e., $R1$ is greater than 2.0) and CF >= CFTHRESHEX, where CFTHRESHEX is the confidence threshold for explosion, the event is identified as an explosion with confidence CF. Alternatively, if the event has earthquake characteristics and CF >= CFTHRESHEQ, where CFTHRESHEQ is the confidence threshold for earthquake, the event is identified as an earthquake with confidence CF. However, if in either case, CF < CFTHRESHEX or CF < CFTHRESHEQ, then the event is classified as unidentified with confidence 0.5. The values of CFTHRESHEQ and CFTHRESHEX can be varied, but are currently set to 0.5.

(v) Lg Spectral Ratio

This discriminant is applied in exactly the same way as the one for *Sn* spectral ratio.

(Note: For both *Sn* and *Lg* spectral ratios, the confidence calculation has been set up to be relatively conservative in identifying explosions because of the great amount of scatter we have observed for blast spectral ratios. Because of this uncertainty, we have set the maximum possible confidence for explosion to be only 0.75, and a very large ratio (4.0) is required to attain this value. The maximum confidence for earthquake, on the other hand, can be as high as 0.95. Note also that these maximum confidence levels and the other threshold settings for the value of the ratios and for the confidence levels are all variables in the rules which can be adjusted and perhaps varied for different regions.)

(vi) Time Independent Spectral Modulations (Ripple Fire)

This discriminant uses a cepstral-analysis method, suggested by Baumgardt and Ziegler (1988), to find significant cepstral peaks which are indicative of time-independent spectral scalloping caused by ripple-firing. A process called Multiple Event Recognition System (MERSY) computes cepstra for multiple phases and finds peaks which occur in two or more sets of cepstra. This is done on a station-by-station basis. If two or more peaks are found, the station votes for EX, which means ripple-fired blast. The total number of votes for ripple-fired explosion, NUMEX, is then counted. Then, a confidence factor for ripple fire, CF, is computed as follows:

$$CF = \{NUMEX/ MAXNUM\} (0.5) + 0.5.$$

Now, if CF >= CFMIN, the event is identified as an explosion (specifically, ripple-fired mine blast) with confidence of CF. If CF < CFMIN, then the event is unknown. Currently, NUMEX = 2 and CFMIN = 0.6. Therefore, only one station needs to find consistent cepstral peaks in order to identify the event as a ripple-fired mine blast.

Note that lack of spectral modulations does not identify the event as an earthquake. It could also be a single explosion. So, this discriminant only identifies mine blasts, not earthquakes.

(vii) Combined Discrimination

A voting scheme is used to obtain the final event identification and a weighted average gives the final confidence of the identification, as follows:

NVeq => number of votes for earthquake

NVex => number of votes for explosion

Initially, NVeq = NVex = 0

If a discriminant, say *Di*, votes for earthquake, then NVeq = NVeq + 1. Similarly, if the vote is for explosion, then NVex = NVex + 1. Now, let Diex be all the confidences of discriminants that voted for explosion, Dieq be all those which voted for earthquake, and Diun be those which voted for unknown. The overall confidence value for explosion is

$$CFex = [\text{Sum (over } i) \{wi * Diex\}]/NVex,$$

where *wi* is the relative weight assigned to the discriminant *i*. Correspondingly for earthquake, we have,

$$CFeq = [\text{Sum (over } i) \{wi*Dieq\}]/NVeq.$$

For unknown, we have

$$CFun = [\text{Sum (over } i) \{wi* Diun\}]/NVun.$$

The final overall identification then is made as follows:

If CFeq > CFex and CFeq > CFun, then the event is earthquake with confidence CFeq.
If CFex > CFeq and CFex > CFun, then the event is explosion with confidence CFex.
If CFun > CFex and CFun > CFeq, then the event is unknown with confidence 0.5.

If the event is identified as an explosion and the ripple-fire discriminant says there is ripple fire, then the event is identified as a mine explosion.

Relative weights, *wi*, are computed from absolute weights, *Wi*, which are assigned to all discriminants as follows:

$$wi = Wi \,/\, \text{Sum (over } i\text{) } \{Wi\},$$

where the sum over *i* is for all discriminants which are applied to a particular event. Currently, the weights are set such that if all six discriminants contribute to the overall discrimination, the *MaxP/Max*, *Pn/Sn*, and *Pn/Lg* amplitude ratios have relative weights of 0.2 each, *Sn* and *Lg* spectral ratios are 0.1, and the ripple-fire discriminant is weighted 0.3. Note that the highest weight is assigned to the ripple-fire discriminant, since it is believed to be very diagnostic of mine blasting if ripple fire is present and should be the dominant discriminant. The spectral ratio discriminants are assigned the lowest weight because we are uncertain if this discriminant is very effective. (Note that the weights are all variables that can be changed if desired.)

These, then, are the ISEIS discriminants as they are currently implemented in the expert system. As we have noted, all the threshold and weight settings are variables which can be changed. Also, facilities are available in ISEIS to deactivate or activate discriminants, if desired for a particular set of events. For example, if we are identifying events in a region where we know there is no *Sn* propagation (such as, for example, the western United States), then the *Pn/Sn* and *Sn* spectral ratio discriminants can be "deactivated" and therefore, not used in discrimination.

Moreover, ISEIS is modular enough to allow the easy addition of new discriminants. A useful function available for this purpose is the "clone" function, which allows a discriminant to be copied. For example, our recent analysis has suggested that the presence of an *Rg* wave might serve as a useful discriminant since it indicates the event might be at a shallow depth. It would be easy to add a discriminant for *Rg* which would be based on an amplitude ratio, like the *Pn/Rg* or *Lg/Rg* ratio, by simply cloning the rules from one of the other amplitude-ratio discriminants and editing the variables. We may, in fact, add an *Rg* discriminant in the future, although we have so

far held off because of uncertainties about how to apply it because we have observed *Rg* waves from mine tremors.

2.6.3 Evaluation of ISEIS Discriminants on the GTD

The discrimination approach described above has been applied to all the events in the GTD for which we have been able to successfully process the data. These include the events, plotted in Figure 2, which were in the Steigen, Vogtland, Lubin, and Upper Silesia regions. We have so far processed a total of about 107 events in these four regions.

To show how the discriminants perform, we counted how many event identifications of any kind were made by each of the discriminants, individually and overall. These counts were made individually for each of the four regions. The results are plotted in the form of barplots, where a barplot of a particular design is assigned to each discriminant. The identification counts were made for one of three source types, "explosion," "earthquake," or "unknown." The counts for "mine blasts" (i.e., ripple-fired blasts) and "generic explosion" (i.e., non-ripple-fired blasts) were combined under the source type "explosion." The width of the bar assigned to each source type is determined by the number of events which are identified as that type.

Figure 11 shows how ISEIS identified all the events in the Vogtland region which are known to be mine blasts. Each of the discriminants are represented in the barplots as a set of parallel lines plotted at different angles and densities as shown in the legend. Note that the overall identifications are the bars with the dense parallel lines going from lower left to upper right at about a 45 degree angle and are always plotted as the top bar. If this bar is missing for a source type, it means there were no overall votes for that source type. Figure 11 shows that ISEIS identified all the events as either "explosion" or "unknown." Although there were some discriminants for "earthquake," mostly the *MaxP/MaxS* amplitude ratio discriminants, there were no overall votes for "earthquake." Note that the very thin bar at the top for "earthquake" is the one vote from the *Lg* spectral ratio, which came from the "anomalous *Lg* spectral ratio" event recorded at GERESS that we discussed above.

Many of the unidentified identifications resulted from the fact that the ripple-fire discriminant failed to identify the events. (Recall that if ripple fire is not found, the discriminant always votes "unknown.") In our earlier study of these events (Baumgardt et al, 1992), we noted our failure to see ripple-fire effects in the GERESS data for mine blasts. Wuster (1993), on the other hand, identified most of these events as ripple-fired using a sonogram method. However, he had access to broader-band data, which was sampled at about 120 Hz. We only had access to data sampled at 40 Hz. Thus, our Nyquist bandwidth was limited to 20 Hz, or actually 16 Hz, because

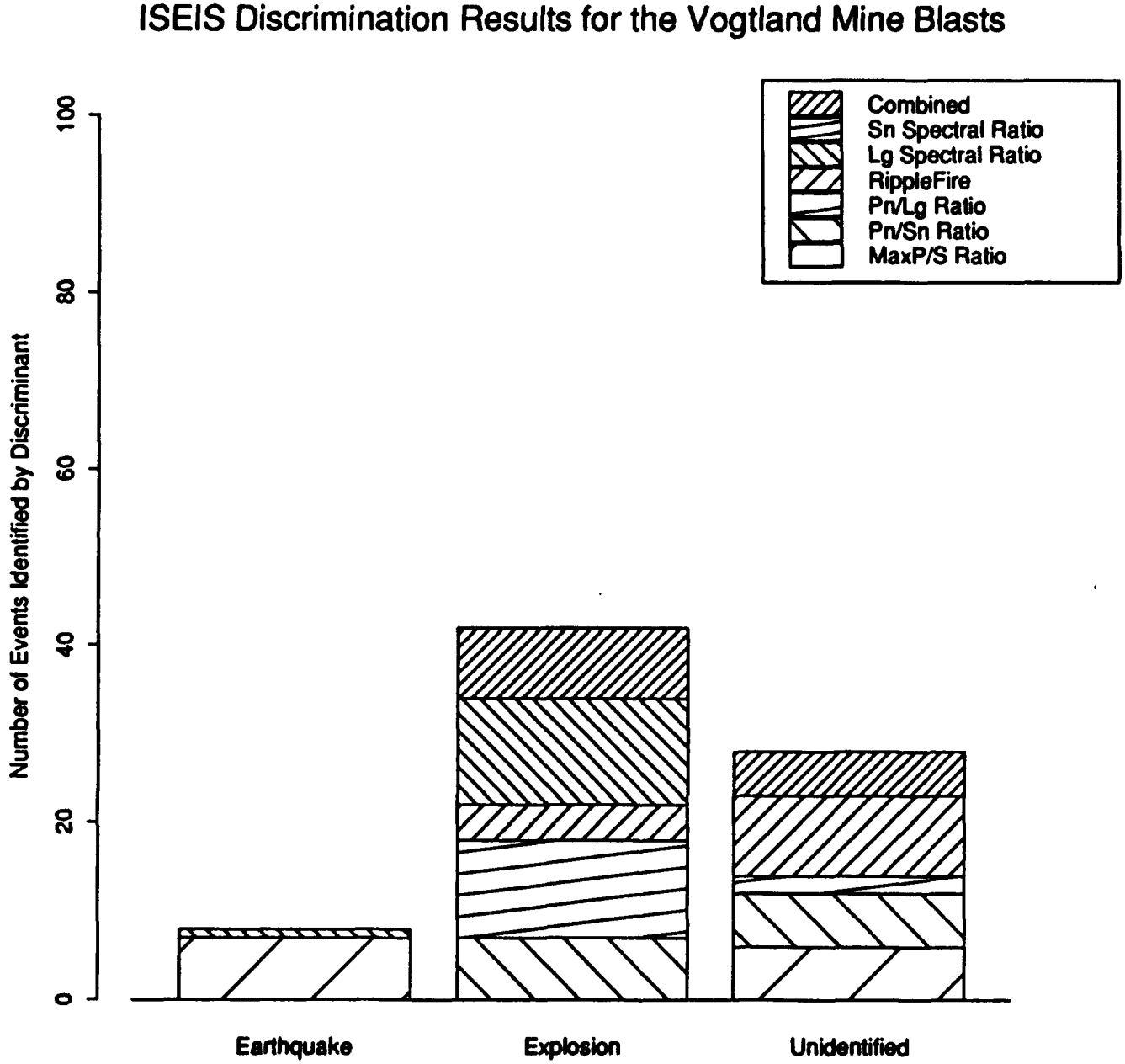

FIGURE 11: Barplots of the discrimination results for the Vogtland mine blasts.

of the sharp anti-aliasing filter, whereas Wuster (1993) had a bandwidth of up to 60 Hz. Evidently, many of the Vogtland mine blasts had short delay ripple fire (< 0.050 seconds) which requires the broader-band data to resolve the higher-frequency spectral nulls. At least three other discriminants must vote for explosion in order to overcome the "unidentified" vote of the ripple-fire discriminant because of its high weight. This explains why so many of the Vogtland events came out "unidentified "

Baumgardt et al (1992) and Wuster (1993) both pointed out that most of the Vogtland blasts had well observed *Rg* waves. If we had included an *Rg* discriminant, we would have identified most of the events which were unidentified in Figure 11.

Figure 12 shows the results for the Vogtland earthquakes, all of which were identified by ISEIS as "earthquake." The ripple-fire discriminant voted for one event to be "explosion," which appears to be an error. (We have had some problems with spurious cepstral peaks caused by the sharp cutoff anti-alias filter at GERESS.) Most of the votes for "earthquake" came from the amplitude-ratio and *Lg* spectral ratio discriminant, which we showed in the previous section were very strong discriminants.

The results for the Lubin region are shown in Figure 13. Because we believe most of these events are mine tremors, we expect that most of these events should be classified as "earthquake," and in fact, Figure 13 shows that most of the events, about 16, were classified as "earthquake." However, six of the events were also classified as "explosion," based mainly on the ripple-fire discriminant, and seven were unidentified. The *Pn/Lg* and *Lg* spectral ratio were the strongest contributors to the "earthquake" classifications.

Figure 14 shows the results for the Upper Silesia region, another region believed to mainly have mine tremors. However, as shown in Figure 14, the predominant identifications were "explosion" and "unidentified." The strongest discriminants for "earthquake" were *Pn/Lg* and *MaxP/MaxS* amplitude ratios and the strongest discriminants for "explosion" were ripple fire and *Lg* spectral ratio. Figure 14 reveals a great deal of uncertainty about these events. This may be due to the fact that they may be a combination of mine tremor and explosion, which results in a large number of "unidentified" classifications.

Finally, Figure 15 shows the results for the Steigen-swarm events located in northern Norway. Note that these events were classified primarily by data from the ARCESS and NORESS arrays. All these events are known to be earthquakes, and ISEIS was very successful in identifying these events. Only 1 of the 24 events processed was "unidentified" and none of the

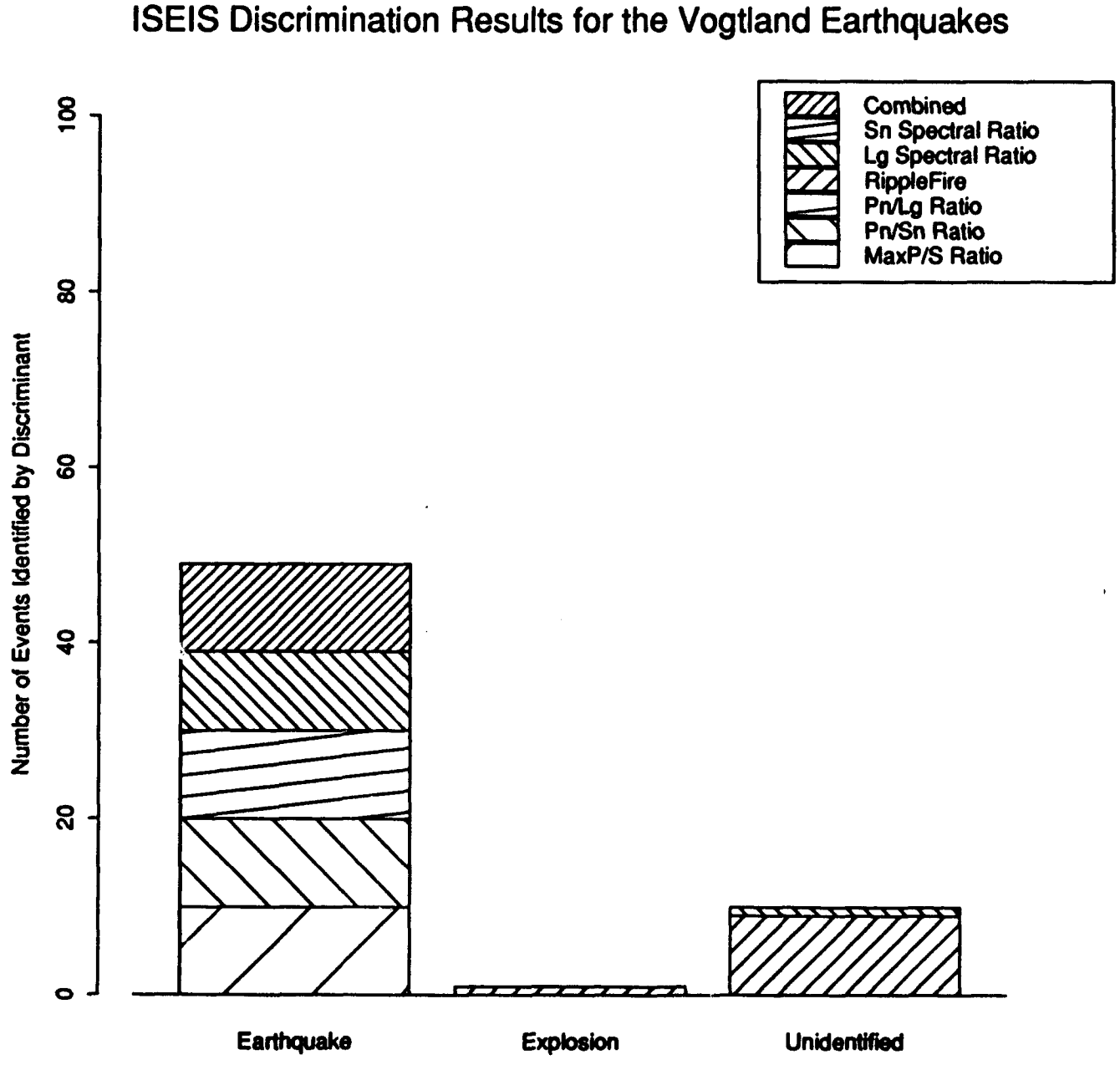

FIGURE 12: Barplots of the discrimination results for the Vogtland earthquakes.

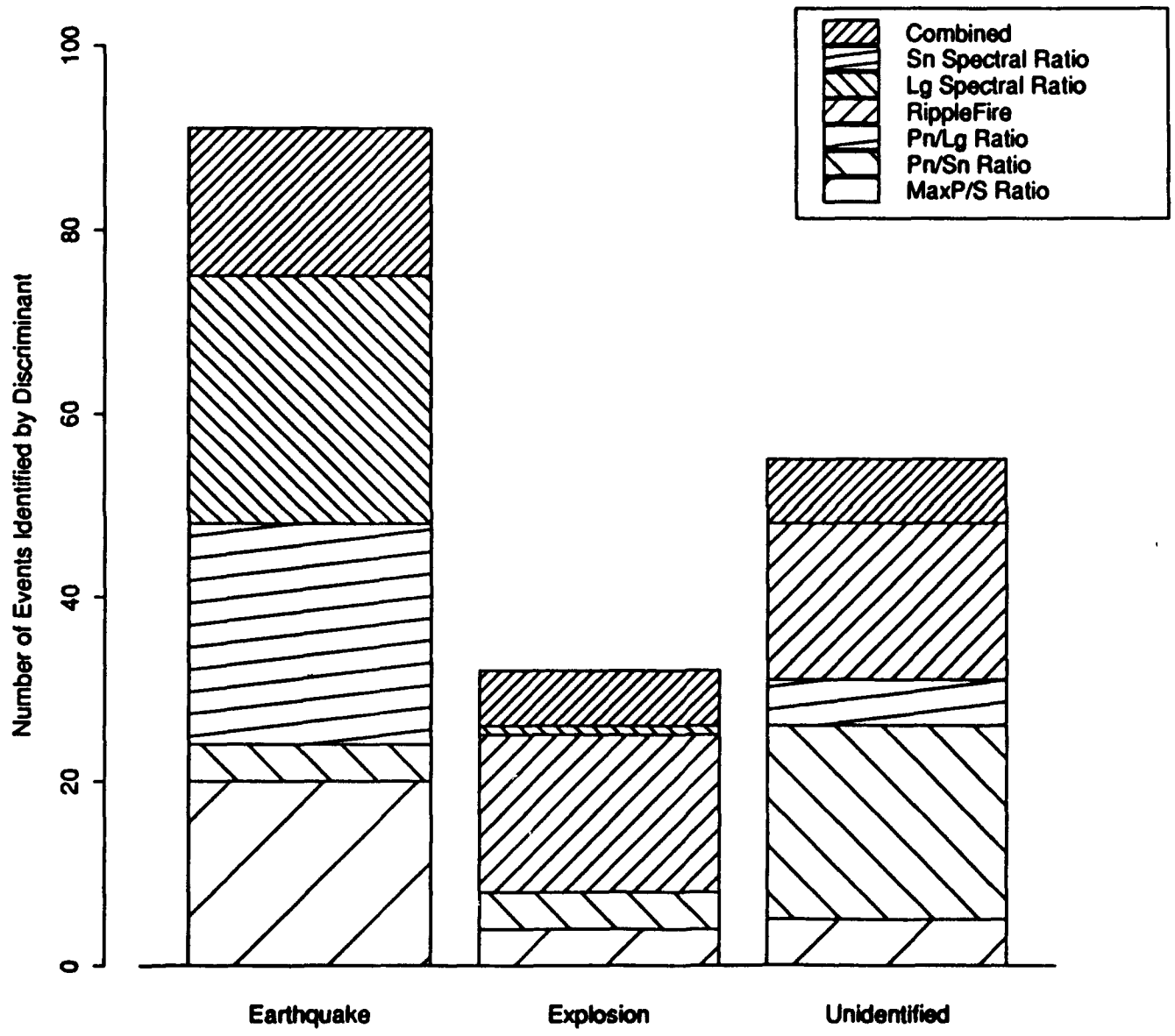

FIGURE 13: Barplots of the discrimination results for the Lubin mine tremors.

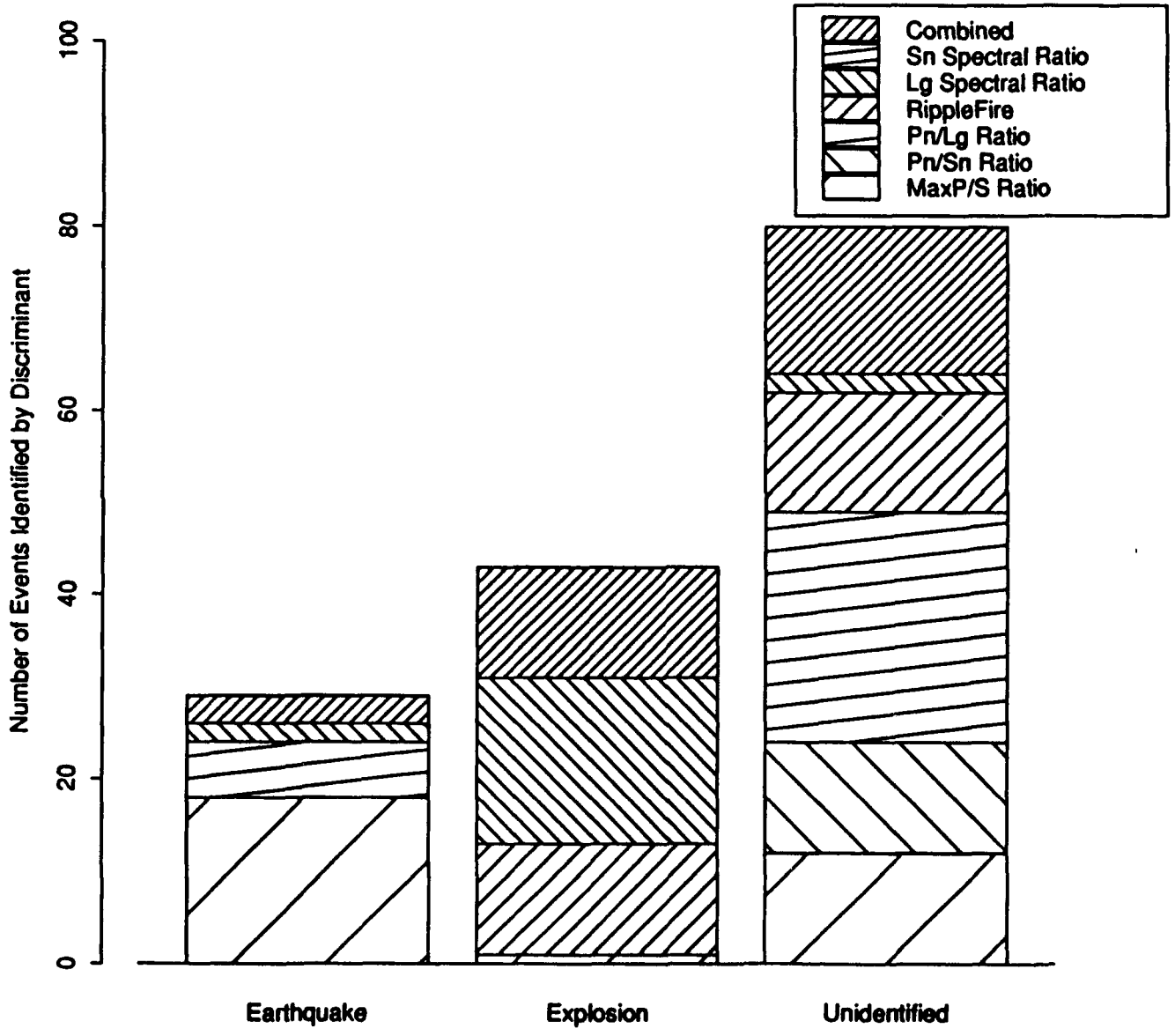

FIGURE 14: Barplots of the discrimination results for the Upper Silesia mine tremors.

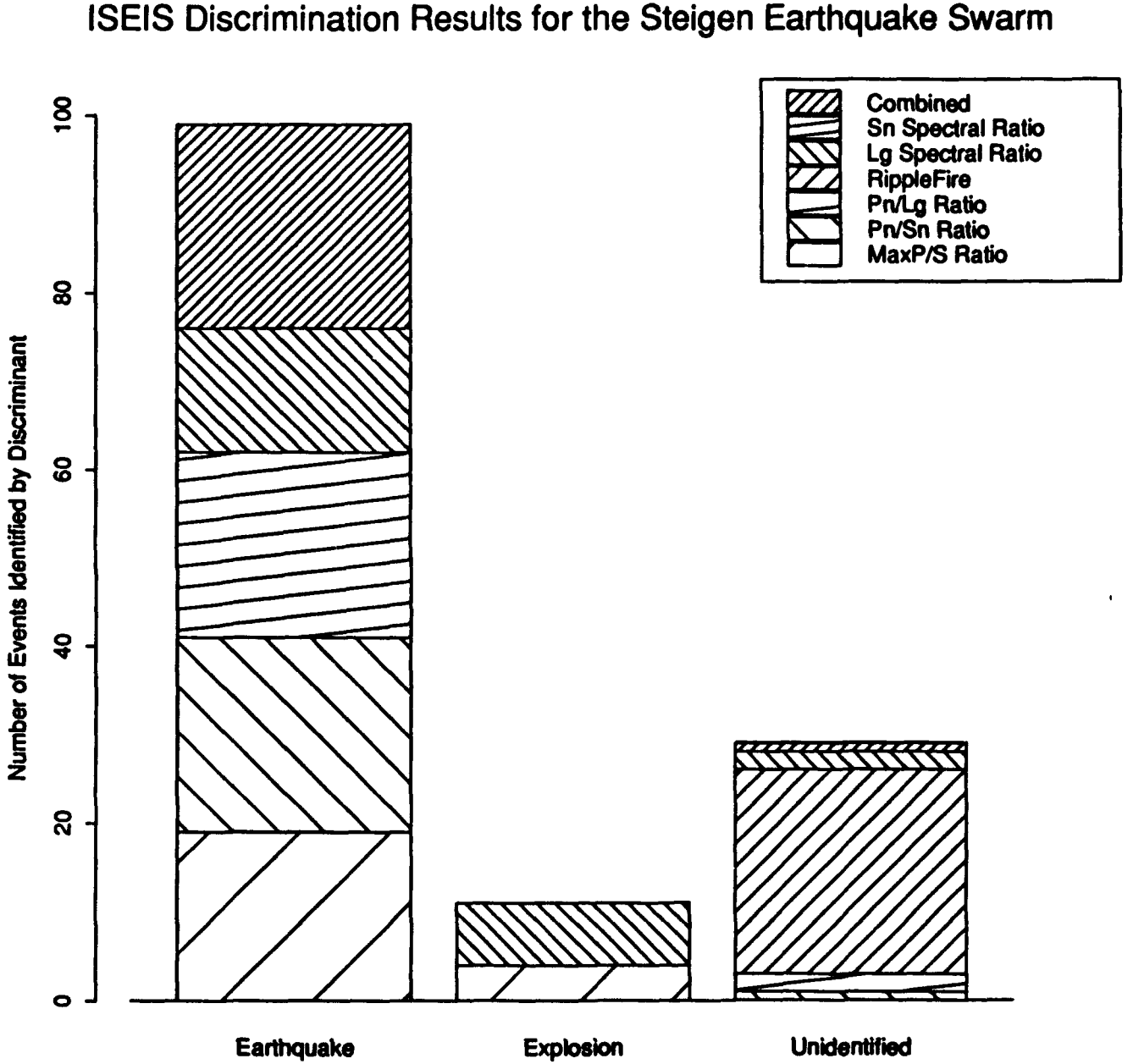

FIGURE 15: Barplots of the discrimination results for the Steigen earthquakes.

events were classified as "explosion." The best discriminants were the combination of *Pn/Sn*, *Pn/Lg*, and *MaxP/Max* ratios which drove the overall classification for earthquake. The only explosion votes came from *MaxP/MaxS* and the unreliable *Lg* spectral ratio. Note that these "earthquake" classifications overcame the strong vote for "unidentified" coming from the ripple-fire discriminant, which found no evidence that any of the Steigen earthquakes were multiple events.

2.7 SUMMARY AND CONCLUSIONS

This section has completed the analysis of the GTD begun by Baumgardt et al (1992). This has included the additional analysis of presumed mine tremors in Poland, and an assessment of the discriminant rules in ISEIS. As a result of this overall study, we make the following conclusions:

(1) The regional *P/S* ratio discriminant seems to be a very good discriminant at high frequency. Mine tremors seem to resemble earthquakes in that they have small *P/S* ratios. Even for events which may be combined mine blast and tremor, we have observed earthquake-like *P/S* ratios.

(2) The *Lg* spectral ratio has given somewhat enigmatic results. It seems to effectively separate the explosion and earthquake populations at Vogtland in the way observed by Bennett and Murphy (1986) for nuclear explosions and earthquakes; i.e., the earthquakes seem to have higher frequencies than the explosions. Our analysis of the spectra have shown that the reason that this discriminant works at Vogtland is that Vogtland earthquakes have a strong spectral peak at about 4 Hz, which seems to be missing in the explosions, and hence, earthquakes have much flatter spectra than the explosions. We have suggested possible source effects, including depth of focus differences and source-mechanism differences, as the cause of the success of this discriminant. However, we have found greater scatter in these spectral ratios for the Lubin and Upper Silesia events. Moreover, our studies in other regions of Scandinavia have shown that this discriminant is not as effective in shield regions in separating earthquakes and explosions.

(3) Our analysis of the performance of the ISEIS discrimination rules have shown them to be surprisingly successful. As expected, the *P/S* ratio discriminants work best to classify earthquakes whereas ripple-fire works best to classify explosions. Also, at Vogtland, *Lg* spectral ratio helps to classify many of the events. We have a large number of "unidentified" events, many of which could later be identified by an analyst using the ISEIS interactive graphics visualization tools. Moreover, the addition of an *Rg* discriminant would eliminate many of the unidentified blasts, although care must be used for very shallow mine tremors and also earthquakes.

(4) The Lubin and Upper Silesia events need more analysis. We have found that these events tend to look earthquake-like, which we might expect for such events, but we have also observed some explosion-like characters as well. For many mines in Scandinavia, we have frequently observed large scatter in the *P/S* ratios which may be due to induced spall. However, many of these events may actually not be pure blasts, but rather some combination of blast and induced tremor. This has significance for conceiving possible evasion scenarios, because it appears to be possible to generate earthquake-like sources in mines. Thus, it might be possible to detonate a nuclear explosion in a mine, perhaps with some combination of conventional blasts, in such a way as to produce ' ~ ong shear waves at the observing stations which might be identified as mine tremor or earthquake.

3.0 SEISMIC WAVEFORM FEATURE ANALYSIS AND DISCRIMINATION OF THE DECEMBER 31, 1992 NOVAYA ZEMLYA EVENT

3.1 INTRODUCTION

On December 31, 1992 (hereafter 921231), a seismic event of unknown identity occurred at Novaya Zemlya near Matochkin Shar, the primary Russian nuclear test site. Natural seismicity has occurred in this region, although it is very rare (W. Leith, personal reference). Thus, proximity to this known test site does not automatically identify the event as an explosion. The objective of the study described in this paper was to characterize the high-frequency waveform signals detected at the Scandinavian regional arrays for this event, to compare them with historical events of known identity, and thereby to determine whether the event was a nuclear explosion, a chemical explosion, or an earthquake.

The 921231 event produced seismic signals at two regional arrays in Scandinavia, NORESS and ARCESS, a sensor called Apatity on the Kola Peninsula, and a newly installed array at Spitzbergen. The signals detected by these sensors were processed by the Intelligent Monitoring System (IMS) (Bache et al, 1991), which located the event and determined its local magnitude to be 2.2. The analysis described in this report utilized waveform edits produced by the IMS for the event as recorded at the regional arrays.

The approach in this study was to analyze the waveforms in the IMS database at the Center for Seismic Studies (CSS), utilizing a new research discrimination prototype, called the Intelligent Seismic Event Reference System (ISEIS), described by Baumgardt (1991a), and Baumgardt et al (1992). In brief, the processing steps include: (1) incoherent beam computation in nine primary filter bands, ranging from 0.5-2.5 Hz (for possible Rg phases analysis) to 8-16 Hz; (2) phase selection for key phases and amplitude computation (maximum and average) within preset windows keyed-on IMS phase identifications; (3) regional *P/S* amplitude-ratio computation (same frequency) for selected regional phases; (4) array-stacked spectral density computation in the phase-selection windows; (5) spectral ratio computation for all phases; (6) cepstrum calculation for ripple-fire detection and depth estimation; (7) storage of all key features to an Oracle database; (8) rule-based processing, using rules coded in the NASA expert systems shell, CLIPS, to identify events on the basis of individual discriminants extracted from the database; and (9) overall event identification using a voting scheme.

ISEIS has been designed to accept as input events formed by the IMS, including all associated phase identifications and waveforms, and to make a number of time and frequency domain

measurements on the regional seismograms. Interactive graphics interfaces facilitate the comparison of waveform features with the same features measured at the same sensors for historical events which were processed earlier through IMS and ISEIS. In this study, we used ISEIS to compute and compare waveform features from the 921231 Novaya Zemlya event to those of historical events to determine what kind of source (i.e., chemical blast, nuclear explosion, or earthquake) the event most resembles.

Ideally, the historical events should be the same type as those of interest (i.e., chemical explosions, earthquakes, nuclear explosions) and in the same geographic region as the event we are characterizing in order to factor out effects on the waveforms caused by propagation path differences. However, in the present case, we do not have this ideal arrangement because seismicity is rare, except for nuclear explosions, in the Novaya Zemlya region, and so we must compare the event with historical events in other regions near Novaya Zemlya. However, we try to find historical events whose paths to the sensors are as similar as possible as those for the Novaya Zemlya event. At the least, we try to examine events in the same magnitude range (2.0 to 3.0) as the Novaya Zemlya event and which are at comparable distance as the Novaya Zemlya event is from the regional arrays. However, even for paths of similar distance, the differences in crustal structure along different paths need to be considered when comparing regional waveform signatures.

In this section, we first discuss the characteristics of the waveforms of this event and other earthquakes, chemical blasts, and nuclear explosions recorded at the ARCESS and Spitzbergen arrays. After a review of the processing methods, we discuss the discrimination results for the ARCESS array. At NORESS, the signals were very weak and only a *P* wave was detected. However, we present an analysis of a larger event which occurred in 1986, identified as a possible earthquake (Ryall et al, 1987), and which had strong *Pn* and *Sn* signals recorded at the NORESS array. Although this event occurred before the ARCESS array was installed and cannot be directly compared to the 921231 event, it nevertheless has certain similarities to the 921231 event, which has important ramifications about the identification of both events.

3.2 DISCRIMINATION ANALYSIS OF THE 921231 EVENT AT ARCESS AND SPITZENBERG

ARCESS Waveforms

Figure 16 shows a map of the locations of the ARCESS arrays relative to Novaya Zemlya. Also shown on the map are the locations of the reference events that were recorded at ARCESS and the great-circle propagation paths. These events consist of previous nuclear explosions at Novaya Zemlya, mine explosions on the Kola Peninsula, earthquakes from a swarm in northern

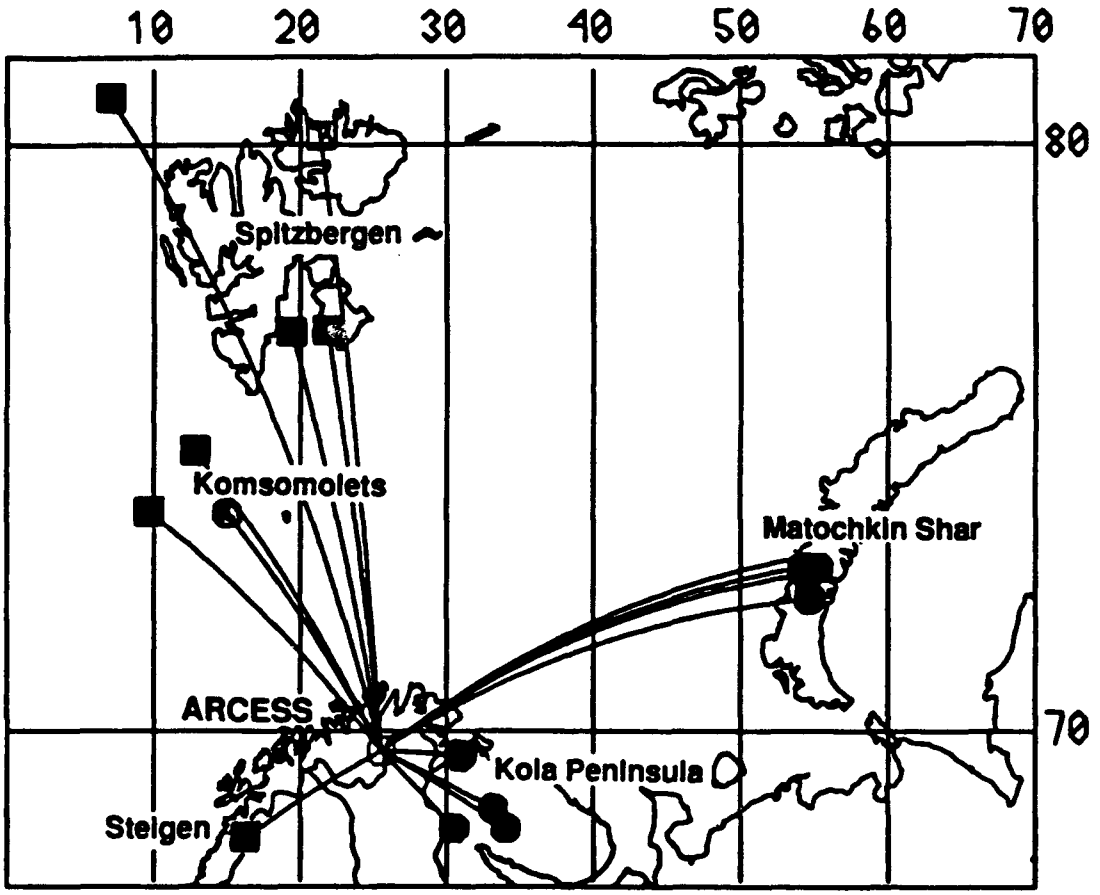

FIGURE 16: Map showing the locations of the ARCESS and Spitzbergen arrays and the reference events recorded at ARCESS used to characterize the 921231 event. The great circle paths between the 921231 event from the reference events to ARCESS are shown. Square and circle symbols indicate earthquake and explosion locations, respectively.

Norway in the Steigen region, the presumed Komsomolets submarine-implosion off the northern coast of Norway (Baumgardt, 1991b), and earthquakes in the Spitzbergen-Greenland Sea regions. Note that the nuclear explosions, mine blasts, and earthquakes all occurred in different regions and the paths from the different events to ARCESS are all different. The distances from ARCESS range from 200 to 300 km for the Kola events, 400 to 500 km for the Steigen earthquakes, and 900 to 1100 km for the Greenland Sea earthquakes and the Novaya Zemlya events. The Spitzbergen-Greenland Sea earthquakes occurred well east of the Mohns-Ridge mid-oceanic spreading center so that the seismic propagation paths to ARCESS should be similar to those from Novaya Zemlya to ARCESS.

The 921231 Novaya Zemlya event wrote excellent waveforms at ARCESS, although it was necessary to apply bandpass filters to reject the high noise levels. Figures 17, 18, and 19 compare the waveforms recorded on the ARB1sz channel of ARCESS for the 921231 event with selected historical events recorded on the same channel. In each plot, the waveforms have been bandpass-filtered with a recursive Butterworth filter in the 8 to 10 Hz band. (As we shall discuss later, this frequency band was the best for discrimination of the different source types in this region.) Strong signal-to-noise ratios were observed in all bands above 2 Hz, with the highest frequencies near 10 Hz for all events. Two large arrivals were identified as the *Pn* and *Sn* regional phases.

Figure 17 shows a comparison of three Kola Peninsula mine blasts with the 921231 event. The Kola blasts occurred much closer to the ARCESS array than the Novaya Zemlya event, as evidenced by the shorter time delay between *Pn* and *Sn* for these events. However, the presumed mine blasts have nearly the same amount of *Pn* and *Sn* energy in this 8 to 10 Hz band as is also observed for the 921231 event.

Figure 18 compares the three known Novaya Zemlya nuclear explosion tests, which have occurred since ARCESS was installed, with the 921231 event. Although both *Pn* and *Sn* phases are observed at ARCESS for these events, no direct *Lg* waves are observed. Presumably, *Lg* is blocked in its propagation across the Barents Sea from Novaya Zemlya to ARCESS, as discussed by Baumgardt (1991c). (Note: The energy in the coda of the *Sn* observed on the 921231 trace is probably an interfering local event.) This comparison shows that the *Sn* waves are not as strong relative to *Pn* for the nuclear explosions in the 8 to 10 Hz band as for the 921231 event.

Figure 19 compares the ARCESS traces from three Greenland Sea earthquakes with the 921231 event in the 8 to 10 Hz filter band. No *Lg* is observed from these earthquakes as well as from the Novaya Zemlya events, presumably because of the largely oceanic propagation path from the Greenland Sea region to ARCESS. However, the *Sn* waves from the Greenland Sea earth

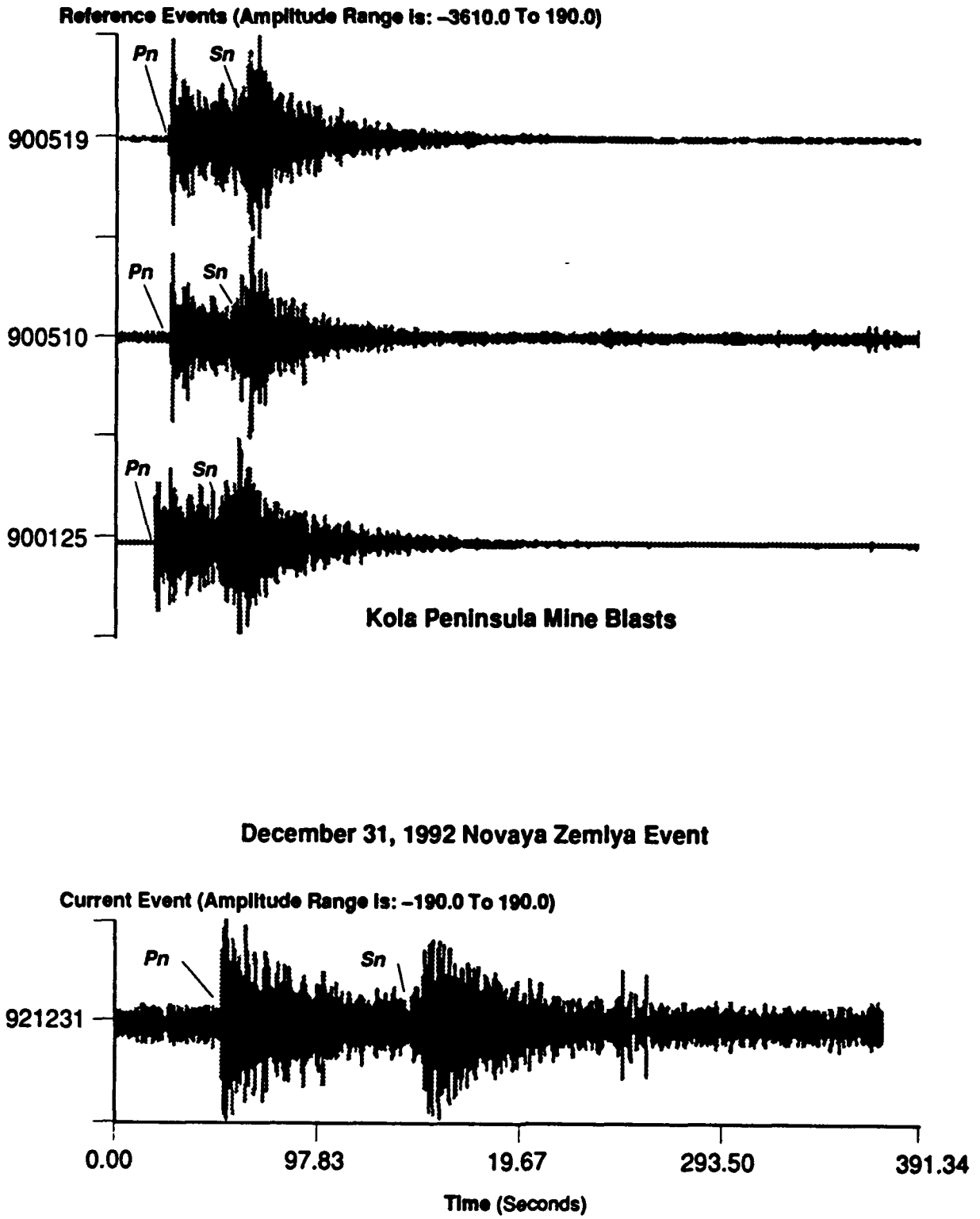

FIGURE 17: Comparison of waveforms from the 921231 event (bottom) and three Kola Peninsula mine blasts. All traces are bandpass-filtered from 8 to 10 Hz.

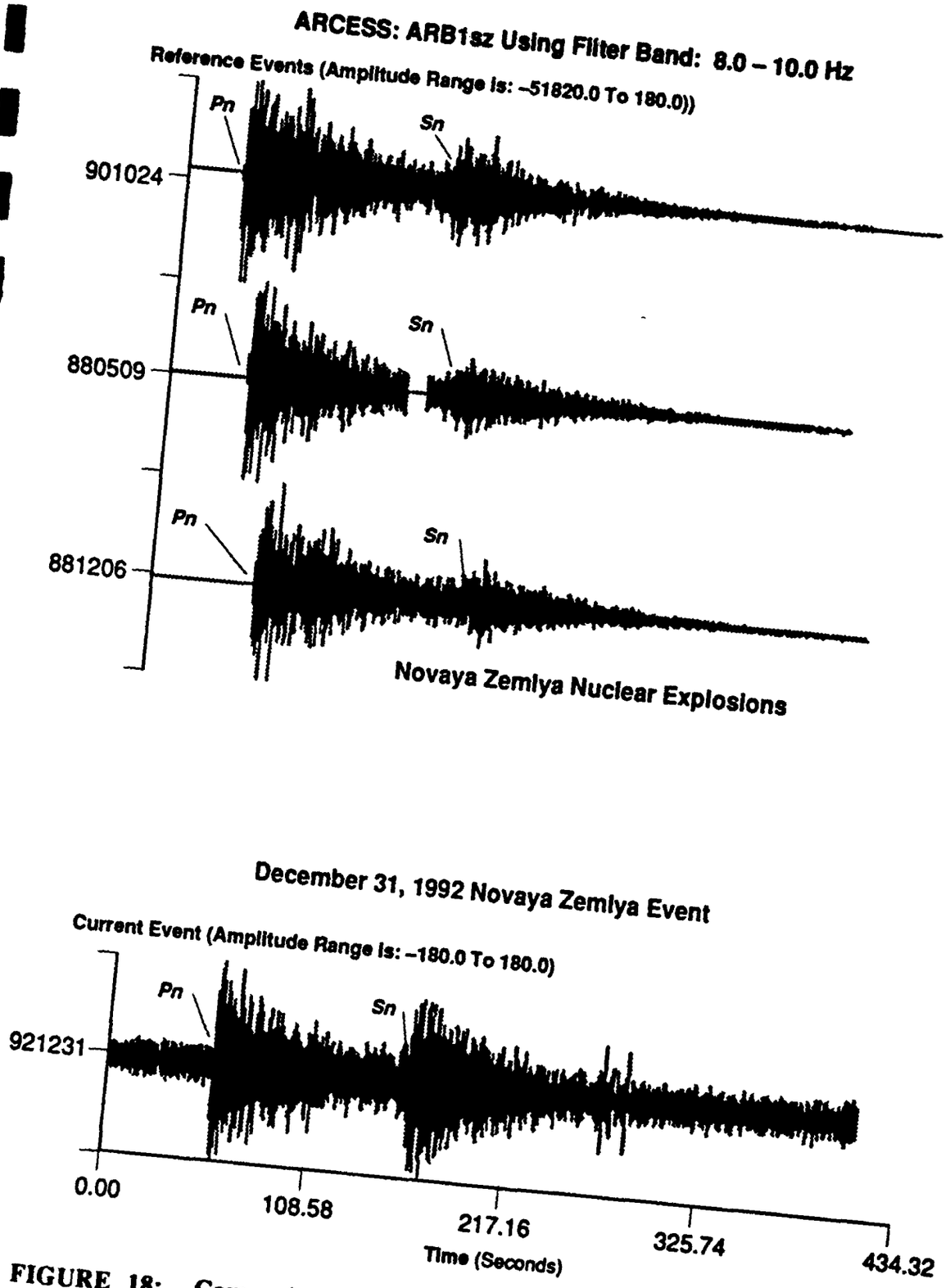

FIGURE 18: Comparison of waveforms from the 921231 event (bottom) and three Novaya Zemlya nuclear explosions. All traces are bandpass-filtered from 8 to 10 Hz.

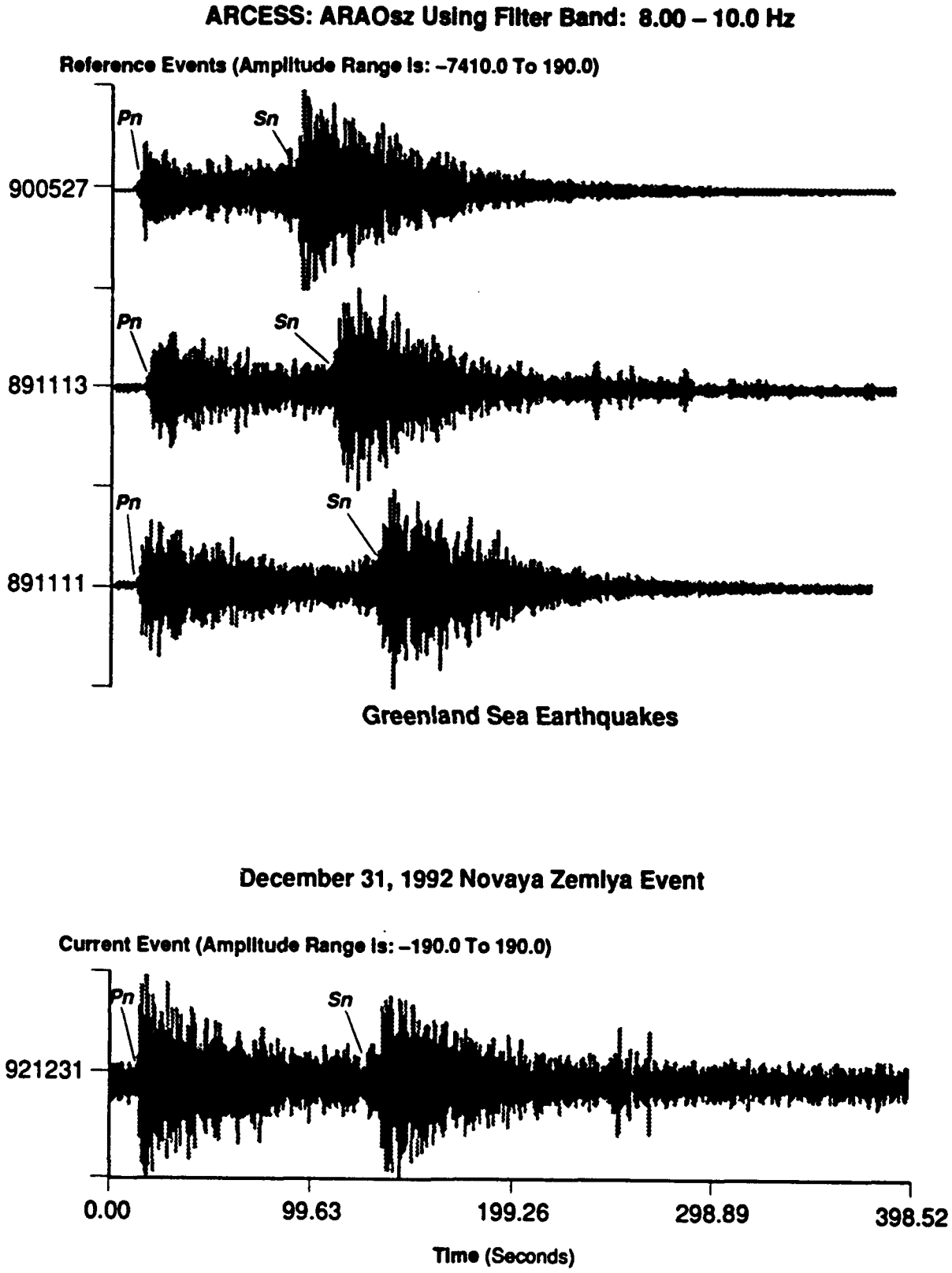

FIGURE 19: Comparison of waveforms from the 921231 event (bottom) and three earthquakes in the Greenland Sea near the mid-Atlantic ridge. All traces are bandpass-filtered from 8 to 10 Hz.

quakes are strong in the 8 to 10 Hz band. The 921231 event generates more *Pn* energy relative to *Sn* than do the earthquakes. This comparison is significant, because the earthquakes and Novaya Zemlya events are nearly the same distance from ARCESS, albeit on different azimuths. The paths are different, but they should have similar distance dependent effects.

These three plots show that the 921231 event does not resemble the nuclear explosions. It most closely resembles the Kola blasts, but there may be significant propagation-path difference effects which must be considered in such a comparison.

Spitzbergen Waveforms

Figure 20 shows a single channel output (SPB2) recording of the December 31, 1992 event recorded at the new Spitzbergen array. The installation of this array has not been completed, so not all the sensor data is available. Moreover, the SPB2 channel records the highest signal-to-noise ratio. In fact, the only Spitzbergen channels which recorded an observable signal for this event were SPA3, SPB1, SPB2, and SPB5.

Incoherent Beam Analysis at ARCESS

ISEIS feature processing relies extensively on incoherent beams computed on multiple-bandpass-filtered waveform data for regional-phase definition and feature extraction, as discussed by Baumgardt (1991a) and Baumgardt et al (1992). Incoherent beams in ISEIS are computed by first bandpass-filtering the trace in one of nine frequency bands ranging from 0.5 to 2.5 Hz on the low end to 8 to 16 Hz on the high end. Then, on the filtered traces, the average log-rms amplitudes in one second windows, shifted down the trace in one second increments, are computed on each vertical component array element and these log-rms amplitudes are averaged across the array.

Figure 21 shows the log-rms incoherent beams in the eight frequency bands computed for the ARCESS array. The 0.5 to 2.5 Hz beam has not been plotted because it is mostly noise. The beam windows begin about 40 seconds before the onset of *Pn* and extend well into the *Sn* coda. Each beam, corresponding to a different filter band, has been shifted up for viewing purposes. The *Pn* and *Sn* picks of the CSS seismic analyst are shown on top of the incoherent beams. Note that these picks were made by the analyst on the seismogram itself, probably on a coherent beam, and <u>not</u> on the incoherent beam plots in Figure 21. These plots show that both the *Pn* and *Sn* phases are evident in the 2.5 to 4.5 Hz band and up, although the highest signal-to-noise ratios can be found in the 8 to 10 Hz and 8 to 16 Hz bands. The *phase selections* used for RMS amplitude measurements and spectral analysis windows begin at the phase pick times and extend to a

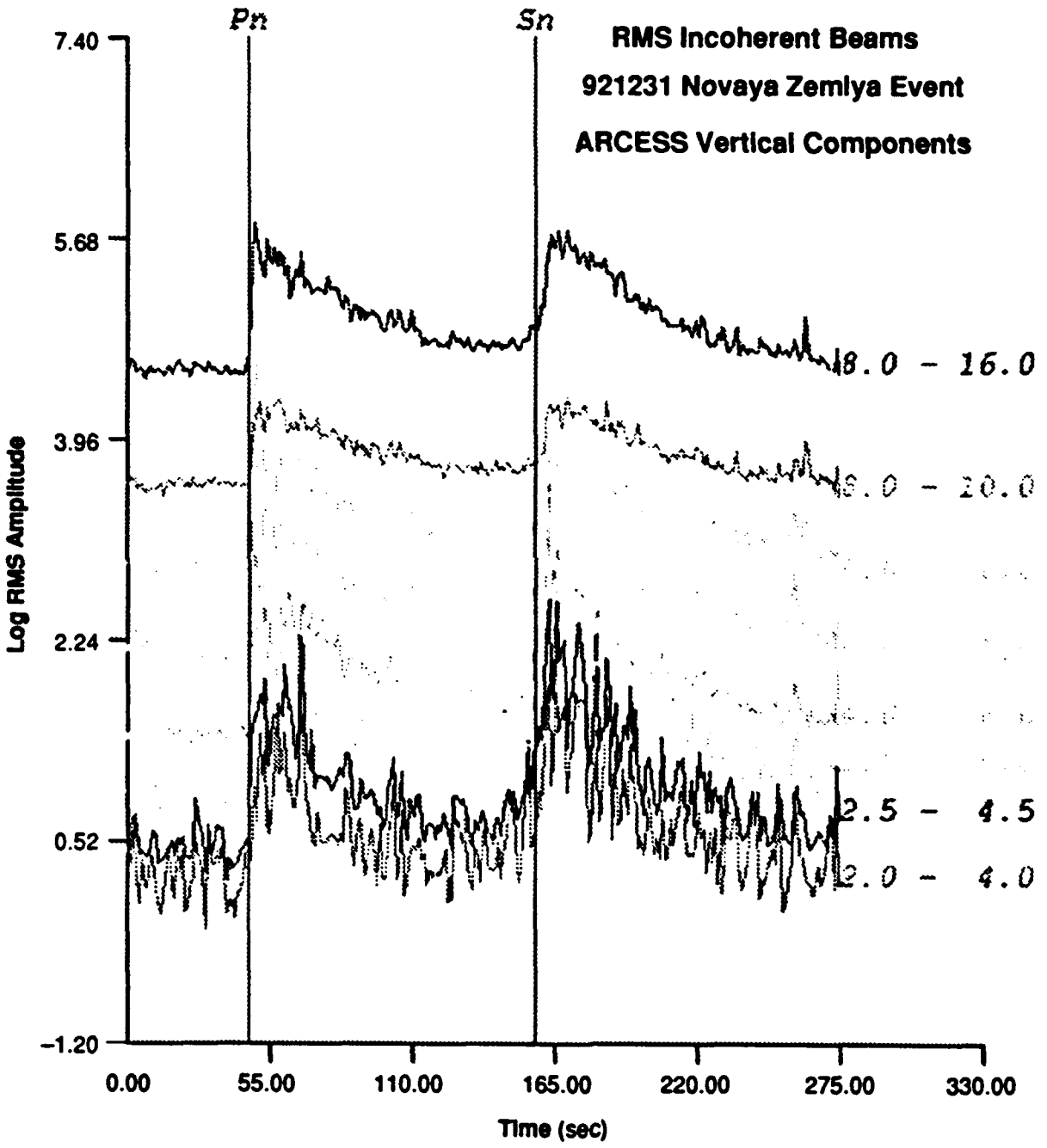

FIGURE 20: Plots of multifiltered log-rms incoherent beams recorded at ARCESS (ARA0). The *Pn* and *Sn* lines indicate the picks the analyst made on a coherent beam.

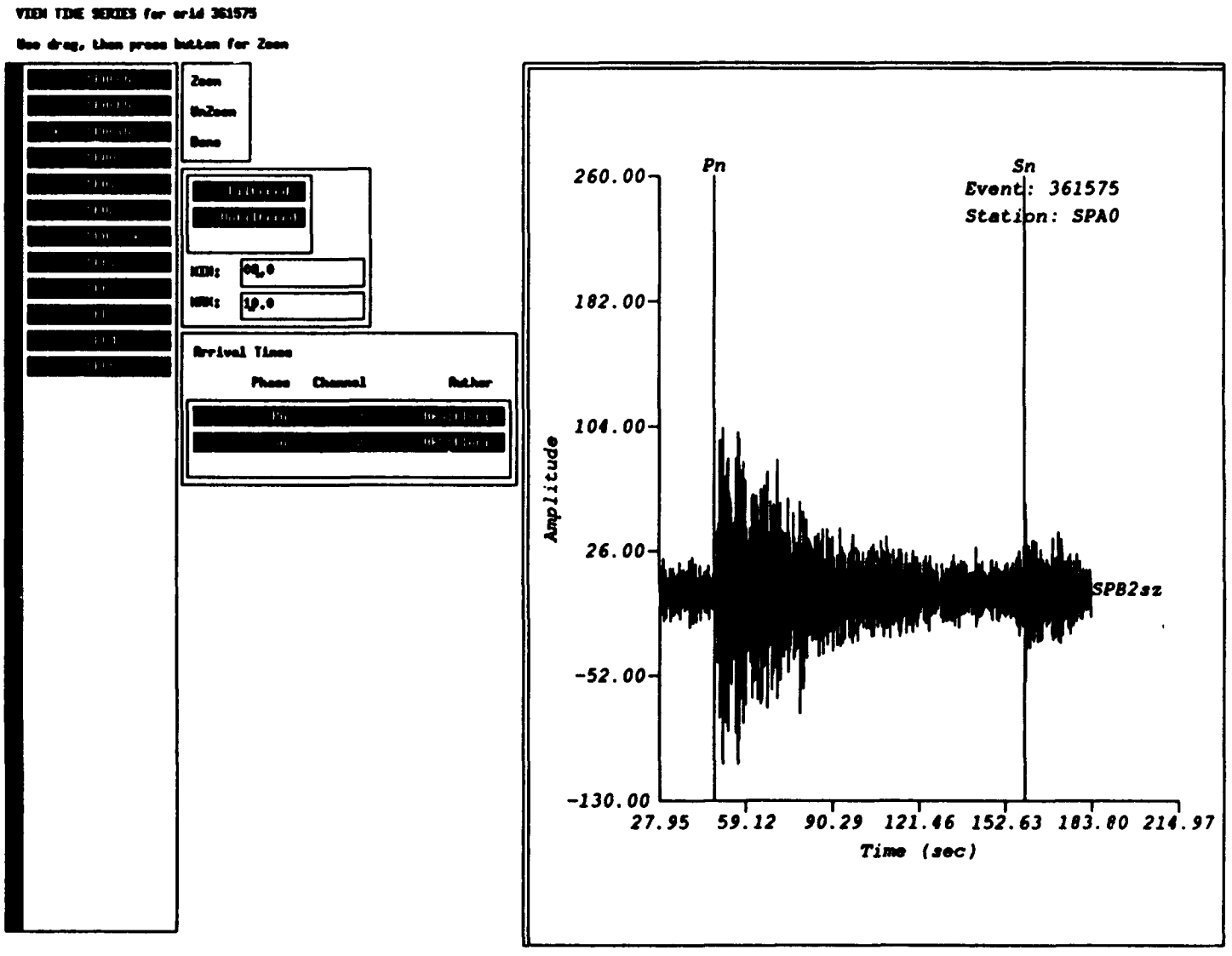

FIGURE 21: Coherent beam trace for the 921231 Novaya Zemlya event recorded at the Spitzbergen array.

specified time, based on an assumed group velocity for each regional phase (8.1-7.8 km/sec for *Pn* and 4.5 to 4.0 km/sec for *Sn*).

Incoherent Beam Analysis at Spitzbergen

Figure 22 shows the incoherent beams computed for the Spitzbergen array, designated SPA0. These beams were computed only from the channels which had visible signal, as mentioned above, which included SPA3, SPB1, SPB2, and SPB5. Again, the highest noise levels can be found in the low-frequency bands, below 2.5 Hz, with the signal emerging strongly in the high-frequency bands above 8 Hz. In both the ARCESS and Spitzbergen recordings, it is notable that the signal onset for *Pn* is almost impulsive in the high-frequency band.

As shown in Figure 16, both the ARCESS and Spitzbergen arrays occur near coastlines, although the SPA0 array is actually on an island. Because this data was recorded in winter, the microseismic-noise levels are probably higher, due to the more intense wave action, and the spectra of microseismic noise falls off very fast with frequency, which is evident from the comparison of noise and signal spectra at these arrays. This probably best explains why the signal-to-noise ratios for *Pn* and *Sn* are so much higher at both these arrays in the high-frequency band; i.e., the noise spectra fall off more rapidly at high frequency than do the signal spectra.

Spectral Analysis at ARCESS

As discussed above, with reference to phase selection, ISEIS computes spectra for phase-selection windows defined on the incoherent beams. Each spectrum is computed by windowing the phase on each channel after a cosine taper, computing the FFT, smoothing with a Hanning window convolution in the frequency domain, and then averaging the spectra across all the array channels.

Figure 23a shows array-averaged *Pn* and *Sn* spectra for the 921231 event, compared to the noise background to *Pn*. The instrument response for ARCESS has been deconvolved from both the signal and noise spectrum. This plot shows that the signals are above the noise levels above about 2-3 Hz. Both spectra are generally simple, showing a nearly linear drop-off with frequency. There is no evidence of time-independent spectral modulations, which were observed by Baumgardt and Ziegler (1988) for ripple-fired explosions, so the event appears to be a single event.

Figures 23b and c, respectively, compare *Pn* and *Sn* zoomed spectra for the 921231 event, with the same-phase spectra for the Novaya Zemlya explosions, and one of the Greenland Sea

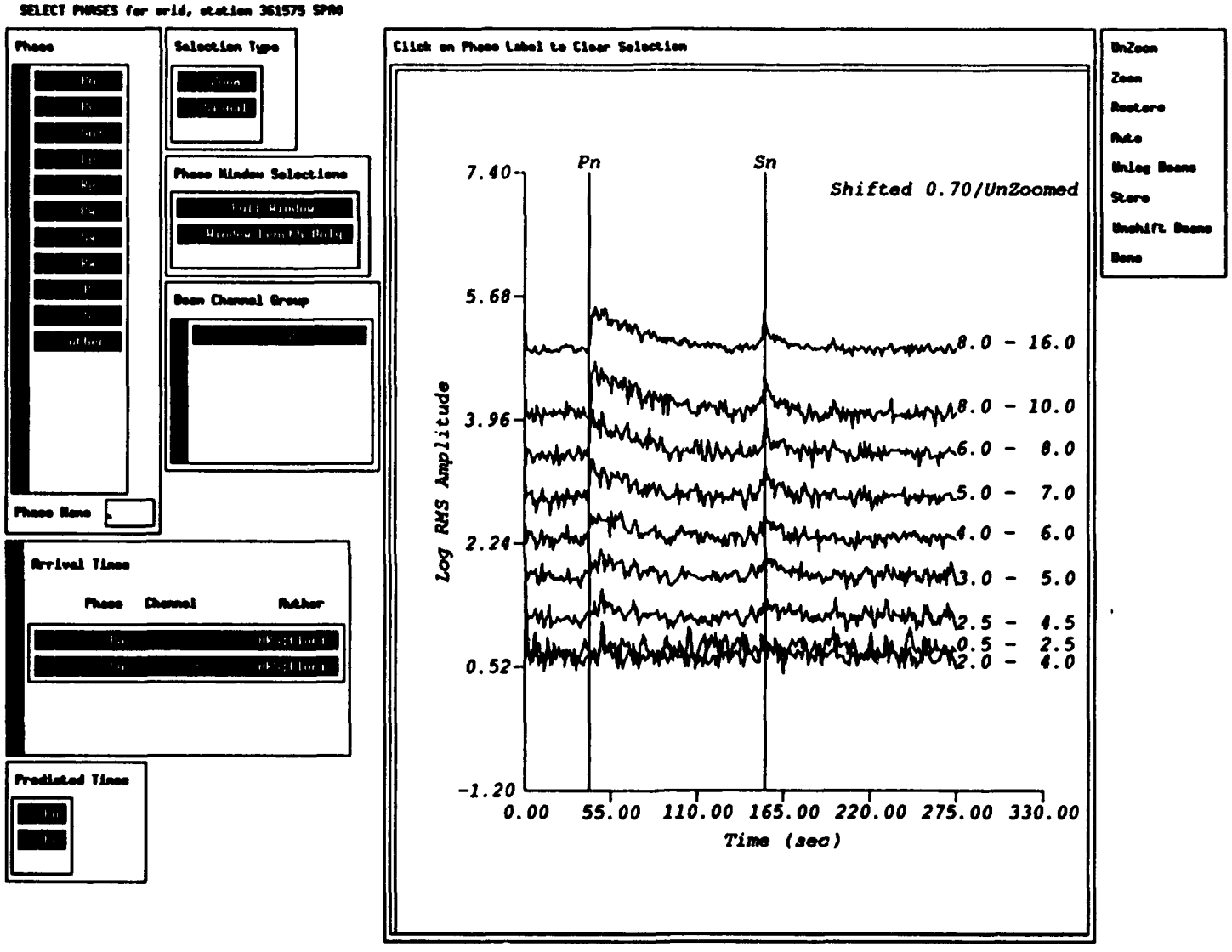

FIGURE 22: Incoherent beam traces in different frequency bands for the 921231 Novaya Zemlya event recorded at the Spitzbergen array.

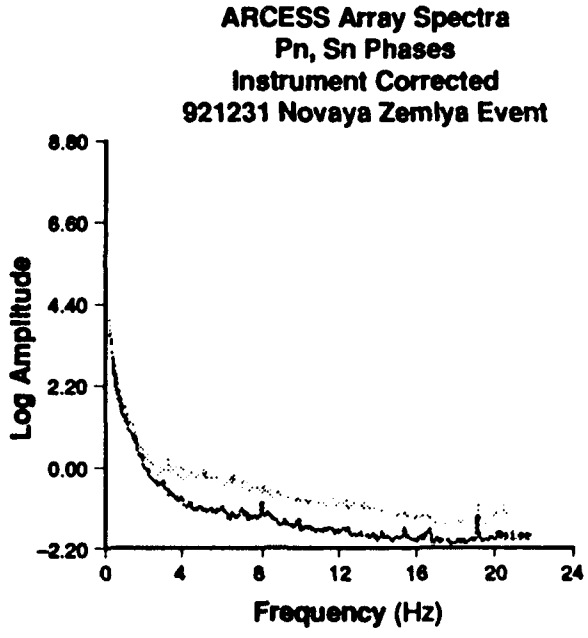

FIGURE 23a: Array-averaged signal and noise spectra for the 921231 event recorded at ARCESS. Spectra have had ARCESS instrument response removed.

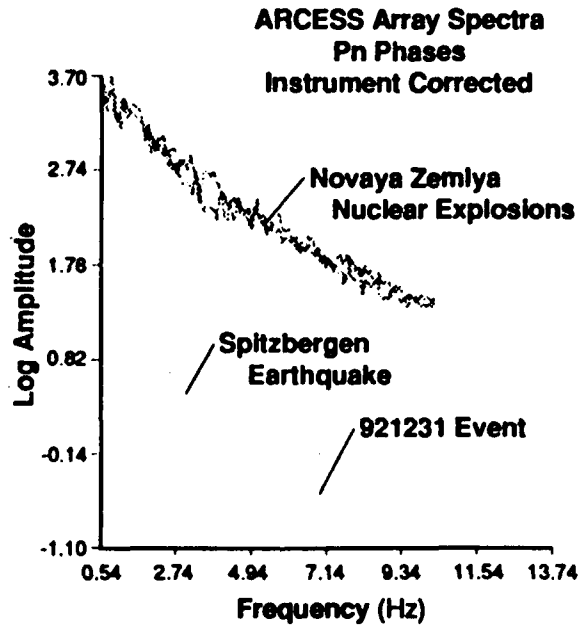

FIGURE 23b: Comparison of the instrument-corrected spectra for *Pn* for the Novaya Zemlya nuclear explosions and the 921231 event.

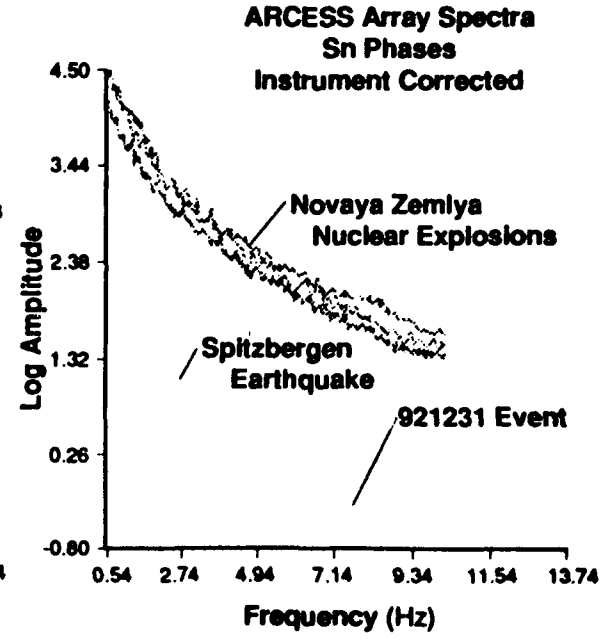

FIGURE 23c: Comparison of the instrument-corrected spectra for *Sn* for the Novaya Zemlya nuclear explosions and the 921231 event.

earthquakes. The expected difference in absolute level is evident since the nuclear explosions are at least three orders of magnitude larger than the 921231 event. Also, the high-frequency *Pn* and *Sn* spectral slopes of this event are less than those of the nuclear explosions but comparable to those of the earthquake. These slope differences are probably related to spectral scaling differences caused by the large differences in magnitude. These spectra show that the Novaya Zemlya nuclear explosions and the earthquake are also simple, with no indication of strong spectral modulations, as expected for single sources.

Pn/Sn Amplitude Ratio Features

The amplitude ratio between *P*- and *S*-type phases has been found to be a very promising discriminant in a number of studies (e.g., Bennett et al, 1989; 1991; Baumgardt and Young, 1990). It is based on an old idea that earthquakes should generate more shear wave energy relative to compressional wave energy and thus, earthquakes should have smaller *P/S* type amplitude ratios than explosions. Recent research has shown that this discriminant seems to work better at high frequency than at low frequency. Baumgardt (1992) and Baumgardt et al (1992) studied this discriminant extensively using ISEIS and data from the Scandinavian arrays and concluded that earthquakes and mine blasts can be discriminated using high-frequency *Pn/Sn* and *Pn/Lg* ratios.

In this study, we compared amplitude ratios of the 921231 event with the same measurements for many mine blasts, earthquakes, and the three nuclear explosions recorded at ARCESS. For Novaya Zemlya events, we must rely entirely on the *Pn/Sn* ratio since virtually no *Lg* energy is recorded at ARCESS (Baumgardt and Young, 1990; Baumgardt et al, 1991).

ISEIS used phase selection windows to measure features on each phase, where the window starts at the IMS phase-pick times shown in Figure 21. The average and maximum rms amplitudes in each window were measured and stored in the database along with the time limits of the window. Array-averaged spectra were then computed for each phase, which we will discuss in the next section. For amplitude ratios, we have found the maximum rms amplitude in each phase window to be the best discriminant, rather than the average rms amplitude, because the latter depends critically on the window length which may not always be consistently set.

For all comparative feature analysis, reference events were assigned to *reference regions*, which are geographic regions whose boundaries were set by the average location of the events assigned to the regions. So, for example, the Novaya Zemlya reference region is an area about 50 km in extent, which encloses the IMS locations of the three nuclear explosions which have occurred there since the ARCESS array was installed. The mine sites include the numerous Kola

Peninsula mine sites (K1, K3, K4, K5, K8, and K9), identified in the Helsinki bulletin, and one additional one called Kola Zapelyarnyi, the location of two known test charges. Three earthquake regions include the Spitzbergen and Svarlbard regions, defined by the Greenland Sea events, and the Steigen swarm region. Also, the one presumed underwater implosion event, which is believed to be the Komsomolets submarine disaster of 1989 (Baumgardt, 1991b), has been included since it occurred in the same region as the Spitzbergen and Svarlbard earthquakes. This event was assigned to the Svarlbard region. In this study, these regions include a total of about 96 events.

Figure 24a shows a scatterplot versus frequency of the *Pn/Sn* ratios computed from the maximum rms amplitudes in each phase-selection window on each incoherent beam. The frequency ranges printed on the abscissa correspond to the frequency band of each filter. Because there are so many points in the plot, only the average for each event type (earthquake, quarry or mine blast, marine explosion, and nuclear explosion) are plotted as four different symbols, shown in the legend in the upper left part of the plot. Each point has an error bar which is the standard deviation of values for each event type. The triangle with the superimposed asterisks are the computed values for the current event of interest, the 921231 event.

Figure 24a shows that the separation of nuclear explosions from other event types is greatest at high frequencies, beginning at about the 4 to 6 Hz band. Below this frequency band, most of the event types have overlapping error bars. At high frequencies, the event types separate with the nuclear explosions having the highest values, the presumed Komsomolets marine implosion and mine blasts having the next highest, and the earthquakes having the lowest values for *Pn/Sn* ratios. This agrees with the concept that earthquakes generate more *Sn* energy relative to *Pn* energy than explosions and therefore have lower *Pn/Sn* ratios. The nuclear explosions have the highest ratios at high frequencies, even larger than the mine explosions. The best separation is in the 8 to 10 Hz band. The 921231 event falls almost exactly on the average value for all the mine blasts, which is well below the ratios observed for the nuclear explosions. However, the ratios only slightly exceed those observed for the earthquakes used in this study.

The problem with comparing amplitude ratios for event types like this is that there may be significant propagation-path differences which could affect these ratios. To examine these more closely, we plot in Figure 24b the *Pn/Sn* amplitude ratios in the 8 to 10 Hz band, which is the most discriminatory band in Figure 24a, as a function of epicentral distance. This plot shows the separation of the nuclear explosions and all other events in the 8 to 10 Hz band. Note, however, that on this plot, the mine explosions and earthquakes are much closer together. Baumgardt (1992) and Baumgardt et al (1992) have studied in detail the separation of mine blasts and earthquakes in this region and have pointed out that mine blasts have much greater variance in this ratio than

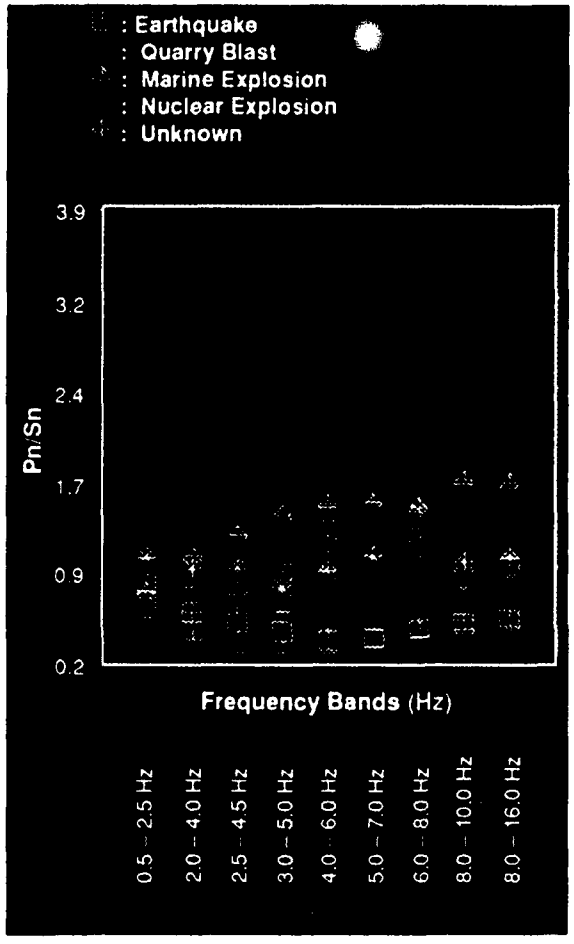

FIGURE 24a: Plot of the average *Pn/Sn* amplitude ratios measured in nine frequency bands at ARCESS, using maximum rms measurements, for the reference events shown in Figure 16. The triangle with the asterisks through it indicate the values of the 921231 event. Error bars shows the standard deviations in the values for all events of a given source type.

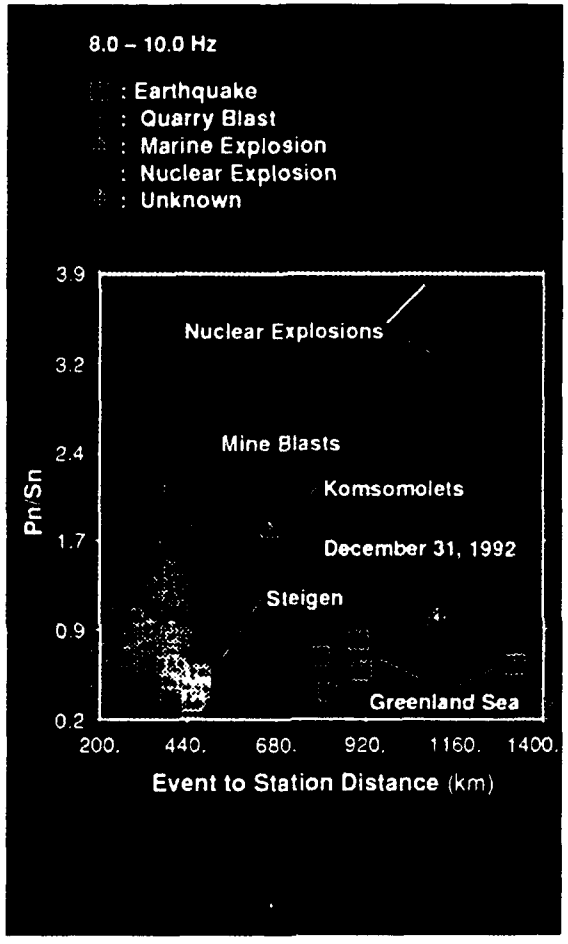

FIGURE 24b: Scatterplot showing the values of the *Pn/Sn* amplitude ratios in the 8-to-10 Hz band as a function of epicentral distance from ARCESS for all the event types and the 921231 event. Legend in the upper left identifies the symbols used in the plot.

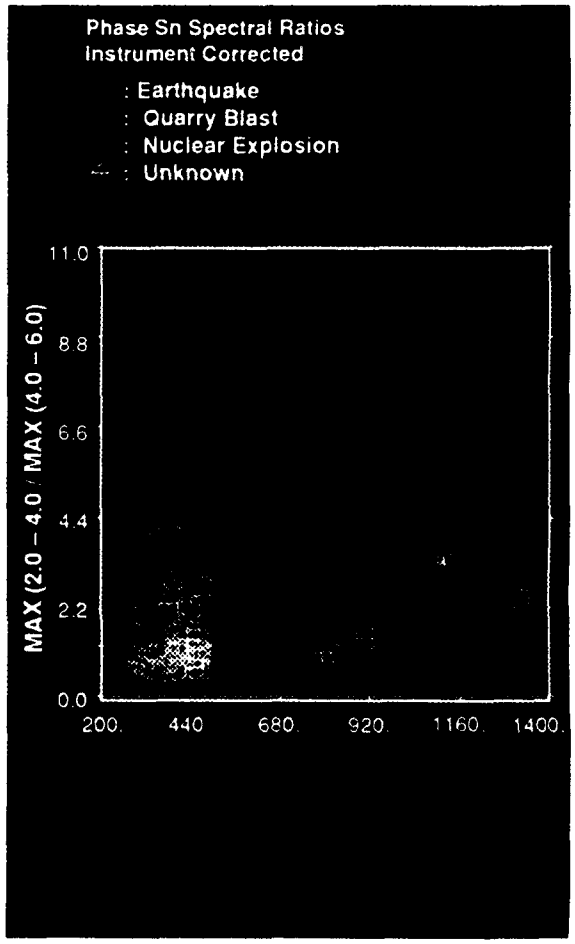

FIGURE 24c: Scatterplot of *Sn* spectral ratios (2-4 Hz/ 4-6 Hz) measured at ARCESS as a function of epicentral distance. The 921231 event is the asterisks/ triangle overstrike symbol.

earthquakes. This was explained as being caused by differences in shear excitation due to rock spalling and fracturing effects in the blasts. The tight clustering of the Steigen earthquakes at around 440 km was noted by Baumgardt et al (1992) and may be accounted for by the fact that these earthquakes occurred as a swarm in the same region and thus, may have had very similar source mechanisms. However, the five Greenland Sea earthquakes, between 900 and 1400 km, have very similar ratios. The reason for this apparent stability of the *Pn/Sn* ratio at high frequency for earthquakes and its large variance for mine explosions is not yet clear, but has important implications for interpreting the separability of classes of event types based on this feature.

This plot shows that the 921231 event in question falls in the middle of the range for mine blasts but just barely above the values of the earthquakes in the same distance range as the Novaya Zemlya event. However, the mine blasts are at closer distances (about 400 km) than the Greenland Sea and Novaya Zemlya events (about 900 to 1100 km). So, we cannot rule out the possibility of there being propagation-path differences which might affect these ratios.

From Figures 24a and 24b, we conclude that the 921231 event was probably not a nuclear explosion. However, identifying the event as a conventional blast is still problematic because the ratio is not much higher than those observed for earthquakes in the same distance range, although the ratio is comparable to those of mine blasts at shorter distance ranges and significantly higher than earthquakes in that shorter distance range.

Sn Spectral Ratio Features

Murphy and Bennett (1982), Bennett and Murphy (1986), and Taylor et al (1988, 1989) found that the ratio of low-frequency to high-frequency spectral energy for *Lg* discriminated nuclear explosions and earthquakes in the western U.S., with the earthquakes having lower spectral-ratios (higher frequencies) than explosions. Baumgardt et al (1992) found that this discriminant separated blasts and earthquakes in Germany but not in Scandinavia. Taylor and Denny (1991) presented a theoretical argument that the *Lg* spectral-ratio discriminant may work if earthquakes and explosions occur at different depths and the explosions occur in a shallow, low-Q medium. Baumgardt et al (1992) have suggested that such conditions may not apply to Scandinavian mine blasts and earthquakes and thus, we would not expect the spectral-ratio discriminant to work in Scandinavia.

A scatterplot of spectral ratios for *Sn* from the 921231 event and other events are shown in Figure 24c. These ratios were computed by taking the maximum spectral densities in the *Sn* spectra in the 2 to 4 Hz and 4 to 8 Hz bands, and ratioing these values. As in the previous plots, the

921231 event is indicated by the triangle and asterisks overstrike symbol. These plots show that the nuclear explosions have higher spectral ratios in *Sn* than for the other event types. The 921231 event has a slightly higher ratio than the earthquakes at the same distance. However, looking at the points in the 200 to 450 km distance range, there appears to be significant overlap in the points for chemical blasts and earthquakes.

The apparent separation in spectral ratio between the nuclear events and all the others may be more due to magnitude differences in the events than in any intrinsic source differences. Looking at the spectra in Figure 23c, it can be seen that there is an enhancement of the 921231 spectrum in the low-frequency band, below about 2.74 Hz. However, this enhancement is caused by noise contamination at low frequency, which can be seen clearly in the comparison of the signal and noise spectra in Figure 23a. This low-frequency enhancement causes the lower spectral ratios for the smaller mine blasts, earthquakes, and the 921231 event compared with the nuclear explosions. These results are consistent with the apparent magnitude scaling in the spectra, as shown in Figure 23c. Thus, we conclude that there appears to be no discrimination of source types in this region based on spectral ratio of *Sn* or any other phase.

3.3 SIGNAL CHARACTERISTICS AT NORESS

We now consider the signal characteristics of Novaya Zemlya events at NORESS. NORESS has operated much longer than ARCESS, so there is a greater record of historical data at NORESS than ARCESS. Unfortunately, NORESS is farther away from Novaya Zemlya (about 2300 km) compared with ARCESS (about 1100 km). Figure 25 shows on a map the great circle propagation paths from the Novaya Zemlya region to NORESS. The 921231 event was so small that weak signals were detected at NORESS. However, we will later reconsider another event at Novaya Zemlya, the August 1, 1986 event, which was identified as an earthquake.

As mentioned above, the 921231 event was very small, with an estimated *Ml* of 2.2, and its signals at NORESS were very weak. Only a direct *P* wave could be identified on a filtered beam. Figure 26 shows a plot of a NORESS beam trace for an 8 km/sec velocity directed at the azimuth of the event and bandpass-filtered between 4 to 6 Hz. The *P* pick made by the analyst, which was called *Pn* in ISEIS, is indicated. It was not possible to see this phase on any individual trace.

Figure 27 shows the ISEIS incoherent beams for the event, with the ISEIS phase picks superimposed. A tentative identification of an *Sn* phase was made, as indicated in Figure 27, which was not made by the IMS system or analyst. It can be seen on the beam trace in Figure

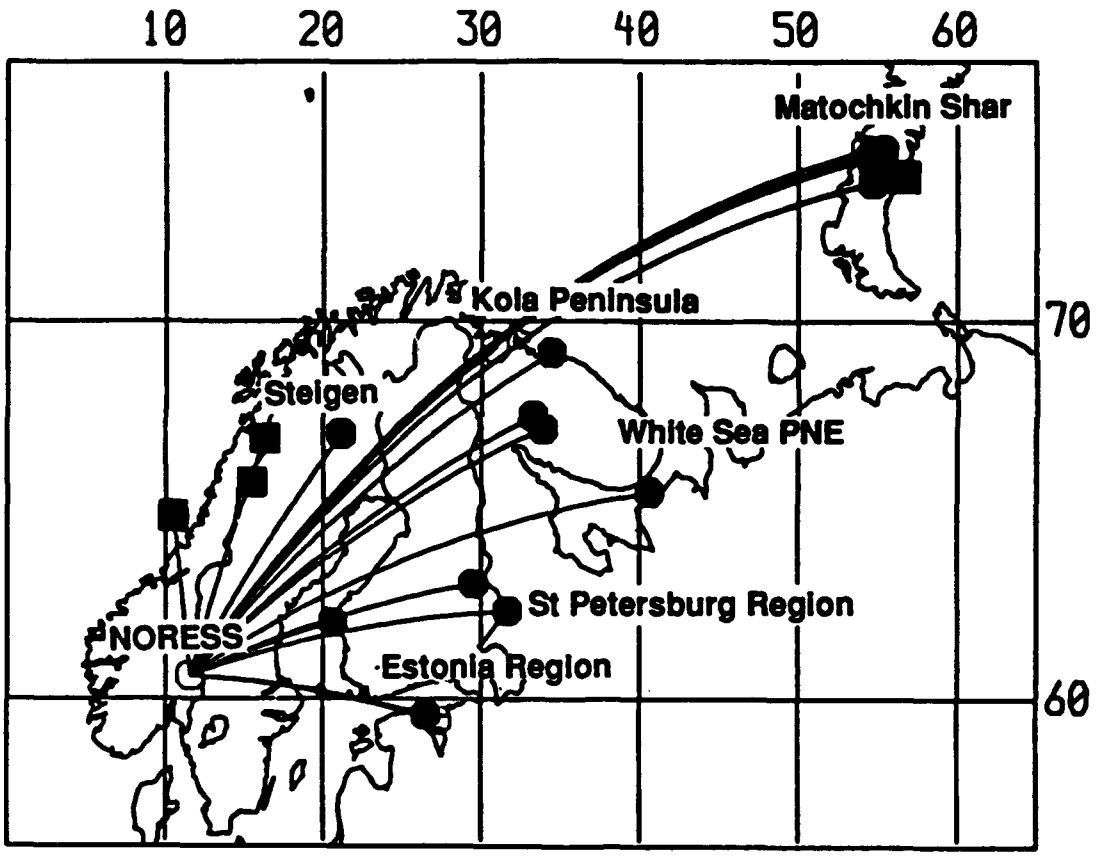

FIGURE 25: Map showing the locations of the NORESS array and the reference events recorded at NORESS used to characterize the 860801 event. The great circle paths between the Novaya Zemlya events and other reference events to NORESS are shown. Square and circle symbols indicate earthquake and explosion locations, respectively.

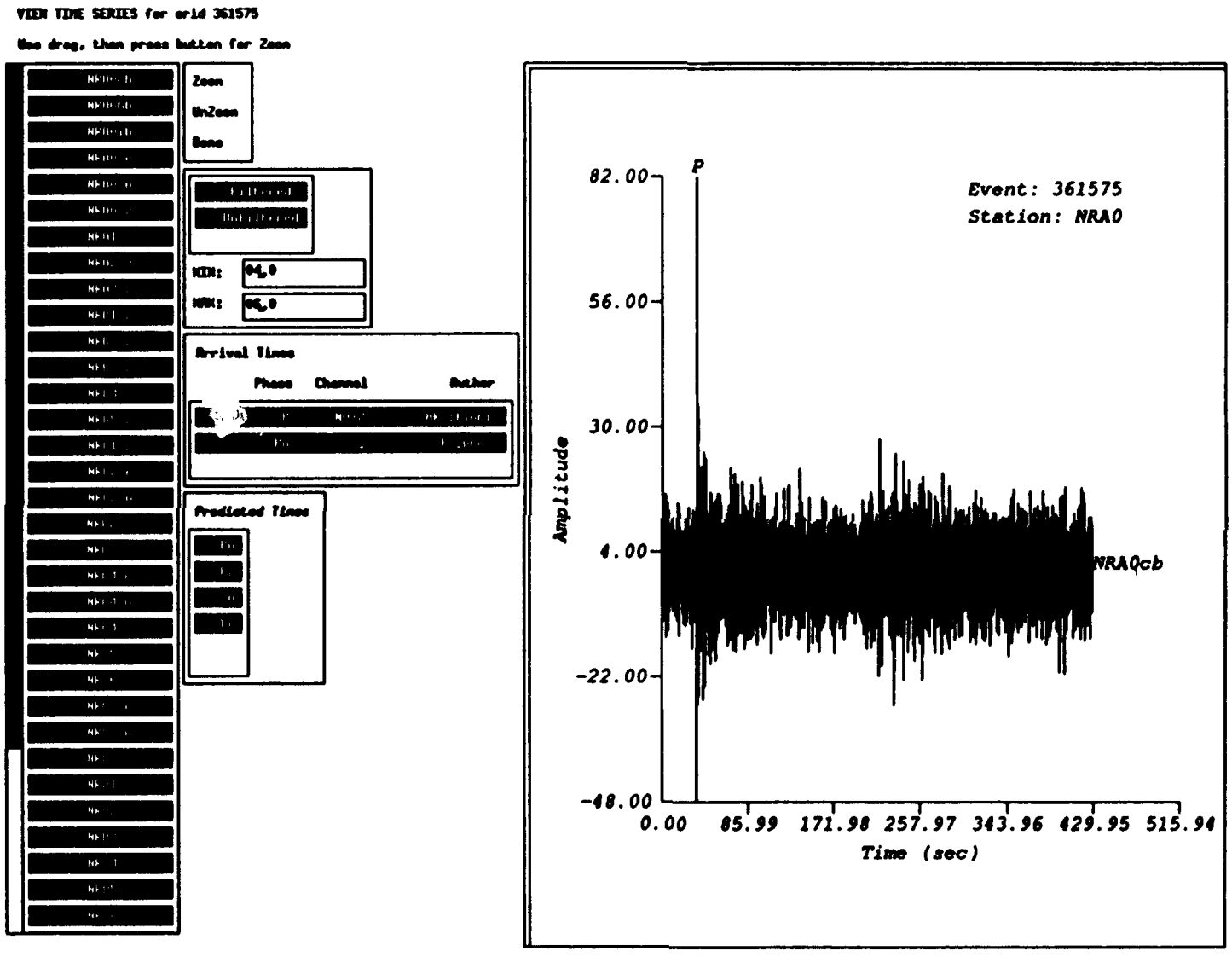

FIGURE 26: Filtered coherent beam of the 921231 Novaya Zemlya event recorded at NORESS. The *P* pick made by the analyst in the ARS is shown. Energy near 257 seconds corresponds to the expected time of *Sn*, but this phase was not identified in the IMS.

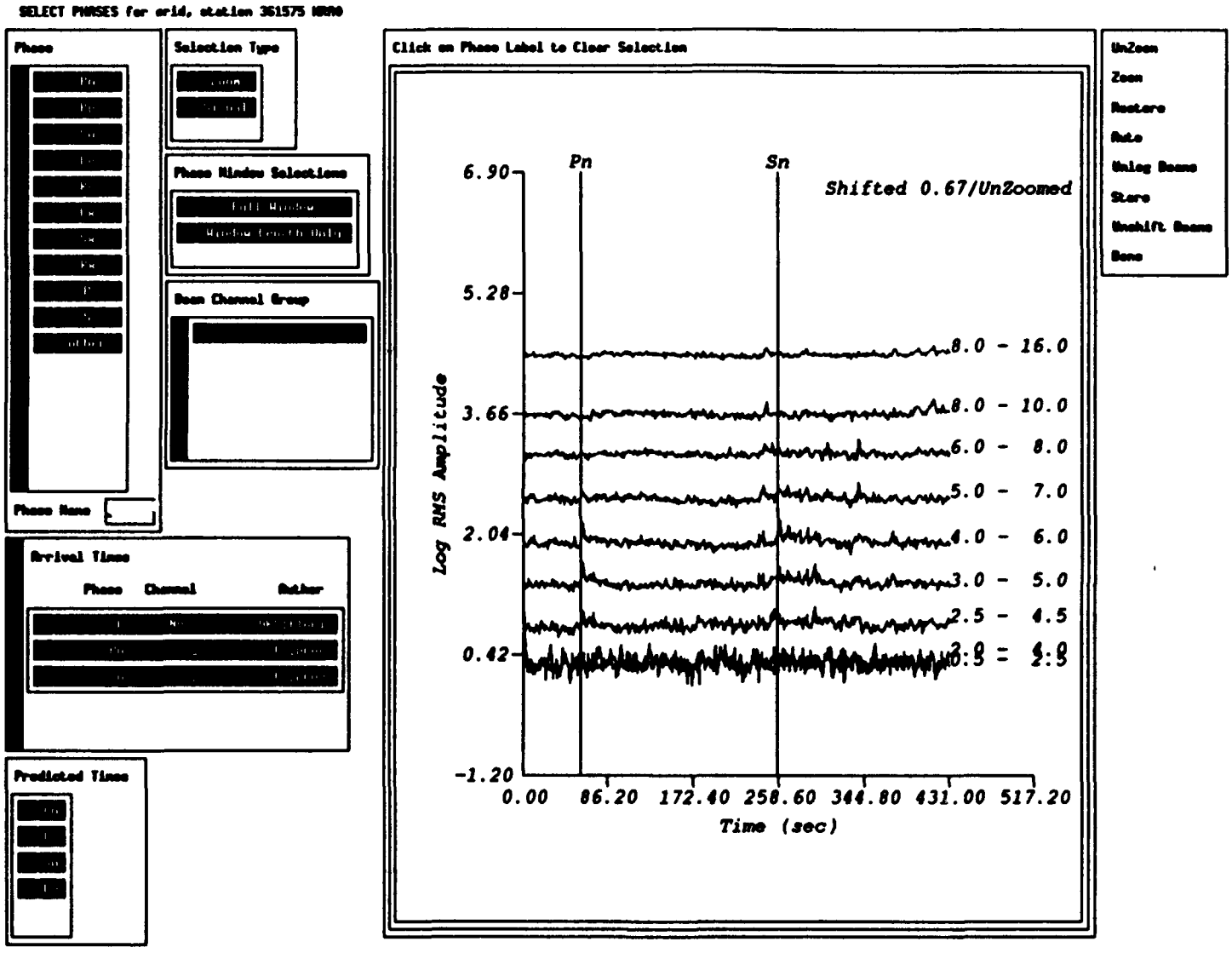

FIGURE 27: Multifrequency incoherent beams at NORESS for the December 31, 1992 event. *Pn* and suspected *Sn* time is indicated.

26 as an increase in energy at about 258 seconds. This energy comes in at the expected time for *Sn* from Novaya Zemlya. If this phase is truly *Sn* from the December 31, 1992 event, it would be significant because its amplitude would be comparable to the *Pn* amplitude.

To determine if, in fact, an *Sn* phase was recorded at NORESS, we applied a process in ISEIS called *continuous fk* and *fk template analysis*. *Continuous fk* spectra are computed by running a window down the trace, starting in the noise before the *Pn* onset, and computing broadband *fk* spectra in each window. For each *fk*, the peak is found and the velocity, azimuth, and f-statistic of the signal energy in the peak are determined and stored. *Fk templates* are then displays of these estimates as a function of time. Figures 28 and 29 show the *fk* templates for the event in the 4 to 6 Hz band, which we determined from the incoherent beam analysis in Figure 27 to be the band for the best signal-to-noise ratio for the suspected *Pn* and *Sn* phases. The upper left plot shows a plot of one channel, filtered in the 4 to 6 Hz band. The lower left plot shows the f-statistic, plotted as a function of time. F-statistic is a measure of signal coherence. We regard f-statistics above 2 or 3 to be significant. In the upper right, the azimuth estimate is plotted as a function of time, with a horizontal line showing the suspected azimuth of the event, or about 33 degrees. In the lower right is shown the velocity template, with the horizontal lines drawn at 6 and 10 km/sec.

In Figure 28, the time window suspected for the *Pn* was selected and the average f-statistic, azimuth, and velocity in the window have been computed. This phase appears to be on the correct azimuth and has a velocity of 13.7 km/sec, closer to that of direct *P* rather than *Pn*. Moreover, the average f-statistic is 7.6 which indicates that the measurements are relatively coherent. Figure 29 shows the same analysis done in the time range of the suspected *Sn*. This plot shows that the phase is in fact <u>not</u> *Sn* from Novaya Zemlya but rather a teleseism from another azimuth. In fact, Figures 28 and 29 show that the *Pn* window, just before 80 seconds into the templates, is the <u>only</u> signal from the 921231 event.

Thus, we conclude that only a direct *P* wave was recorded above the noise level at NORESS from the December 31, 1992 event and no *S* waves were recorded at all. So, not much can be said about the identity of this event from the NORESS data.

3.4 DISCRIMINATION ANALYSIS OF THE 860801 NOVAYA ZEMLYA EARTHQUAKE AT NORESS

As mentioned earlier, the small size of the 921231 event precluded our analyzing it at NORESS as we did at ARCESS. Baumgardt (1993) has analyzed the NORESS waveforms from

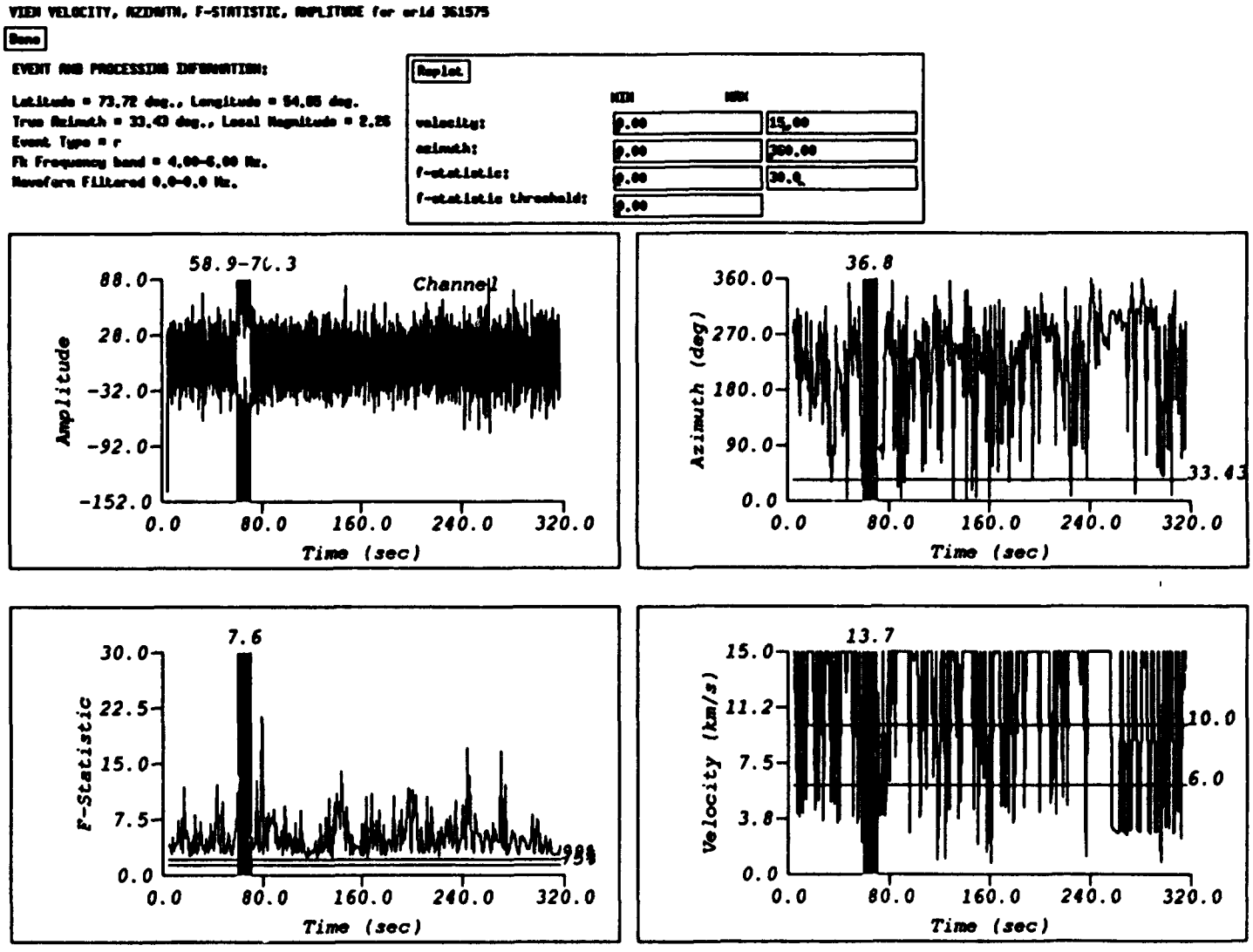

FIGURE 28: Results of continuous *fk* analysis of the December 31, 1992 event recorded at NORESS. Shown are the 4-6 Hz filtered NRA0 channel (upper left), the f-statistic template (lower left), and azimuth template (upper right), and the velocity template (lower right). The darkened area is a window on the suspected *Pn* phase and the average value on each template is shown.

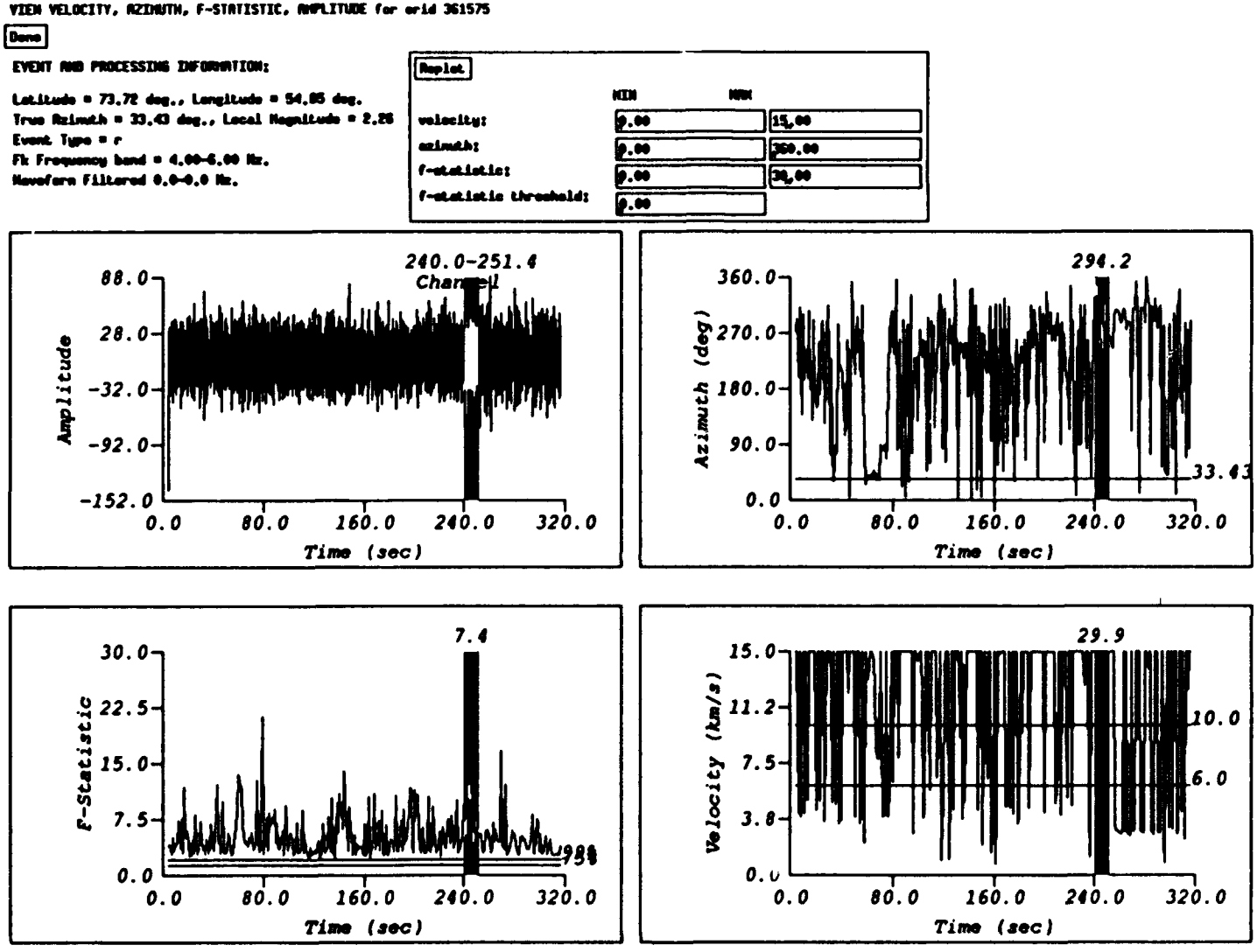

FIGURE 29: Same as Figure 28 with the window on the suspected *Sn* time. No phase of *Sn*-type velocity or azimuth of Novaya Zemlya appears in the coda. *Sn* apparently was not detected at NORESS.

the 921231 event and found that only a single *P*, but no shear waves, were detected. Since we cannot actually study the 921231 event at NORESS for discrimination purposes, we consider instead an earlier, larger event which was recorded at NORESS on August 1, 1986 (860801) and located near the test sites at Novaya Zemlya. At the time this event occurred, only the NORESS array was operating. However, we do have the NORESS recordings of the Novaya Zemlya nuclear explosions which can be compared with the 860801 event at NORESS in the same way that we compared the same nuclear explosions with the 921231 event at ARCESS.

The 860801 event was studied in detail by Ryall et al (1987), who considered many signal characteristics of the event recorded at NORESS. Moreover, they relocated the event, using teleseismic data from other stations, to be south of the test site but offshore to the east. Based on an *Ms-mb* analysis at the Hagfors array, the event was plotted in between earthquakes and explosions on the *Ms* vs. *mb* plot, but slightly closer to the earthquake population. Subsequent *Ms* vs. *mb* analysis of this event with other stations has placed this event more in the earthquake category (A. Ryall, personal reference). Finally, the event magnitude was about 4.6, which is much too large to be a conventional chemical explosion. Thus, the event appears to have been an earthquake.

Earthquakes are rare at Novaya Zemlya. However, they have been detected by the Kola Scientific Center of the former Soviet Union, now Russia, including this event (W. Leith, personal reference). These earthquakes in the region may result from stresses associated with uplift caused by glacial unloading.

Ryall et al (1987) did not do a *Pn/Sn* analysis of this event and compare it with NORESS recordings of Novaya Zemlya explosions, since these events had not occurred yet. In this section, we reconsider this event, using the same *Pn/Sn* analysis which was done for the ARCESS recording of the 921231 event, and compare it to historical events recorded at NORESS.

NORESS Waveforms

Figure 25 shows the locations of the Novaya Zemlya nuclear explosion and several mine blast and earthquake sites along with great circle seismic propagation paths for the events which have been studied at NORESS.

In Figure 30, the NRB1sz channels for the 860801 event and the three Novaya Zemlya explosions are plotted. Note that these traces are broadband with no filtering.

Baumgardt (1990; 1991c) has studied Novaya Zemlya explosions recorded at NORESS and NORSAR and has shown that, like at ARCESS, no direct *Lg* was recorded at NORESS.

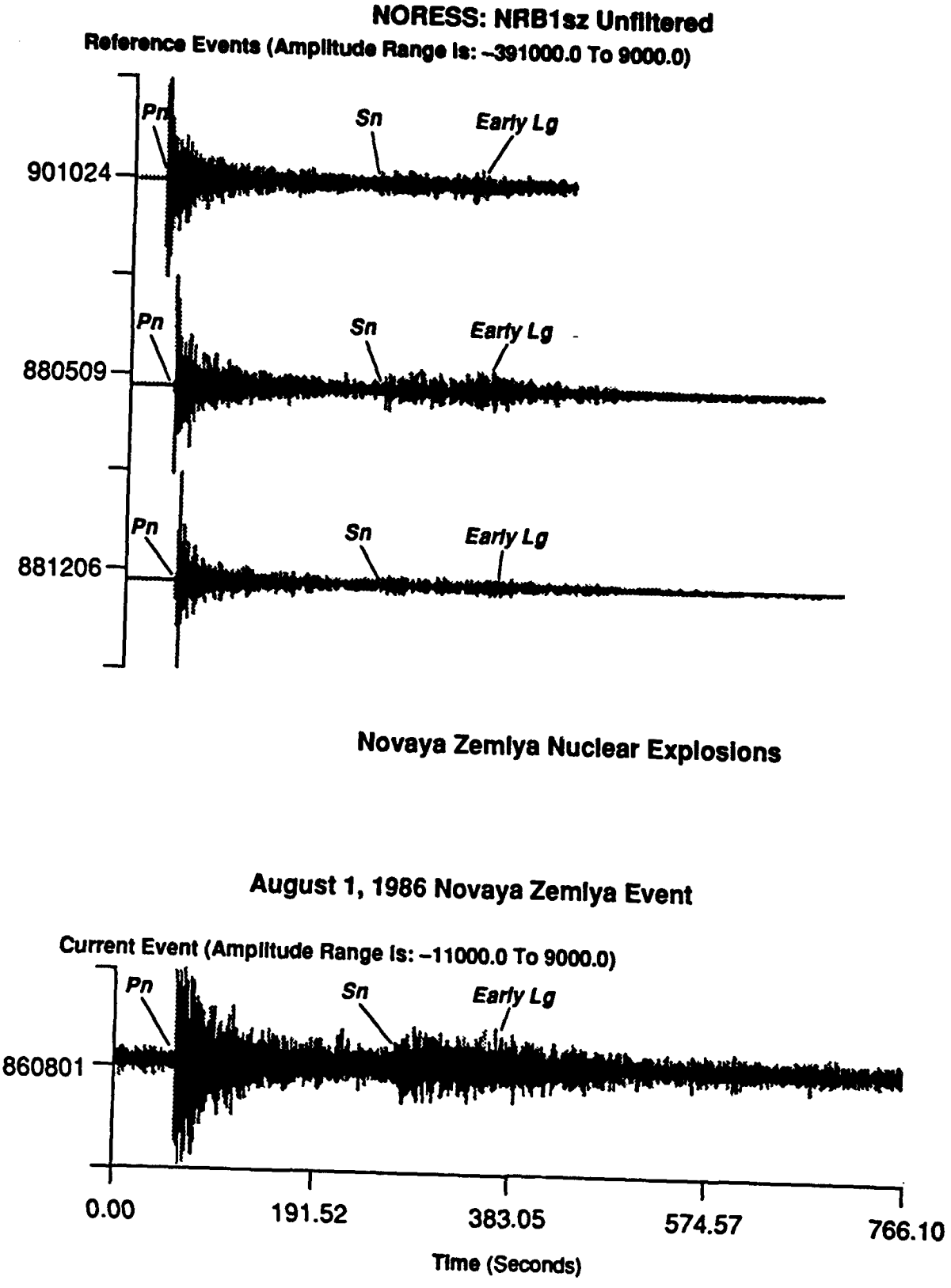

FIGURE 30: Comparison of unfiltered waveforms recorded on the NORESS NRB1sz channel from the 860801 Novaya Zemlya event (bottom) and the three Novaya Zemlya nuclear explosions.

However, an "early *Lg*" was observed which Baumgardt and Young (1990) (also Baumgardt (1991c)) have explained as being due to an *Sn* to *Lg* mode conversion at the Barents Sea-Kola coastline interface. Direct *Lg* itself seems to have been blocked by the Barents sedimentary basin. The 860801 event shows the same lack of direct *Lg* but the presence of an early *Lg*.

The 860801 event differs from the nuclear explosions in that it has larger shear waves. To consider if this can be expected for blasts, we compare the event with three other event types in Figure 31. These events, including the 860801 event, have all been filtered in the 2 to 6 Hz band. The top trace is an earthquake in central Norway, the second trace is a small (*Ml* = 2.8) Kola Peninsula explosion, and the third trace is a presumed peaceful nuclear explosion (PNE) which occurred near the White Sea in northern Russia. The 860801 event looks most like the PNE, both in terms of the impulsiveness and strength of the *P* relative to the coda, and in the strength of the shear waves which are comparable. In Baumgardt's (1991c) study of this event, he showed that the *Lg* was not blocked on the White Sea PNE-to-NORESS path since it does not cross any sedimentary basins. Again, based on a subjective comparison of the plots in Figure 31, the 860801 event most resembles a PNE nuclear explosion. However, it should be noted that the epicentral distances of the events in Figure 31 are shorter than that from Novaya Zemlya to NORESS, and the paths all differ in that they do not cross the Barents Basin.

Amplitude Ratio Features

The multispectral incoherent beam analysis and amplitude measurements, described above for ARCESS, were also applied to the NORESS recordings of the 860801 event and other reference events. The reference events include the Novaya Zemlya nuclear explosions, including one which occurred in 1984 prior to the installation of ARCESS (Baumgardt and Young, 1990), the White Sea PNE, mine blasts on the Kola Peninsula which were recorded at NORESS, mine explosions in the St. Petersburg and Estonia regions, and earthquakes in central Sweden, central Norway, and the Steigen region in northern Norway. (Note: In all the analyses, we interpret the first arrival *P* as *Pn*, even in the distance range where *Pn* is not the first arrival. However, in most of these cases, the measurement windows are made long enough so that they include the *Pn* in the coda. However, for the case of most events beyond about 1000 km, *Pn* actually refers to direct *P*.)

Figure 32a shows a plot of *Pn/Sn* ratios as a function of the filter frequency band. The 860801 event is again plotted as a triangle/asterisks overstrike symbol. This plot shows that the *Pn/Sn* ratios are lower than those of nuclear explosions but above those for earthquakes and mine blasts. Note that the nuclear explosions do not include the PNE.

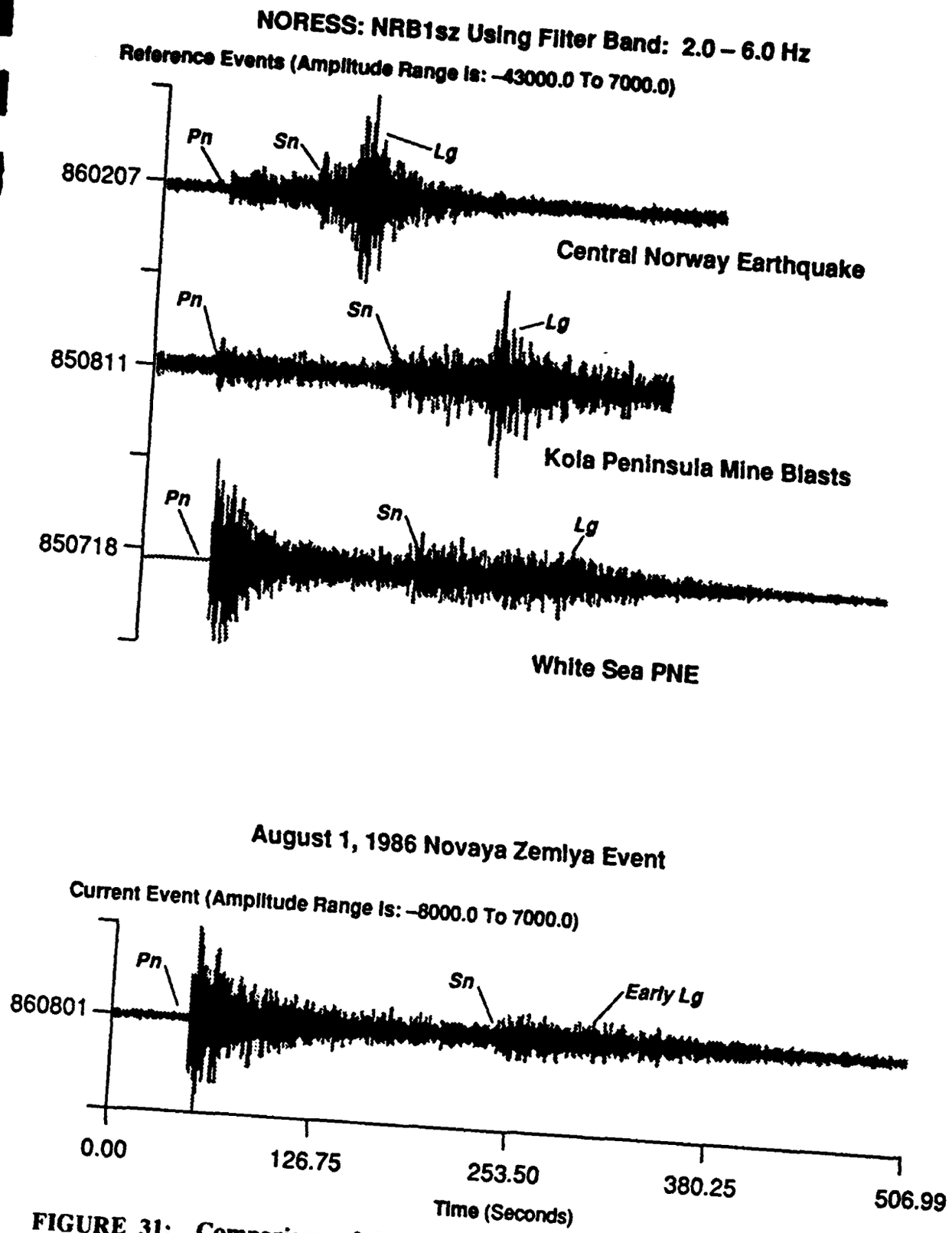

FIGURE 31: Comparison of 2-6 Hz filtered waveforms recorded at the NORESS NRB1sz channel from the 860801 Novaya Zemlya event (bottom) with three reference events. *Orid* 69 is an earthquake, *orid* 49 is a Kola Peninsula mine blast, and *orid* 47 is the White Sea PNE.

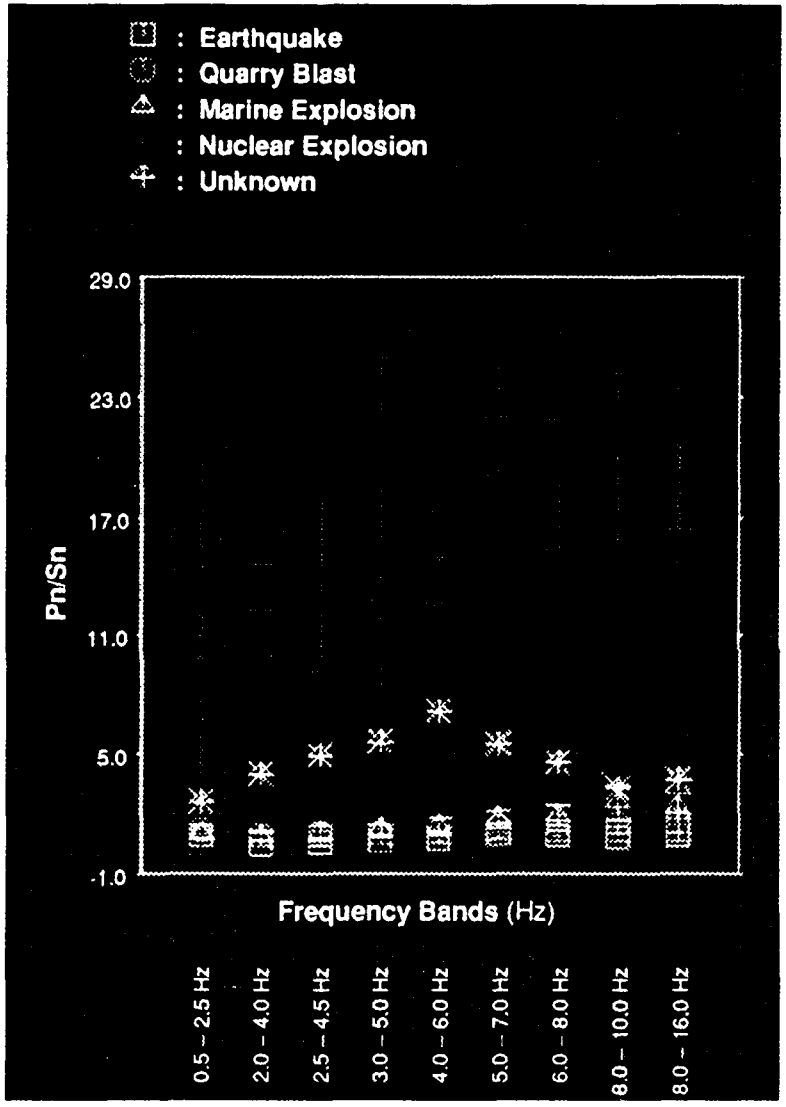

FIGURE 32a: Plot of the average *Pn/Sn* amplitude ratios measured at NORESS, using maximum rms measurements, for the reference events shown in Figure 8. The triangle with the asterisks through it indicate the values of the 860801 event. Error bars show the standard deviations in the values for all events of a given source type.

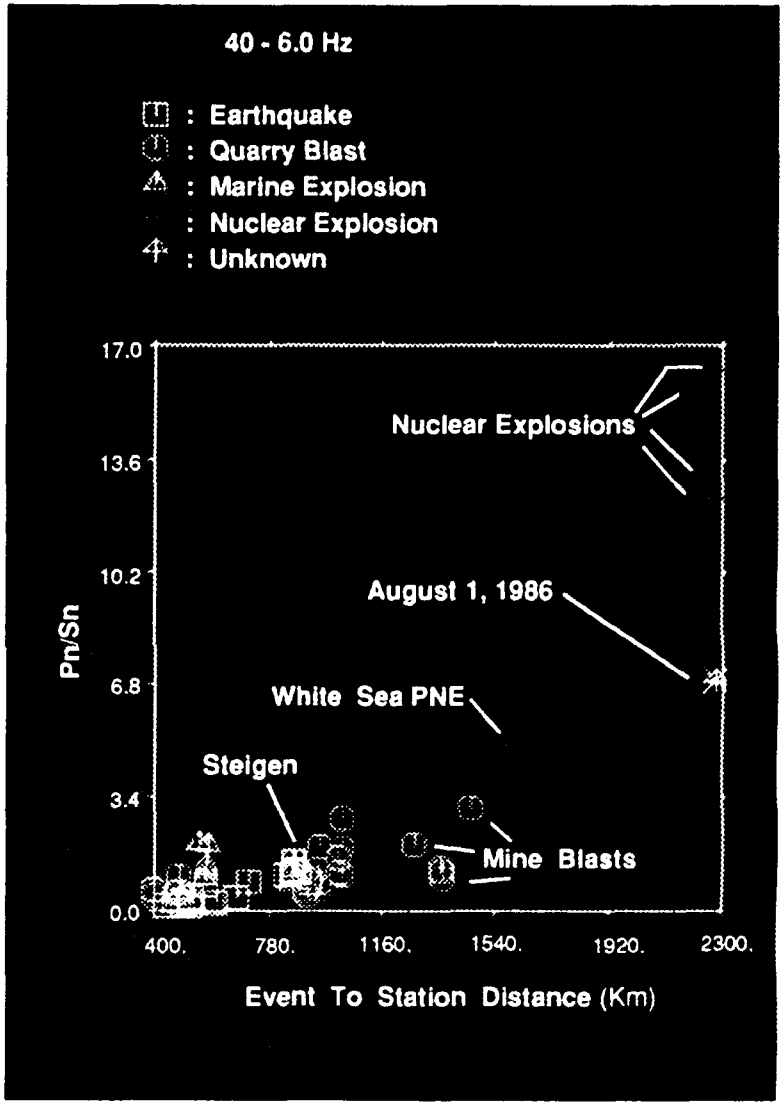

FIGURE 32b: Scatterplot showing the values of the *Pn/Sn* amplitude ratios in the 4-to-6 Hz band as a function of epicentral distance from NORESS for all the event types and the 860801 event. Legend in the upper left identifies the symbols used in the plot.

The greatest separation of the 860801 event and the nuclear explosions is in the 4 to 6 Hz band. Figure 32b shows a plot of the ratio in this band as a function of distance. This plot shows that the *Pn/Sn* ratio for the 860801 event is significantly less than the Novaya Zemlya explosions. However, it is comparable to that of the White Sea PNE at 1540 km distance, this in spite of the fact that the PNE was located 800 km closer to NORESS than the Novaya Zemlya. Mine explosions have smaller ratios than any of these events and earthquakes at short distances have even smaller ratios, usually less than one.

The problem with these comparisons is the lack of any earthquake data points in the distance range of 1000 to 2300 km. Thus, although the 860801 looks like mine blasts in this distance range, we do not know for sure what an earthquake would look like in this distance range. Second, there is a great gap in observations of any kind in the distance range of 1540 km to 2300 km. We know that *Lg* waves from Novaya Zemlya are blocked by the Barents Sea sedimentary basin. However, we are uncertain about what happens to *Sn* waves in this region. Perhaps they are partially blocked in the Barents Sea basin, which may explain the large *Pn/Sn* ratios for the Novaya Zemlya explosions. However, we might also expect *Pn* to be blocked as well, which might stabilize the *Pn/Sn* ratio. To check this, however, data from a known earthquake whose *Sn* waves cross the basin need to be studied.

Spectral Characteristics

Finally, we discuss the spectral characteristics of some of these events. Figure 33a shows the *Pn*, *Sn*, and noise spectra from the 860801 event. These spectra have been corrected for the NORESS instrument response. They show that the signal is quite limited in bandwidth, with the signal disappearing into the noise at about 9 Hz. Furthermore, the spectra are quite simple and, with the exception of some detail in the low-frequency part of the *Pn* spectrum, there are no spectral modulations which may indicate ripple fire or multiple events. The spectra of the Novaya Zemlya nuclear explosions look the same as this event in terms of bandwidth and lack of spectral modulations.

Figure 33b shows a plot of the spectra for the *Pn*, *Sn*, and *Lg* phase from the White Sea PNE. In contrast to all the Novaya Zemlya explosions, this explosion does exhibit spectral modulations in the low-frequency band which appear in all the spectra. Note that the spectral modulations are strongest at low frequency and die out above about 4.48 Hz. Cepstral analysis of these modulations produces a peak at about 0.9 seconds, indicating that these modulations are consistent with a double event delayed in time by about 0.9 seconds. The fact that the modulations do not extend to high frequency, in spite of the fact that the bandwidth for these phases extends beyond

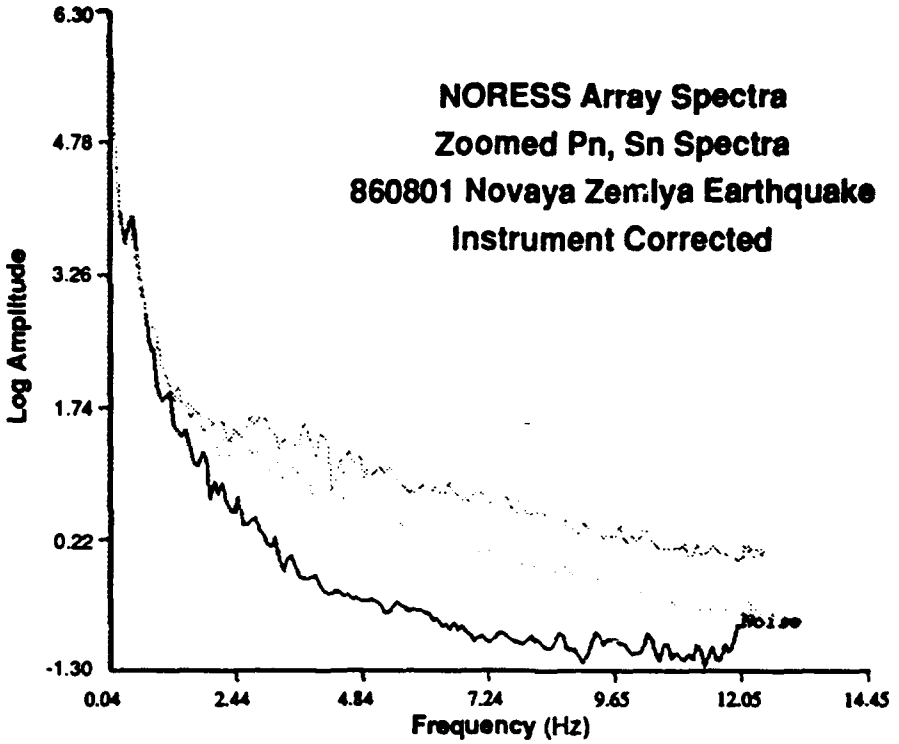

FIGURE 33a: Array-averaged spectra for signal and noise at NORESS for the 860801 Novaya Zemlya event. Each spectrum has been corrected for the NORESS instrument response.

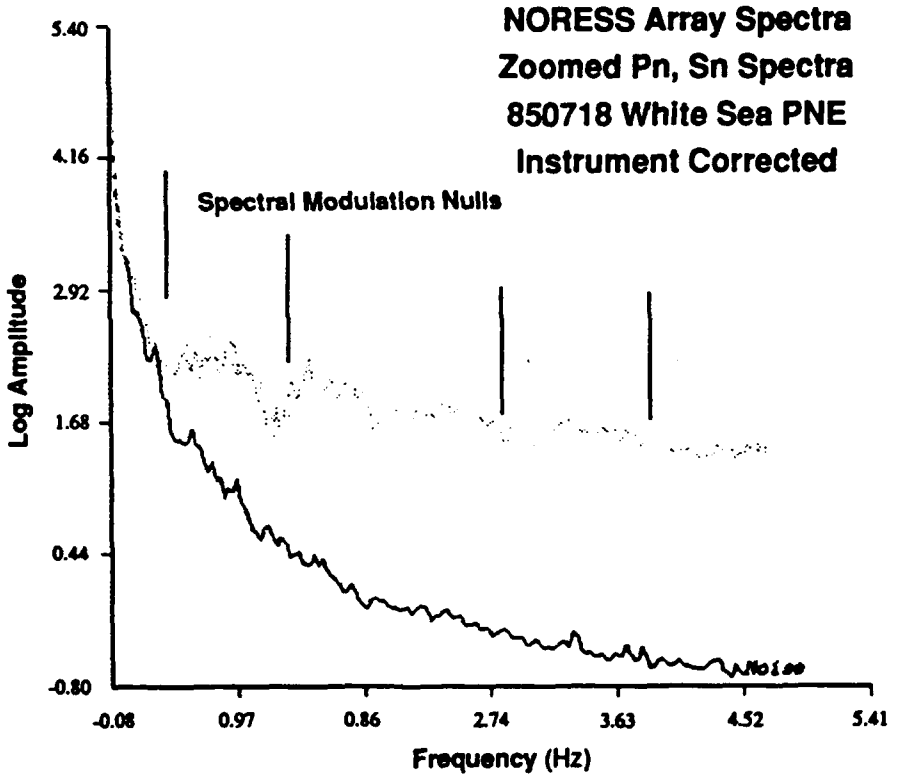

FIGURE 33b: Instrument-corrected signal and noise spectra for the White Sea PNE recorded at NORESS. These spectra show spectral scalloping in both *Pn*, *Sn*, and *Lg* but not in the noise, indicating that there are two shots with a delay time of about one second. The arrows indicate the troughs of the scalloping.

10 Hz, may indicate that these modulations are produced by two shots, a large one and a small one. Because the large shot may have less high-frequency content than the small one, the signals may not correlate beyond a high-frequency limit.

Thus, like the 921231 event, the 860801 was a single event, like the Novaya Zemlya explosions. However, as we have seen in the case of the White Sea event and for other PNEs studied by Baumgardt and Ziegler (1988), many Russian PNEs have time-independent spectral modulations indicative of two or more delayed shots. Moreover, it would have been possible to detect at NORESS time-independent spectral modulations caused by multiple sources, had they occurred for the 860801 event, at a distance of 21 degrees, because Baumgardt and Ziegler (1988) observed such effects in PNEs at even greater distances from NORESS and NORSAR.

3.4 WERE THE 921231 EVENT AND THE 860801 NOVAYA ZEMLYA EARTHQUAKE SIMILAR?

We now address the following question: Had the 921231 event been large enough so that *Pn/Sn* ratios could be observed at NORESS, would they have been the same as the 860801 event? An affirmative answer to this question would argue strongly that the 921231 event was an earthquake, assuming that the 860801 event was an earthquake. To answer this question, we statistically analyze the *Pn/Sn* ratios of the 921231 and 860801 events relative to the same nuclear explosions which were recorded at both arrays.

The plot of *Pn/Sn* ratios against distance in Figure 32b shows a strong distance dependence in the ratio, caused by differences in attenuation of the *Pn* and *Sn* phases over large distance. The *Sn* phase has stronger attenuation than *Pn*, causing the *Pn/Sn* ratio to decrease exponentially with distance. Thus, to compare the *Pn/Sn* ratios recorded at the ARCESS and NORESS arrays from Novaya Zemlya events, this differential attenuation effect needs to be taken into account.

The distance dependence of attenuation is usually expressed as follows:

$$A_{Pn} = A_{op} e^{-\pi \Delta t_P^*}$$

and

$$A_{Sn} = A_{os} e^{-\pi \Delta t_S^*} \quad ,$$

where A_{Pn} and A_{Sn} are the measured amplitudes of the *Pn* and *Sn* phases, respectively, at an array at distance, Δ, A_{op}, and A_{OS} are the source excitations of *P* and *S*, respectively, and t_p^* and t_S^* are the attenuation coefficients for *P* and *S* waves, respectively. The ratio of the *Pn* to *Sn* amplitudes can be written:

$$R = \frac{A_{Pn}}{A_{Sn}} = \frac{A_{op}}{A_{os}} e^{-\pi\Delta(t_p^* - t_s^*)},$$

where the exponential distance decay results when $t_p^* < t_S^*$. Consider now the log of the ratios, $LR = \log R$, in order to make the attenuation terms additive. If we difference the logs of the ratios for two events in the same region and at the same distance, Δ, from an array, the additive attenuation terms subtract out, as follows:

$$\log R^1_{NORESS} - \log R^2_{NORESS} = \log R^1_{ARCESS} - \log R^2_{ARCESS}.$$

where $R^i NORESS$ and $R^i ARCESS$ are the *Pn/Sn* amplitude ratios for event *i* at NORESS and ARCESS, respectively. Thus, the difference log of the *Pn/Sn* ratios for two events in the same region should be the same at both NORESS and ARCESS. If the 921231 event was another type of earthquake like the 860801 event, then we would expect the difference in the logs of the *Pn/Sn* ratios with the nuclear explosions in the same region to be the same at both arrays.

Now, we test the hypothesis that the 921231 and 860801 were the same kind of events. We first difference the *Pn/Sn* ratios in all frequency bands observable at both arrays with the ratios for each nuclear explosion and average the logs of the ratios:

$$\mu_1 = \frac{1}{N_1} \sum_{j=1}^{N_1} \left\{ \sum_{i=1}^{nf} \left[LR^{921231}_{ARCESS}(f_i) - LR^j_{ARCESS}(f_i) \right] \right\}$$

for the ARCESS recordings and

$$\mu_2 = \frac{1}{N_2} \sum_{j=1}^{N_2} \left\{ \sum_{i=1}^{nf} \left[LR^{860801}_{NORESS}(f_i) - LR^j_{NORESS}(f_i) \right] \right\}$$

for the NORESS recordings, where *LR* refers to the log ratio, $N1$ and $N2$ are the number of nuclear explosions recorded at ARCESS and NORESS, respectively, and *nf* is the number of frequency bands for which the log *Pn/Sn* amplitude ratios have been measured. Thus, if the 921231 and 860801 events are the same type of sources, then we expect that $\mu 1 = \mu 2$.

Figure 34a shows boxplots of the log ratios in four frequency bands (2-4 Hz, 2.5-4.5 Hz, 3-5 Hz, 4-6 Hz) of the 921231 event at ARCESS and the 860801 event at NORESS alongside the corresponding ratios for the nuclear explosions recorded at the two arrays. These frequency bands were chosen because they were the ones for which both *Pn* and *Sn* had good signal-to-noise ratios at both arrays. For NORESS, four nuclear explosions are plotted, including one in 1984, along with the three explosions that occurred after 1988 and were also recorded at ARCESS. Although the *Pn/Sn* ratios at NORESS are larger than those at ARCESS, because of the differential attenuation effect on *Pn* and *Sn*, the differences in the log ratios appear to be about the same.

We now test whether the means in the differences in the log ratios are the same, i.e., $\mu 1 = \mu 2$. Figure 34b shows box plots of the differences in the log ratios between two events in question and the nuclear explosions at the respective arrays. The white lines in each boxplot are the median values of the difference in ratios. The mean differences, which are nearly the same as the medians, are $\mu 1 = -0.7$ at ARCESS and $\mu 2 = -1.1$ at NORESS. Testing the null hypothesis that $\mu 1 = \mu 2$ using the t test and the nonparametric Wilcoxcon test, we can accept the null hypothesis using the t test at the 98% confidence level and with the Wilcoxcon test at the 96% confidence level. Based on this analysis, we conclude that had the 921231 event been observed at NORESS, it would have had almost the same mean log *Pn/Sn* ratios relative to the nuclear explosions as does the 860801 event. Therefore, if the 860801 was most likely an earthquake, the similarity in relative scaling of log *Pn/Sn* amplitude ratios relative to the nuclear explosions at the two arrays strongly implies that the 921231 event was also an earthquake.

3.6 CONCLUSIONS

Our analysis of the waveform features of the 921231 event has shown that the event was probably not a nuclear explosion. Based on the comparison of *Pn/Sn* amplitude-ratio features with historical events, including earthquakes and mine explosions, we conclude that, based on the ARCESS data, the event is consistent with a mine blast on the Kola Peninsula and also resembles earthquakes in the Greenland Sea, although the *Pn/Sn* ratios of the 921231 event are slightly higher than those of the earthquakes. An earthquake identification cannot be ruled out because there are limited earthquakes in the same distance range and none in the actual Novaya Zemlya region, except for the 860801 event, which was only recorded at NORESS.

The event was too small to produce measurable *S* waves at NORESS. However, we reconsidered the 860801 event, which was larger and well recorded at NORESS. Our relative scaling analysis provided indirect evidence that these two events might have been very similar, other than their size, and thus, may have been the same source type. The evidence supported the

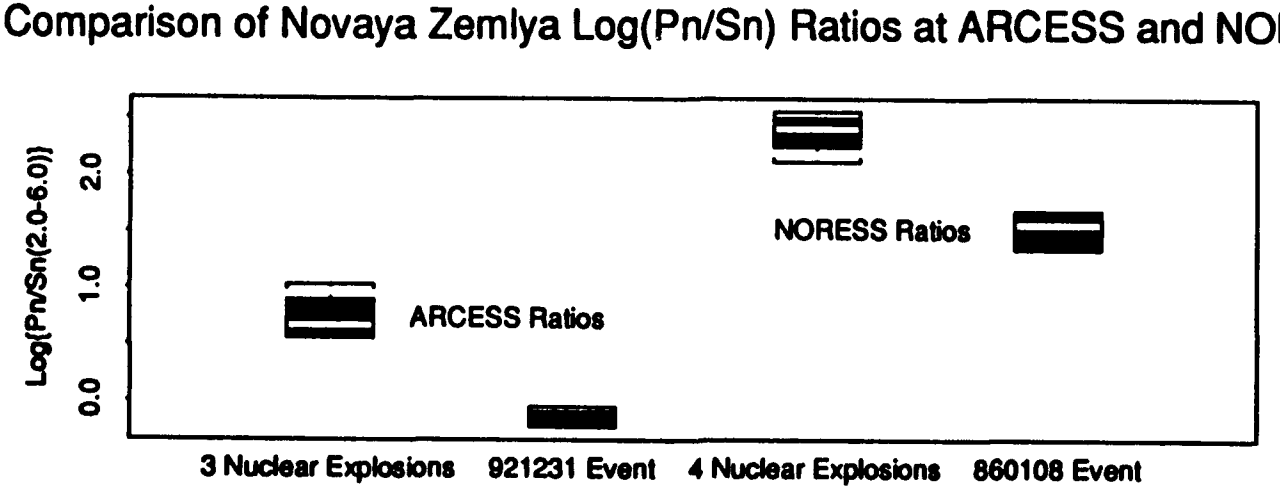

FIGURE 34a: Boxplots of the log *Pn/Sn* ratios of the 921231 event and three nuclear explosions, measured at ARCESS, and the 860801 event and four nuclear explosions at NORESS. The horizontal white lines indicate the medians of the data and the height of each box encloses the first to the third quartiles of the data. The whiskers are plotted at the extreme values.

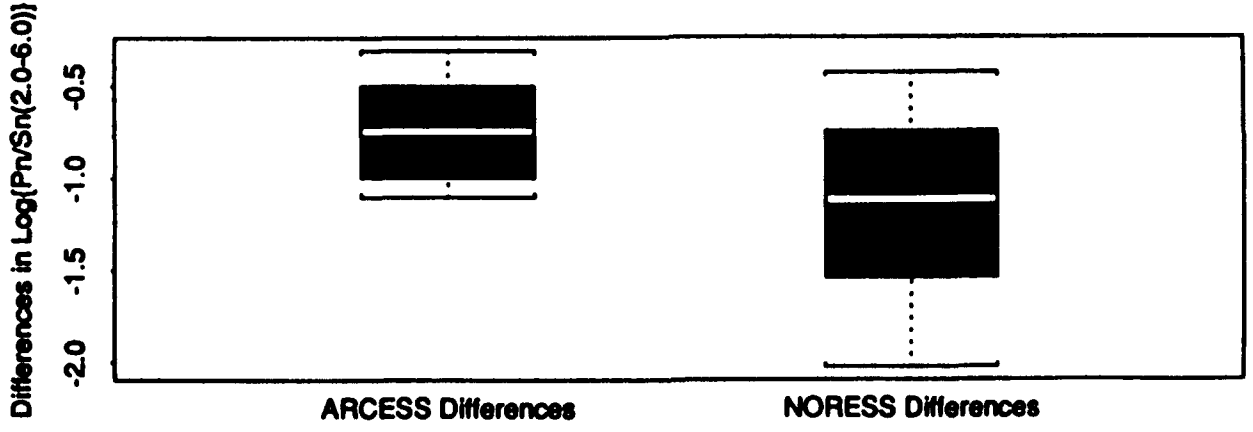

FIGURE 34b: Boxplots of the differences in the log *Pn/Sn* ratios between the 921231 and 860801 events, recorded at ARCESS and NORESS, respectively, and each of the nuclear explosions recorded at each of the arrays.

conclusion that both events were not nuclear explosions, and if the 860801 event was an earthquake, as indicated by other discriminants (e.g., Ryall et al, 1987), then the 921231 was also an earthquake.

This study points up the importance of carefully considering propagation-path differences when trying to compare known explosions and earthquakes with events of unknown identity. If we compared the 921231 *Pn/Sn* features with Kola mine blasts and Greenland Sea earthquakes while ignoring propagation path differences, the first impression would be that the event was a mine blast. However, the Novaya Zemlya events occurred several hundred kilometers farther from ARCESS than the Kola explosions, and *Sn* probably attenuated more rapidly than *Pn* with distance resulting in *Pn/Sn* ratios increasing with distance.

Novaya Zemlya earthquakes, by virtue of source mechanism differences, might look more like explosions than Greenland Sea earthquakes. The similarity in relative scaling of log *Pn/Sn* ratios that we found for the 921231 event at ARCESS and the 860801 event at NORESS, relative to nuclear explosions, supports this conclusion.

Thus, we conclude that the 921231 event was probably an earthquake which resembled mine blasts in other regions. Analysis of more events, particularly earthquakes, may provide a better understanding of the identification of this event. Further ISEIS analysis of other events in the future, including analysis of earthquakes outside of Scandinavia, will continue to supply more reference events. We expect to process more data from the Spitzbergen array, which is not affected by the propagation anomalies from Novaya Zemlya of the Barents Sea, as in the case of NORESS and ARCESS. Thus, by studying more mine blasts and earthquakes at the Spitzbergen and other Scandinavian arrays and comparing waveform-feature discriminants with the 921231 event, we will be able to better characterize this event and others which may occur at Novaya Zemlya in the future.

REFERENCES

Anderson, J., W.E. Farrell, K. Garcia, J. Given, H. Swanger (1990). Center for Seismic Studies, version 3 database: schema reference manual, Technical Report C90-01, Center for Seismic Studies, Arlington, VA.

Bache, T.C., S.R. Bratt, J. Wang, R.M. Fung, C. Kobryn, and J.W. Given (1991). The Intelligent Monitoring System, *Bull. Seism. Soc. Am.*, **80**, 1833-1851.

Baumgardt, D.R., and K.A. Ziegler (1988). Spectral evidence of source multiplicity in explosions: application to regional discrimination of earthquakes and explosions, *Bull. Seism. Soc. Am.*, **78**, 1773-1795.

Baumgardt, D.R., and G.B. Young (1990). Regional seismic waveform discriminants and case-based event identification using regional arrays, *Bull. Seism. Soc. Am.*, **80**, 1874-1892.

Baumgardt, D.R., S. Carter, M. Maxson, J. Carney, K. Ziegler, and N. Matson (1991a). Design and development of the intelligent event identification system, volumes I, II, and III, *PL-TR-91-22298(I)*, Final Report, ENSCO, Inc., Springfield, VA.

Baumgardt, D.R., G.B. Young, and K.A. Ziegler (1991b). Design and development of the Intelligent Event Identification System: design considerations and processing for regional event identification, *PL-TF-91-2211*, Scientific Report #1, ENSCO, Inc., Springfield, VA.

Baumgardt, D.R. (1991a). Intelligent Seismic Event Identification System, volume II: users manual, Final Report, PL-TR-91-2298(II), ENSCO, Inc., Springfield, VA.

Baumgardt, D.R. (1991b). Possible seismic signals from a nuclear submarine accident in the Norwegian Sea, abstract in *EOS*, **72**, 343.

Baumgardt, D.R. (1991c). High-frequency array studies of long range *Lg* propagation and the causes of *Lg* blockage and attenuation in the Eurasian continental craton, Final Report, SAS-TR-91-50, ENSCO, Inc., Springfield, VA.

Baumgardt, D.R. (1992). Investigation of seismic discriminants in Eurasia, SBIR Phase I, Final Report, SAS-TR-92-81, ENSCO, Inc., Springfield, VA.

Baumgardt, D.R., J. Carney, M. Maxson, and S. Carter (1992). Evaluation of regional seismic discriminants using the intelligent seismic event identification system, Semi-Annual Technical Report, SAS-TR-93-38, ENSCO, Inc., Springfield, VA.

Bennett, T.J., and J.R. Murphy (1986). Analysis of seismic discrimination capabilities using regional data from western United States events, *Bull. Seism. Soc. Am.*, **76**, 1069-1086.

Bennett, T.J., B.W. Barker, K.L. McLaughlin, and J.R. Murphy (1989). Regional discrimination of quarry blasts, earthquakes, and underground nuclear explosions, Final Report, *GL-TR-89-0114*, S-Cubed, La Jolla, CA.

Bennett, T.J., A.K. Campanella, J.F. Scheimer, and J.R. Murphy (1991). Regional discrimination of Soviet nuclear explosions, earthquakes, and mine blasts, *Papers Presented at 13th Annual PL/DARPA Seismic Research Symposium*, 8-10 October 1991, Keystone, CO, 78-84.

Bennett, T.J., J.F. Scheimer, A.K. Campanella, and J.R. Murphy (1992). Seismic discrimination of rockbursts in mines, in *Papers Presented at 14th Annual PI/DARPA Seismic Research Symposium*, 16-18 September 1992, Lowes Ventana Canyon Resort, Tucson, AZ, 29-35.

Der, Z., and D. Baumgardt (1992). Automated seismic analysis using supervised machine learning (Phase I), SBIR Phase I Final Report, SAS-TR-92-92, ENSCO, Inc., Springfield, VA.

Der, Z.A., M.R. Hirano, and R.H. Shumway (1990). Coherent processing of regional signals at small seismic arrays, *Bull. Seism. Soc. Am.*, **80**, 2161-2176.

Der, Z.A., M.R. Hirano, K.A. Ziegler, and R.H. Shumway (1991). Broadband studies of seismic sources at regional and teleseismic distances using advanced time-series analysis methods, Final Report, SAS-TR-91-49, ENSCO, Inc., Springfield, VA.

Der, Z.A., R.H. Shumway, and M.R. Hirano (1992). Time domain waveform inversion - a frequency domain view: how well do we need to match waveforms?, *Bull. Seism. Soc. Am.*, **81**, 2351-2370.

Dysart, P.S., and J.J. Pulli (1990). Regional seismic event classification at the NORESS array: seismological measurements and the use of trained neural networks, *Bull. Seism. Soc. Am.*, **80**, 1910-1933.

Gibowicz, S.J. (1984). The mechanism of large mining tremors in Poland, *Proc. First Intl. Cong. on Rockbursts and Seismicity in Mines*, Johannesburg.

Gibowicz, S.J. (1985). Seismic moment and seismic energy of mining tremors in the Lubin Copper Basin in Poland, *Acta Geophys. Pol.*, **XXXIII**, 243-257.

Grant, L., J. Coyne, and F. Ryall (1993a). CSS ground-truth database: version 1 handbook, SAIC Scientific Report No. C93-05, August 1993.

Grant, L., F. Ryall, and J. Coyne (1993b). Use of beta stations and gamma networks for calibration of the GSE system - a case study, Scientific Report #1 (Draft), Center for Seismic Studies, June 18, 1993.

Harjes, H.P., N. Gestermann, M. Jost, J. Schweitzer, and J. Wuster (1992). Advanced waveform research methods for GERESS recordings, Annual Report, 15 February 1991 -14 February 1992, *PL-TR-92-2142*.

Harris, D.B. (1991). A waveform correlation method for identifying quarry explosions, *Bull. Seism. Soc. Am.*, **81**, 2395-24118.

Kennett, B.L.N. (1993). The distance dependence of regional phase discriminants, *Bull. Seism. Soc. Am.*, **83**, 1155-1166.

Kim, W.Y., D.W. Simpson, and P.G. Richards (1993). Discrimination of regional earthquakes and explosions in eastern United States using high-frequency data, *EOS*, **74**, 212.

Lynnes, C., and R. Baumstark (1991). Phase and spectral ratio discrimination in North America, *PL-TR-91-2212 (II)*, Final Report, 18 July 1991, Teledyne Geotech, Alexandria, VA.

Murphy, J.R., and T.J. Bennett (1982). A discrimination analysis of short-period regional seismic data recorded at Toronto Forest Observatory, *Bull. Seism. Soc. Am.*, **72**, 1351-1366.

Mykkeltveit, S., and H. Bungum (1984). Processing of regional seismic events using data from small-aperture arrays, *Bull. Seism. Soc. Am.*, **74**, 2313-2333.

Ryall, A.S., A. Jurkevics, P.S. Dysart, and J.J. Pulli (1987). Note on seismic discrimination and the 1 August 1986 Novaya Zemlya event, in *Technical Report of the Period 1 October-31 December 1986*, Technical Report C87-01, Center for Seismic Studies, Arlington, VA.

Shi, J., W.Y Kim, and P.G. Richards (1993). Quantification of intraplanet earthquakes in New York State and adjacent areas, abstract in EOS, **74**, 212.

Taylor, S.R., and M.D. Denny (1991). An analysis of spectral differences between Nevada Test Site and Shagan River nuclear explosions, *J. Geophys. Res.*, **96**, 6237-6245.

Taylor, S.R., N.W. Sherman, and M.D. Denny (1988). Spectral discrimination between NTS explosions and western United States earthquakes at regional distances, *Bull. Seism. Soc. Am.*, **78**, 1563-1579.

Taylor, S.R., M.D. Denny, E.S. Vergino, and R.E. Glaser (1989). Regional discrimination between NTS explosions and western U.S. earthquakes, *Bull. Seism. Soc. Am.*, **79**, 1142-1176.

Wuster, J. (1993). Discrimination of chemical explosions and earthquakes in Central Europe - a case study, *Bull. Seism. Soc. Am.*, **83**, 1184-1212.